Doctoral Theses at NTNU, 2007:6

Jon Eirik Brennvall

New techniques for measuring thermal properties and surface heat transfer applied to food freezing

Doctoral Thesis

NTNU
Norwegian University of
Science and Technology
Thesis for the degree of
doktor ingeniør
Faculty of Engineering Science and Technology
Department of Energy and Process Engineering

NTNU
Innovation and Creativity

Jon Eirik Brennvall

New techniques for measuring thermal properties and surface heat transfer applied to food freezing

Thesis for the degree of doktor ingeniør

Norway, Trondheim, February 2007

Norwegian University of Science and Technology
Faculty of Engineering Science and Technology
Department of Energy and Process Engineering

NTNU
Innovation and Creativity

NTNU
Norwegian University of Science and Technology

Thesis for the degree of doktor ingeniør

Faculty of Engineering Science and Technology
Department of Energy and Process Engineering

ISBN 978-82-471-0119-3 (printed ver.)
ISBN 978-82-471-0122-3 (electronic ver.)
ISSN 1503-8181

Doctoral Theses at NTNU, 2007:6

Printed by Tapir Uttrykk

Preface

The intention of this work is to improve knowledge about the thermal properties of food and the boundary conditions of food during freezing. This knowledge will be basic input to food freezing models.

The work is founded by the Research Council of Norway through the Strategic Institute Programme:
"Technology for competitive processing of food".

I thank my supervisors Doctor Viðar Harðarson and Professor Ola M. Magnusen at Department of Energy and Process Engineering for initiating my work, and for their professional counselling. Further I will thank my co-workers and the personnel at the laboratory and the engineering workshop at the same department for their help. I particularly acknowledge Robert Olsen for his help with Fortran programming and Latex. I will also thank my friends and family for their assistance and support.

In connection with the process of designing and building the thermal multimeter I will take this opportunity to thank SINTEF and NTNU for making the project possible.

Trondheim, February 2. 2007

Jon Eirik Brennvall

Summary

This thesis presents two different works. The first part introduces a thermal multimeter which measures heat capacity, thermal conductivity and density. *The instrument gives continuous measurement data within a temperature range*. With some exceptions this also holds for the prototype of a thermal multimeter which is built and tested. The measuring method is constant heating of one side of a slab. The slab is insulated on all other sides. After some time there will be equilibrium where there is a constant *temperature difference* over the slab. The thermal conductivity can be calculated from this temperature difference. The heat capacity can be calculated from how fast the temperature rises. Measurements of the slab thickness give density as function of temperature.

The second part discusses a practical method for measuring the heat transfer coefficient (α). The method is based on shell freezing of clear jelly which has the same shape as the product of interest. Transparent jelly is transparent before it freezes and white when frozen. If the sample is removed from the freezer and cut through before it is completely frozen the freezing front is distinct and the thickness of the frozen layer can be measured. By measuring time the jelly sample was in the freezer and thickness of the frozen layer the heat transfer coefficient can be calculated by using Plank's equation. The method is suitable for measuring local α because it can be shown that tangential heat flow can be neglected when the frozen layer is thin.

Computer simulations, automated data acquisition and data processing are a considerable part of this thesis, even though it is not obvious from the results presented. There are more lines in the data code written to obtain the results presented here then the number of lines in this thesis. The size of selected simulation results and processed data from the measurements are 6.3 GB.

Contents

List of Figures

List of Tables

List of Symbols

Symbol	Property	Si-unit
A	area	m^2
A, B, C	integration constants	
$\hat{A}, \hat{B}, \hat{C}$	part of integration constants	
a	thermal diffusivity	m^2/s
Bi	Biot's number	$-$
$c_p,\ c$	specific heat capacity	$J/\left(kgK\right)$
C	heat capacity	J/K
D, l, r, R, z	dimension	m
Fo	Fourier number	$-$
Gr	Grashof number	$-$
g	gravity at earth surface	$9.81\ m/s^2$
h	specific enthalpy	J/kg
Δh_{ice}	latent heat of melting of ice	J/kg
k	thermal coefficient	W/K
m	mass	kg
Nu	Nusselt number, average	$-$
Pr	Prandtl number	$-$
r^*	reduced position	$-$
Re	Reynolds number	$-$
$\dot{q}$	heat flux	W/m^2
$\dot{Q}$	heat flow	W
Q	accumulated heat	J
$\vec{r}$	position vector	m
T	absolute temperature	K
u	specific internal energy	J/kg
u_∞	free stream velocity	m/s
V	volume	m^3
v	specific volume	m^3/kg
x, y, z	Cartesian coordinates	m
α	heat transfer coefficient (HTC)	$W/(m^2K)$
ε	emissivity	$-$
λ	thermal conductivity	$W/\left(m \cdot K\right)$

Symbol	Property	Si-unit
μ	dynamic viscosity	Pa/s
ν	kinematic viscosity	m^2/s
ρ	density	kg/m^3
τ	time	s
σ	Stefan-Boltzmann constant	$5.67 \cdot 10^{-8}\ W/\left(m^2 K^4\right)$
ϑ^*	reduced temperature difference	$-$
Subscript	Describes	
0	initial	
a	ambient	
A	air	
B	bottom	
D	diameter	
E	edge	
c	center of cell, convection, conduction	
C	container	
Cu	copper	
f	fluid	
ff	freezing front	
G	guard	
I	insulation	
i	inner	
i, j	node index	
l	heat leakage	
L	left	
o	outer	
p	pressure	
r	radiation, radius	
R	right, reference, radius	
s	surface	
S or Sa	sample	
SaC	sample container	
St	steel	
T	top	
va	variance	
W	water	
x	distance from the surface	

Chapter 1

Introduction

1.1 Summary of state of art for measuring the thermal properties and the heat transfer coefficient in food freezing

In the food industry new products with new composition, size, shape and packaging are regularly introduced to the market. Many of the products are frozen. The refrigeration systems used today are computer regulated which gives new possibilities to customize the freezing process of the product. This makes it possible to reduce cost, product loss and increase the quality. An important tool for customization of the freezing process is numerical simulations. With today's computers and numerical methods non-linear heat conduction problems can be accurately solved, (Wang & Kolbe [1]) but the trustworthiness of the results is directly dependent on the accuracy of the thermal properties and heat transfer coefficient (α) used as input (Hayakawa [2]). The dominating heat transport mechanism for heat in food freezing is conduction. The properties needed to do computer simulations of heat conduction in food include enthalpy, apparent heat capacity, density, thermal conductivity (Simpson [3]).

In the food industry density is usually measured with a box of known volume and a weight. The density change during freezing, of up to 8% for pure water, is usually ignored in the simulations, but it can be included by using volume-based heat capacity instead of mass-based heat capacity (Cleland [4]). Data for the volume change of food during freezing are seldom included in reported measurements

of thermal properties. See also Section 2.1.1.

Heat capacity of food is mainly dependent on the composition. Food can therefore be grinded, heat treated, undergo internal enzymatic or bacteriological processes etc. without any significant change in heat capacity. This makes heat capacity relatively easy to measure. Adiabatic methods give the most accurate result when measuring heat capacity (Magee et al. [5], Nesvadba [6]). These methods are however time consuming if the sample has the size of approximately one cm^3 or larger, but they are the most common methods used for food (Pham [7]). This because food is not homogeneous. If the sample is too small there is a risk of measuring on only one of the materials in the mixture. This will of course not give the average heat capacity which usually is the one of interest since small-scale material variation in food is ignored in most models. The other common methods for measuring heat capacity are differential scanning calorimeters (DSC) and mixing apparatus. See also Section 2.1.2.

Thermal conductivity is *not* only dependent of composition. Fibre orientation, porosity texture etc. also have great influence and will often cause the thermal conductivity to be directional dependent. Unlike heat capacity the thermal conductivity can therefore change when food is handled, and is consequently much more difficult to measure. Water, which is a major component in most food, also complicates the measurements of thermal conductivity. This is because of the difference between the thermal conductivity of ice and water, and because only under special conditions will water freeze to transparent ice free of cracks and bubbles which can decrease thermal conductivity considerably. For frozen samples steady-state methods are recommended because of the strong temperature dependency of heat capacity in the freezing temperature range of most food (Pongsawatmanit et al. [8], Nesvadba [6]). This because theoretically it is mathematically difficult to find thermal conductivity when the heat capacity changes rapidly. Also practically the heat capacity will have large uncertainty since $\partial c_p/\partial T$ is large. According to the Cost90 [9] project which had the goal of supplying the food engineer with reliable thermophysical properties data, the difference between results from different laboratories can vary as much as $\pm 40\%$ where ± 4-24% is caused by deviation between sample which was assumed to be equal. It is therefore necessary to standardize methods for measuring thermal conductivity of food. See also Section 2.1.3

The heat transfer coefficient which usually defines the boundary conditions is also necessary. According to Pham [10] it is "the quantities least amenable to prediction and most subject to variation in practice, and should therefore be a priority area in freezing science". The average heat transfer coefficient (α) for whole

object are usually determined by calculations from the heat balance equation, partitional calorimetry or direct calorimetry (Danielsson [11]). Correlations for α for different objects given as a function of Reynolds, Prandtl and Nusselt numbers are presented by Whitaker [12]. The correlations generally demand simple geometry and well defined fluid flow to give accurate results. See also Section 3.1.1.

The classical method of measuring the local heat transfer coefficient from a solid object's surface to a fluid is to wrap the object in an electrical ribbon which provides constant heat flux. The temperature is then measured over the surface. Packing the object in a ribbon is time consuming and can change the geometry, surface roughness etc. The method is therefore constraining and limited, and the heat transfer coefficient measured differs from what is estimated form temperatures measured in food objects (Kondjoyan & Daudin [13]).

An indirect method for measuring local heat transfer coefficient is presented by Kondjoyan & Daudin [13],[14],[15]. They have wetted objects of plaster and placed them in an air stream where temperature, air speed and air humidity are constant. After a while the plaster will obtain the wet bulb temperature. This temperature will be stable for a long time, until the surface of the objects dries, and water has to diffuse to the surface before it can evaporate. When the temperature is stable, the weight loss per time unit can be measured. All the energy needed to evaporate water is taken from the air, and an energy balance will give the heat flux and the heat transfer coefficient. The method becomes local if the evaporation from different parts of the objects surface is measured.

1.2 Motivation and objectives of the thesis

The investigations done in the Cost90 [9] project indicate that the available data for thermal conductivity of food are insufficient and provide uncertainties of up to 40%. An important reason for this is that with the methods available measuring density, heat capacity and thermal conductivity in a temperature range from -60 to +10 ℃ require at least two different instruments, or alternatively becomes very time consuming. Measuring only thermal conductivity for a temperature interval is also time consuming due to the time needed to reach steady-state conditions for steady-state methods, or suitable initial conditions after previous measurement for transient methods. Since the thermal properties of food are highly temperature dependent it would be preferable with a method which relatively quickly produces data for heat capacity and thermal conductivity for several temperatures in a temperature range with a minimum of sample preparation.

According to Pham [10] methods for finding the heat transfer coefficient are even more insufficient than methods for measuring thermal conductivity, but it seems clear that an effort in both areas is required in order to bring the science of food freezing forward. The objective for this thesis is to develop methods and measuring apparatus for studying heat transfer in food refrigeration. It is emphasized that the methods and apparatuses are to be practical, and suitable for food in the refrigerated environment.

The first part of the thesis presents an instrument called a thermal multimeter that is specially designed for measuring the thermal properties of food. The instrument is easy to use, it measures the thermal properties in a wide temperature range, and can measure corrosive materials. It is also easy to clean and robust and therefore well suited for measuring food. All the thermal properties are found by measuring the temperature development in an otherwise insulated rod which is exposed to a constant heat flux at one end.

The second part of the thesis shows how the local heat transfer coefficient (α) can be measured by using transparent jelly. Jelly changes from transparent to white when frozen. The position of the freezing front can then be found visually by cutting through the jelly. The heat transfer coefficient can then be calculated. This method is cheap and practical and has a wide variety of uses from determining heat transfer coefficient in different parts on the surface of a product placed in an air stream to measuring heat transfer through packaging. It can also be extended if the position of the freezing front can be found by other methods such as magnetic resonance or ultrasound.

1.3 The heat equation

Heat transfer by conduction can usually be described by the heat equation which in its most general form is

$$\frac{\partial \rho c_p T}{\partial \tau} = \nabla \cdot \lambda \left(\nabla T \right) + \dot{q}_{\mathrm{V}} \tag{1.1}$$

The equation is credited to Joseph Fourier (1768-1830), a French mathematician and physicist who has made very significant contributions to the analytical treatment of heat conduction. The left-hand side of (1.1) is the energy change in a control volume. $\nabla \cdot \lambda \left(\nabla T \right)$, which is known as Fourier equation, and gives the net heat conducted through the borders of the control volume and $\dot{q}_{\mathrm{V}}$ is heat generation by chemical reactions, microwaves, electricity etc. inside the control volume.

The heat generation can be negative if there is an endothermic chemical reaction in the material.

Techniques for solving the equation analytically can be found in general books on mathematics, like Penney [16] or Kreyszig [17]. There are three groups of numerically techniques which is much used for solving (1.1). The finite difference technique can be found in a book written by Özisik [18]. The finite volume technique can be found in a book written by Versteeg & Malalasekera [19]. The finite element technique can be found in a book written by Lewis et al. [20]. The heat equation with suitable boundary conditions is used to calculate temperature time development and heat flow in materials where conduction is the dominating heat transport mechanism.

1.3.1 The physics of cooling

In cooling and freezing calculations common objects have the shape of slabs, cylinders or spheres. The word "slab" is here used about objects where two surfaces are parallel and all other surfaces are perpendicular to these two surfaces.

Imagine a slab with infinite width and length (infinite slab), an infinite long cylinder or sphere cooled by a fluid. The fluid has constant temperature T_F. The complex physics of heat transport between the surface of the solid and the fluid is hidden in the heat transfer coefficient (α). α is defined as

$$\alpha \equiv \frac{\dot{q}}{T_s - T_f} \tag{1.2}$$

where T_s is the surface temperature and T_f is the temperature in the fluid far from the surface. A bar over T_s ($\bar{T}_s$) implies that the temperature is an average over the whole surface. T_f in some literature is denoted T_∞. $\dot{q}$ is the heat flux.

α is measured, estimated from tables or empiric equations based on measurements of α in simple geometry. Assume that α is not a function of time and position on the surface. Equation (1.1) will then have the boundary condition

$$\lambda \frac{\partial T}{\partial r} = \alpha \left(T - T_f\right)\Big|_{r=R} \tag{1.3}$$

R is here the external radius or half thickness. The initial condition of (1.1) is a constant temperature

$$T = T_0|_{\tau=0} \tag{1.4}$$

Assuming that λ, ρ, c_p, α and T_f are constant and there is no internal heating or cooling this can be written in unit free form by introducing the reduced temperature difference

$$\vartheta^* = \frac{T - T_f}{T_0 - T_f} \tag{1.5}$$

reduced position

$$r^* = \frac{r}{R} \tag{1.6}$$

Fourier's number

$$\begin{gathered} Fo = \frac{a\tau}{R^2} \\ \left(a = \frac{\lambda}{\rho c_p} \right) \end{gathered} \tag{1.7}$$

and Biot's number

$$Bi = \frac{\alpha R}{\lambda} \tag{1.8}$$

The heat equation in unit free form with boundary and initial conditions then becomes

$$\begin{aligned} &\frac{\partial \vartheta^*}{\partial \left(Fo \right)} = \nabla^2 \vartheta^* \\ &\frac{\partial \vartheta^*}{\partial r^*} = -Bi\vartheta^* \Big|_{r^*=1} \\ &\vartheta^* = 1|_{Fo=0} \end{aligned} \tag{1.9}$$

Equation (1.9) presents analytical solutions for a slab in cosine series in the form

$$\vartheta^* = \sum_{i=1}^{n} C_i \; e^{-\left({A_i}^2 Fo \right)} \; cos \left(A_i \; r^* \right) \tag{1.10}$$

where every A_i satisfies the boundary condition and values for C_i are chosen so that the sum satisfies the initial condition when $Fo = 0$. A_i are positive solutions of

$$A \; tan \left(A \right) = Bi \tag{1.11}$$

There are infinite solutions of (1.11). To find an approximate solution of (1.9) for a given Bi the n first solutions of (1.11) are found. Greater n gives better

approximation. The solutions of (1.11) are then inserted into (1.10) and the values for C_i are found. The solutions of (1.11) are not periodic. Normal Fourier analysis then cannot be used to find values for C_i in (1.10). It is possible to find values for any finite number of C_i by creative use of the least squares method (Anton & Rorres [21]). This is done in the Matlab program "FourierCoolingSlab.m" which can be found among the attached files. Se page 155.

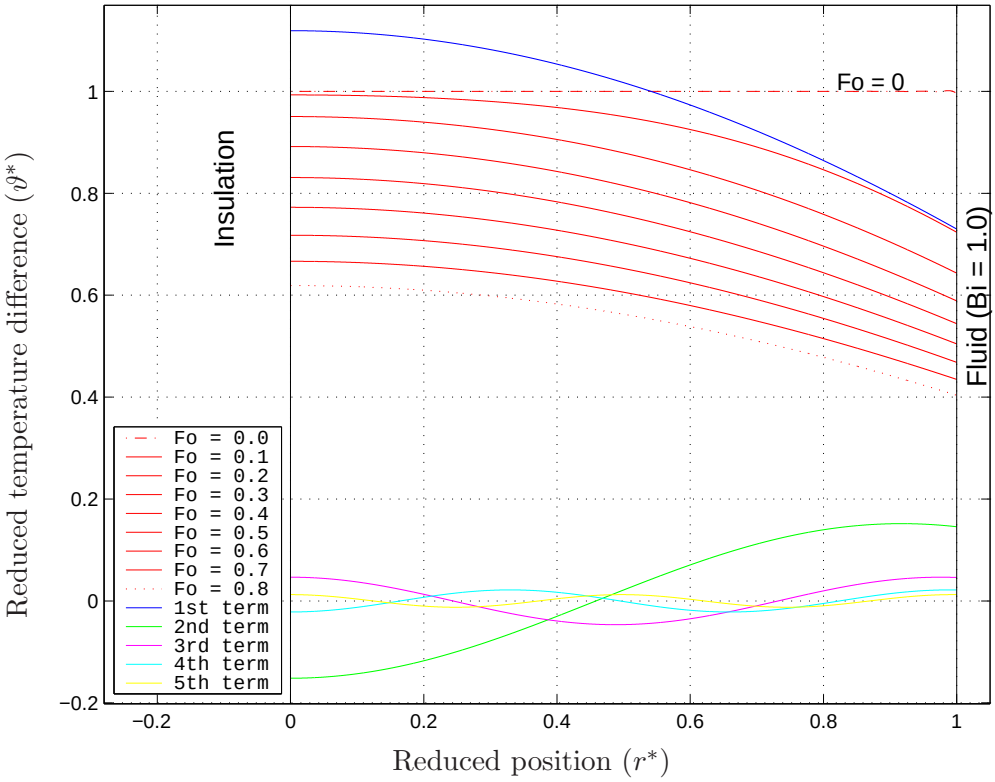

Figure 1.1: Reduced temperature difference as function of reduced position
Fo vary from 0 to 0.8. Bi is 1. The terms are the first five in the sum in (1.10) for $Fo = 0$. Totally 50 terms are used in this approximation. In sum they give the line for $Fo = 0$ which represents the initial condition

In (1.9) only Fo, Bi and r^* can be varied. The number of times (1.9) must be solved with regard to ϑ^* (analytically or numerically) to make charts that are suitable for finding an approximate solution of (1.9) graphic for any Fo, Bi and r^*, is feasible. Such charts are presented in the literature (Özisik [18], Incropera & DeWitt [22], Hewitt et al. [23]).

The physical interpretation of Fo is how long time it takes before a temperature change on the surface is noticeable in the centre of the object. As long as Fo is small the temperature change is small too. In numerical simulation Fo can be calculated for each control volume or node. High Fo then indicates inaccurate or unstable solution. Bi is the ratio between the surface (α) and the internal (λ/R) heat resistance. Low Bi means that the resistance is at the surface and that the temperature variation inside the object at any time is small. By ignoring the small temperature variation inside the object at low Bi (1.9) can be reduced to an ordinary differential equation. High Bi means that the resistance is inside the object, and that the temperature of the surface of the object is approximately the same as the fluid temperature. If Bi is infinite (1.9) becomes

$$\begin{aligned} &\frac{\partial \vartheta^*}{\partial \left(Fo\right)} = \nabla^2 \vartheta^* \\ &\left[\vartheta^* = 0\right]_{r^*=1} \\ &\left[\vartheta^* = 1\right]_{Fo=0} \end{aligned} \tag{1.12}$$

which has a practical analytical solution.

Writing (1.9) on unit free form is mathematically equivalent to reducing the number of parameters to a minimum. Above the heat equation was known before it was written in unit free form. If the heat equation was not known and had to be found from experiments the temperature would be a function of 6 parameters (thermal conductivity, heat capacity, density, α, time and radius).

Experimental science is generally to vary the parameters and look for empirical equations. If n experiments on each parameter were done where one parameter was varied and the rest were kept constant the total number of experiments would be n^6. However since all the parameters have units, they can be multiplied and divided by each other to find dimensionless groups. As shown 3 dimensionless groups would be found reducing the number of experiments needed to have a chance to guess the heat equation to n^3.

This technique has led to many discoveries especially in fluid mechanics and thermodynamics. It is so important that "the reduced number of parameters" is a concept in these special fields. The dimensionless groups are given names after the

people who formulated them and are almost always used in empirical equations which are difficult to explain with basic laws of physics. Most known of these groups is probably the Reynold's number (Re) which describes forced convection, and the fact that the transition between laminar and turbulent flow in a circular pipe occurs at $Re \approx 2300$. Dimensionless groups have also made experiments on scaled models an important tool in science and engineering, since experiments where the dimensionless groups have the same value will have the same result independent of scaling. Sometimes dimensionless groups are used with varying success when the postulation for formulating the group is not valid. Freezing is a typical example since Fo and Bi are defined only for constant thermal properties through the whole radius (half thickness).

1.3.2 The physics of freezing versus cooling

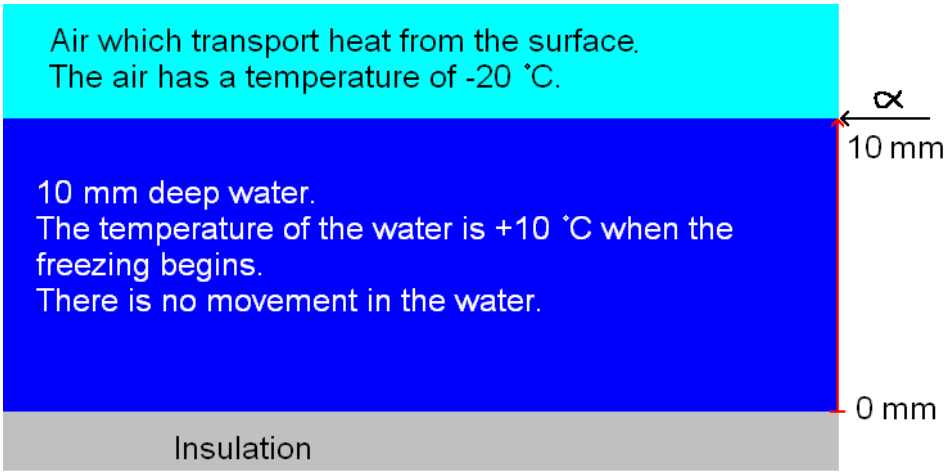

Figure 1.2: Geometry and boundary conditions for the example

Freezing is first cooling down to the temperature when freezing starts. Then there is a period when the object freezes. The temperature in the centre of the object is then almost constant for a long time, because the heat leaving the object is latent heat. At last there is a new period of cooling where the object is cooled below freezing point.

While the object is freezing the thermal properties vary through the object. The premise for introducing Fo and Bi which work so well in cooling are then gone. Fo and Bi can be defined by using average thermal properties for a temperature interval. Then the physical interpretation of Fo and Bi is still valid, but they cannot be used for calculating any temperature inside the object, and it is therefore better to avoid using Fo and Bi in freezing.

The temperature progress in water which freezes is presented as an example of freezing. This is shown in Figure 1.2.

The heat transfer coefficient (α) describes the conductance for heat which leaves the water surface and is taken away by the air. In this simulation α is set to $\alpha = 30\ W/m^2K$ which is a typical value in blast freezing. The thermal properties are those for ice and water. It is assumed that there is no movement in the water. Expansion because of the temperature change is ignored.

In the simulation the heat capacity is infinite during freezing. (1.1) then cannot be discretized directly, but must be formulated in an enthalpy form.

$$\rho \frac{\partial h}{\partial \tau} = \nabla \lambda \left(\nabla T \right) \tag{1.13}$$

In forward Euler form for one dimension, equation (1.13) becomes

$$h_{j,n+1} = h_{j,n} + \lambda \frac{T_{j+1,n} - 2 \cdot T_{j,n} + T_{j-1,n}}{\rho\ dr^2} d\tau \tag{1.14}$$

The temperatures for the next time step must then be calculated from the new enthalpy. This form must be chosen when the heat capacity varies a lot, and it is not sure that the commercial simulation program at hand will do so. The code to solve this problem was written in Matlab. The temperature profile in the water at different times is shown in Figure 1.3.

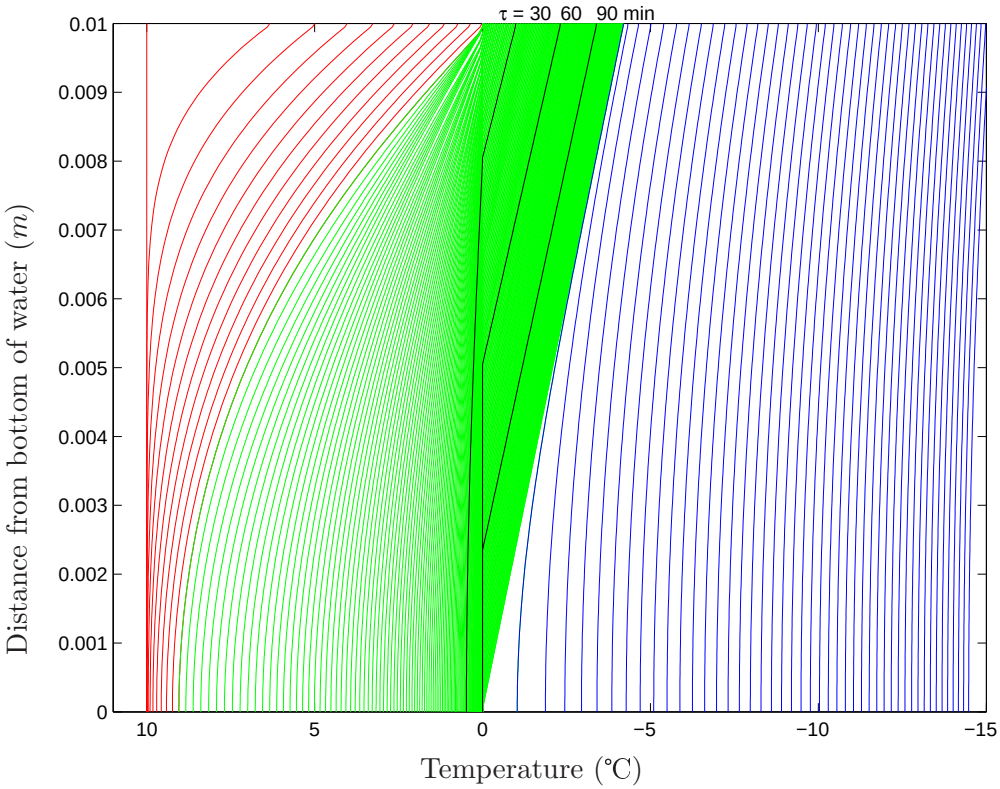

Figure 1.3: Temperatures from simulation of freezing of 10 mm deep water
Temperature profiles at discrete time steps. $\Delta\tau = 20s$

To be consistent with the figure of the system (Figure 1.2) the depth of the water is on the y-axes. There are 20 seconds between each line. Since the temperature is continuously dropping and the temperature axis (x-axis) is reversed the first temperature profile (a red one) is to the left. A later temperature profile is always to the right of an earlier one. In the beginning where the temperature profile lines in Figure 1.3 are red the water is cooling. In this example it takes 4 minutes before freezing starts. Then the temperature changes relatively little for 1 hour and 53 minutes before all the water is frozen. During freezing the lines in Figure 1.3 are green. The colour of the profiles which occur after 30, 60, and

90 minutes are changed from green to black to make the figure more readable. For each of these lines the upper part of the line is below 0 ℃ which indicates that the water has frozen to ice. The lower part of the line is above 0 ℃ which indicates that the water is still liquid. As times passes, a larger and larger part of the temperature profile line is below 0 ℃ indicating that the ice on the top of the water becomes thicker. It is worth noting that when the water is freezing the part of the temperature profile which is below 0 ℃ is almost a straight line. This is because very little heat is transported out of this area compared with the heat transported through it from the level where water freezes, also called the freezing front. The line has a marked knuckle-point (continuous but not derivable) at the freezing front. In the unfrozen water the temperature is close to 0 ℃ everywhere at any time except when freezing has just started. This indicates almost no heat transport in this region. All the heat which is transported through the ice is latent heat released at the freezing front when water freezes to ice. After all the water has frozen it takes 15 minutes before the ice has cooled down below -15 ℃. Here water is freezing 85% of the time from the cooling starts to when the temperature is below -15 ℃. This is typical for freezing of water. The reason is that the latent heat of freezing accounts for more than 80% of the heat which has been removed. Materials with high water content, like food, behave in a similar way.

Because of this behaviour it is possible to describe freezing by an analytical equation by ignoring the sensible heat and assuming that freezing occurs at a fixed temperature. For an infinite slab which freezes from one side the equation can be formulated as

$$\tau = \frac{\rho \Delta h_{ice}}{(T_{ff} - T_A)} \left(\frac{1}{\alpha} L + \frac{1}{2\lambda} L^2 \right) \tag{1.15}$$

This is known as Plank's equation and was first formulated by R. Plank [24, 25]. Cleland and Earle [26] has compared methods for predicting the freezing time of cylindrical and spherical food. In this comparison (1.15) predicts 20 to 40% too short freezing time (read off from the charts in [26]). Equation (1.15) is discussed, modified for several geometries and corrected to include sensible heat by Pham et al. [27, 28, 29], Cleland et al. [26, 30, 31, 32] Hossain [33, 34] and Coskan et al. [35] among others. The simplicity of (1.15) makes it possible to estimate α by measuring the freezing time.

Chapter 2

Thermal multimeter

A description of an instrument for a simultaneous measurement of heat capacity, thermal conductivity and density for food

2.1 Introduction

The physical properties of a material describe how the material will respond to physical influences like tension, pressure, electric field, temperature and light. Physical properties can be strength, flexibility, electric conductivity, thermal conductivity, heat capacity and transparency to light. Physical properties are input to all kinds of engineering. The only way to find the physical properties of unknown materials is to measure them. The results from measurements of all kinds of materials fill engineering handbooks which can be as bulky as extensive encyclopaedia.

Physical properties are arranged according to the kind of physical phenomena they describe. In heat conduction described by the heat equation, (1.1), the physical properties are density ρ, heat capacity c_p, and thermal conductivity λ. Thermal diffusivity a is the ratio $a = \lambda/\rho c_p$, and is used a lot because it will become the only parameter in the heat equation if the thermal conductivity is constant or if thermal conductivity is not a part of the boundary conditions. Some measurement techniques only give thermal diffusivity, and demand an additional measurement of heat capacity to calculate the thermal conductivity. Enthalpy h is the integrated heat capacity with regard to temperature, from a chosen temperature (often -40 ℃ for food materials) to the temperature in the material. The enthalpy is often presented instead of the heat capacity since in an enthalpy - temperature chart fusing heat can be included. Density and heat capacity/enthalpy are properties which

respectively describe the amount of mass and heat in a given volume. They are therefore sometimes denoted as the properties of state. Rahman [36] has written a food properties handbook where the results from several measurements of thermal properties of food are presented.

The number of products and the increasing demand for economical efficiency make quick and accurate methods for finding thermal properties and the heat transfer coefficient increasingly important. If enough measurements are done on a given type of material, some properties of a new material of the same type can often be predicted if the composition of the new materials is known. Today it is common to use such estimates in calculations to save time and money. A reason can be that suitable equipment for measuring the actual property is not available. Comparison of predicted and measured data are also a control that the instrument measures correctly. In chemical analysis of food the amount of protein, fat, carbohydrate, fibre, ashes (salt etc.) and water is measured. The chaep and fast way to find the thermal properties is to estimate them from this chemical composition. The estimation of enthalpy/heat capacity from the composition data using Schwartzberg's model is accurate within 10% (Pham [37]). There are models for estimating thermal conductivity which give satisfying engineering accuracy for homogeneous products (Pham [38]), but since thermal conductivity can be very dependent on the fibre orientation and amount of air in the food, sufficient information is often not available to use these models. Most models for estimating thermal properties from composition demand that the initial freezing point is measured. The models also ignore other phase transitions than the one between water and ice. If composition of the food is not known or a better accuracy then 10% is needed the thermal properties must be measured with a suitable method.

Thermal conductivity/diffusivity describes how heat is transported in the material, and is therefore sometimes denoted as a transport property. A review of measuring and predicting thermal properties of food is written by Lind [39] and Mellor [40]. Results from collaborative measurements which is a part of a European Co-operation in Science and Technology (Cost90) are collected by Jowitt et al. [9] and Kent [41]. In the Cost90 project it was reported that there is as much as $\pm 40\%$ difference in the thermophysical properties for some materials, where 10% was related to the measuring accuracy in one laboratory, $\pm$5-15% was the difference between laboratories and $\pm$4-24% was difference between materials which were assumed to be equal (Hardarson [42]).

2.1.1 Density

The concept of density is known from ancient time. If someone should be credited it must be Archimedes (287-212 BC) with his discovery of buoyancy. The legend says that Archimedes considered why some materials float and some sink. The understanding came to him while he was lying in the bath, probably observing how his body rose and sank in the water while he breathed. The ordinarily sedate Archimedes was so agitated of his discovery that he bounced up from the bath and ran out in the street to tell the passers-by about buoyancy. Density is defined as

$$\rho = \frac{m}{V} \tag{2.1}$$

where m is the mass and V is the volume. For porous materials there can be a question of which volume is to be used. Rahman [36] presents some different definitions of porous density.
True density: is the density of a pure substance or a material calculated from the densities of its components considering conservation of mass and volume.
Substance density: is the density measured when a substance has been thoroughly broken into pieces small enough to guarantee that no pores remain.
Particle density: is the density of a sample which has not been structurally modified, so it will include the volume of all closed pores but not the externally connected porous ones.
Apparent density: is the density of a substance including all pores remaining in the material.
Bulk density: is the density of a material when packed or stacked in bulk.

Density is dependent of temperature and pressure. Sometimes other influences like the magnetic field through the material (terfenol) can also cause a change in density. A change in density because of a change in temperature or pressure is generally so small for solids and liquids that in many cases the change in density can be ignored.

Increased pressure always increases the density. Generally density decreases with increasing temperature and when a substance melts, because of increased molecule movement. One important exception is frozen water melting. Another is water between 0 and 4 ℃. An instrument for measuring density is called a densitometer.

2.1.2 Heat capacity

In 1760, Joseph Black [43, 44] discovered the distinction between temperature and internal energy, and established calorimetry. Calorimetry is a science where the amount of heat gain or release from chemical reactions, biological activity, phase transitions or temperature change is measured. Different methods and measurement equipment have been developed for these purposes. Because of the differences in the nature of the phenomena where calorimetry is used, the property measured varies.

In heat conduction based on Fourier heat equation the property which describes the connection between heat and temperature is heat capacity. Heat capacity is defined as

$$c = \frac{1}{m}\frac{dQ}{dT} \tag{2.2}$$

where dQ is the amount of heat added to an object, dT is the change in temperature in the same object, and m is the mass of the object. The object is assumed to consist of one uniform material. The temperature is also uniform before and after the amount of heat is changed.

Adiabatic methods are generally accepted to give the most accurate result for heat capacity (Magee et al. [5]). These methods are however time consuming if the sample has the size of approximately one cm^3 or larger, but they are the most common methods used on food (Pham [7]). This is because food is not homogeneous. If the sample is too small there is a risk of measuring only one of the materials in the mixture. This will of course not give the average heat capacity. Average heat capacity is usually the one of interest since small scale material variation in food is ignored in most models. Other common methods for measuring heat capacity are differential scanning calorimeters (DSC) and mixing apparatus.

In an adiabatic calorimeter, a known amount of heat, dQ , is added to the sample which is at uniform temperature when the heating starts. After this amount of heat has been supplied, the heating is turned off, and when the temperature is uniform in the whole sample again, the temperature increase, dT, is measured. The total heat capacity is then defined as $C = dQ/dT$. In an actual instrument it is necessary to correct for the heat that is accumulated by the instrument. To satisfy the assumption of adiabatic conditions, no heat must be exchanged with the surroundings. Adiabatic calorimeters are therefore well insulated, and the surrounding temperature is controlled to avoid temperature gradients between the sample container and surroundings. Still according to Pham [7], Riedel [45, 46, 47, 48]

and Flemming [49] have done the most authoritative investigations of food using adiabatic calorimeters. Results from measurements of heat capacity done with different kinds of adiabatic calorimeter are presented by Flemming [49], Pham [7], Lindsay & Lovat [50], Kobashi et al. [51], Tocci et al. [52] and Riedel [46]).

DSCs have a short measuring time compared to adiabatic calorimeters because the sample is so small. The small size of the sample makes it necessary to evaluate in each case if the food is homogeneous enough so that the sample is representative. The DSC is not as accurate as the adiabatic calorimeter. There are two main types of DSCs. In the heat flux DSC the sample and a known reference are placed on a disk. The edge of the disk is in contact with a container of a material with high thermal conductivity. The sample and the reference are positioned symmetrical to each other, so if the sample and the reference are identical and the container is heated or cooled the temperature difference between the sample and the reference are (ideally) zero. See Figure 2.1.

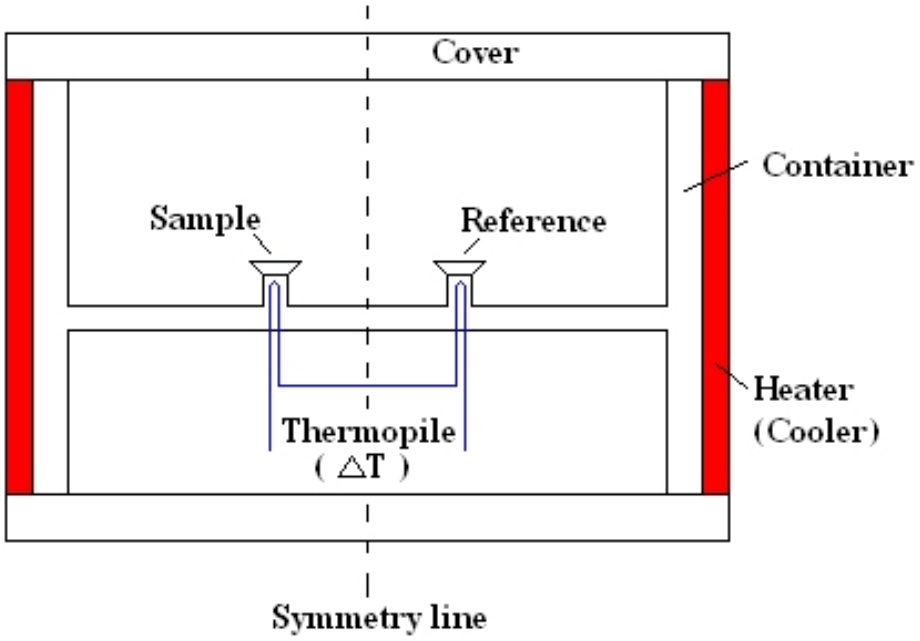

Figure 2.1: Sketch of the principle drawing of a DSC

If the container in the DSC is heated at constant rate and there is a difference in heat capacity (C) between sample and reference there will be a difference in the amount of heat supplied to the sample and the reference. This difference is proportional to the temperature difference between the sample and the reference. The heat flow between the sample and the reference is then given by (2.3)

$$Q_{SR} = (C_{Sample} - C_{reference}) \frac{\partial T}{\partial \tau} \tag{2.3}$$

where $\partial T/\partial \tau$ is the rate which the container is heated. The heat flow between the sample and the reference can also be given by (2.4)

$$Q_{SR} = -K\Delta T_{SR} \tag{2.4}$$

where K is a constant given by the shape and thermal conductivity of the material in the disk, and ΔT_{SR} is the temperature difference between the sample and the reference. Combining (2.3) and (2.4) gives

$$C_{Sample} = C_{reference} - K\frac{\Delta T_{SR}}{\frac{\partial T}{\partial \tau}} \tag{2.5}$$

When calibrating a DSC it is necessary to find K and to correct for any measured ΔT_{SR} when measuring an identical the sample and the reference. If C_{Sample} changes quickly, like in a phase transition, the heat flow between the sample and the reference will not change fast enough so that (2.5) is valid. The enthalpy difference can still be found by integration. The small samples make DSCs especially suitable for finding exact temperature of phase transitions. Other phase transitions than freezing (melting of fat etc.) are from a thermal point of view usually neglible, but can give information about the composition of the food.

An alternative design for DSCs is the power compensated DSC where heat is added electrically to the sample and the reference so the sample and the reference have the same temperature. Here the supplied heat is monitored, and gives the difference in heat capacity between the sample and the reference. This is in principle two small and identical adiabatic calorimeters with equal heat leakage. DSCs are commercially available from several manufacturers and differential scanning calorimetry is a growing field in science. Höhne et al. [53] give a wide descriptions of different types of DSCs. Garti et al. [54], Brill & Gmelin [55], Meuter et al. [56] and Ozilgen & Reid [57] have done measurements with DSC on food.

In a mixing apparatus the sample at one temperature is mixed with a reference (often water) with another temperature. The heat capacity of the sample is then

calculated from the initial and equalizing temperatures, mass of sample, mass of reference, heat capacity of reference, and the heat loss to the container used for mixing. There are several sources of errors, like not correcting for the enthalpy of solutions, or chemical or biological reactions during mixing. The method is simple. Explaining the concept of heat capacity by this method is instructive. Making the mixing apparatus is quick and cheap and can be adapted to almost any shape or size of sample. The experimental time can be long, and the method gives an average heat capacity over a large temperature interval. Hemminger & Höhne [58] have written a comprehensive description of most methods and instruments used to measure heat capacity.

Enthalpy and heat capacity are two of the properties which can be estimated from composition of food as mentioned in Secton 2.1, see also Pham [37, 59, 38] and Choi & Okos [60]. Estimating enthalpy and heat capacity by composition generally gives good accuracy because the structure of the sample has little influence on these properties. Since measurements often give discrete values for different temperatures combining them with theory for estimation of properties from composition gives continuous data, also close to the initial freezing point where enthalpy and heat capacity can be difficult to measure with some measuring methods.

2.1.3 Thermal conductivity

When the difference between heat and temperature was discovered, Fourier defined thermal conductivity in his main work "Théorie analytique de la chaleur" by assuming that

$$\frac{1}{A}\frac{dQ}{d\tau} = \lambda\frac{dT}{dx} \tag{2.6}$$

where dQ is the amount of heat, $d\tau$ is the time difference, A is the area normal to the heat flow, dx is the thickness parallel with the heat flow, dT is the temperature difference over dx and λ is the thermal conductivity. This assumption on how heat is conducted in solid materials was later verified by experiments, and even later explained by the vibrations of molecules.

The heat capacity of a material is the same whether the material is one solid lump or many small pieces. In one solid lump heat can be conducted through the entire cross-section of the material, but if the material is small pieces heat must be conducted from contact point to contact point between the pieces. This makes the thermal conductivity dependent of porosity, orientation of fibres, size and shape of particles etc. Thermal conductivity can also be a directional dependent property because of for instance fibre orientation. A sample must therefore be

defined by more than composition when thermal conductivity is measured. This makes thermal conductivity the most difficult thermal properties to measure, or to estimate from composition data. Again, combining theory with measurement data can be useful.

For food this means that thermal conductivity can alter if the structure of the food is changed due to stirring, impacts etc., or because of chemical changes over time. Ice and water also have thermal conductivity of respectively $2.3W/mK$ and $0.61W/mK$ close to 0 ℃ [61] meaning that the conductivity of the food at one point is dependent on the ratio between ice and water during freezing.

Some methods for measuring thermal conductivity or diffusivity are reviewed by Ohlsson (Chapter 17 in [9]) and Rahman (Chapters 5 and 6 in [36]) The latest review article "Methods for measurement of thermal conductivity and diffusivity of foodstuffs" was written by Nesvadba [6] in 1982! Nesvadba classifies methods for measuring thermal conductivity in steady-state methods and transient methods. The steady-state methods with reference to measurements of food are listed in Table 2.1 from Nesvadba's [6] article.

The most common and most accurate way to measure thermal conductivity is by using plate apparatus (Pham et al. [62, 63], Willix et al. [64]). The weaknesses are that it is a stationary method which only gives thermal conductivity at one temperature. The measured thermal conductivity is an average over a temperature interval. The measuring time is long, and repeated measurements are needed for materials where the thermal conductivity is temperature dependent. The influence of sub-cooling etc. on thermal conductivity cannot be measured.

Transient methods like hot-strip (Gustavsson [65, 66, 67]) or heated probe (Tocci et al. [52]) are also common since they are fast. Buhri & Singh [68] have done measurements on food with a modified DSC. Nesvadba [69] finds thermal conductivity by using the temperature profile in a slab which is heated or cooled. Some of these methods give heat capacity in addition to thermal conductivity. It is possible to measure the influence of sub-cooling etc., but sub cooling can also complicate the interpretation of the measurement. The methods are not as accurate as the plate apparatus. The slow methods seem to be more accurate than the faster ones. Repeated measurements are needed to find temperature dependence.

As mentioned in Section 2.1 it is also possible to calculate thermal conductivity from composition data (Pham [38]).

Table 2.1: steady-state methods of measurement of thermal conductivity of foodstuffs

Method	*Experimental arrangement*	*Foodstuff measured*	*Reference*
Steady-state absolute	Temperature difference across slab sample measured, heat flux estimated from power supplied to electric heater, from rate of sublimation of ice or measured by heat flux meter	Frozen vegetables, fruit, fish and meat	Smith et al., 1952
		Fish and meat	Hatfield, 1953
		Honey	Helvey, 1954
		Fats, meats frozen and unfrozen, heat flow parallel and perpendicular to fibres	Hill et al., 1967
		Freeze-dried beef	Massey and Sunderland 1967
		Freeze-dried mushrooms	Keppeler and Cowart, 1972
		Minced meat	Sörenfors, 1974
	Two slab samples, one on each side of a planar heater (mirror image concept)	Meats, gelatine gels, ice	Lentz, 1961
		Frozen and unfrozen beef, heat flow Parallel to fibres	Miller and Sunderland 1963
	Slab sample guarded, mirror image concept	Burley tobacco	Duncan et al., 1966

Table 2.1 – continued

Method	*Experimental arrangement*	*Foodstuff measured*	*Reference*
Steady-state absolute	Sample filling space between two co-axial cylinders	Dried baby food	Varshney and Ojha, 1974
		Paddy grain and its by-products	Dua and Ojha, 1969
	Co-axial cylinders, guarded	Freeze-dried milk	Gentzler and Schmidt, 1972
		Frozen and unfrozen Fish	Long, 1957
	Concentric spheres	Flour	Köhegyi-Margittai, 1974
Steady state comparative	Slab	Starch granules standard = cardboard	Roth et al., 1970
	Co-axial cylinders	Soybean oil meal, standard = carbon black	Hougen, 1957
	Thermal compactor	Bone	Morley, 1966

According to Nesvadba the advantages of the steady-state methods are the simplicity of the mathematical processing and the high degree of control of experimental variables which is reflected in a high precision in the result.

The disadvantages are;

(1) the long equilibrium period (up to several hours);
(2) the need to prevent heat losses, making the apparatus rather complex;
(3) the difficulty in using Laplace's equation when λ is temperature-dependent in the interval from T_1 to T_2 and T has to be measured at several points;
(4) only λ can be determined (a separate method is required for a or ρc_p determination;
(5) moisture migration can be a problem, due to long measurement times; and
(6) the measurements of liquids poses difficulties due to the onset of convection currents.

Transient methods for measuring thermal conductivity and diffusivity are listed in Table 2.2. The transient methods with reference to measurements on food are listed in Table 2.3. These tables are also from Nesvadba's [6] article.

Table 2.2: Classification of transient methods

Duration of experiment (min)	*Position of heat source with respect to sample*	
	External	*Internal*
<0.01	Heat pulse method	
0.1-10		Heated probe
5-15		Internal heater and a non-integral sensor
10-20	Fitch method	
10-80	External heater and a non-integral sensor	
10-100	Direct use of temperature profiles to identify thermal properties	
10-200	Temperature matching	
40-80	Regular phase methods	

Table 2.3: Transient methods of measurement of thermal properties of foodstuffs

Method	*Experimental arrangement*	*Quantity measured*	*Foodstuff measured*	*Reference*
Heat pulse (analytical solution)	Thin disk sample, theoretically instantaneous heat pulse applied to the front surface, temperature on the rear surface monitored	a	Freeze-dried beef, potatoes, apples	Vacek, 1977
Heater integral with a temperature sensor (heated probe method)	Spherical thermistor bead acting as heater and sensor; power supplied at controlled rate to maintain a a constant temperature rise	a, λ	Glycerol, agar gel, biological materials	Balasubramaniam and Bowman, 1977
	Linear heater in a theoretically infinite sample; constant power supplied to heater	λ	Dairy products	Sweat and Parmalee, 1978
		λ	Fruits and vegetables	Sweat, 1974
		λ	Chicken meat frozen and unfrozen	Sweat and Haugh, 1974 Sweat et al., 1973
		λ	Wheat, butter, margarine	Hooper and Chang, 1953
		λ	Fresh and dry fish	Annamma and Rao, 1974
		λ	Wheat	Jankowski et al., 1977
		λ	Wheat	Chandra and Muir, 1971
		a, λ	Potatoes	Rao et al., 1975
	Cylindrical heater (r = 15 mm), cylindrical annular sample; constant power supplied	a, λ	Wheat with varying moisture content	Serykh and Gergesov, 1976
	Metal strip serving as heater and sensor	λ	Glycerol	Gustafsson et al., 1979
Methods using internal heater and non-integral sensor	Sensors at x = 0, x = 5 mm away from planar heater, sample symmetrically disposed on both sides of heater	a, λ	Agar and sugar dissolved in water (food model)	Badari Narayana and Krishna Murthy, 1975
	Sensors at r = 0, r = 10.7 mm away from linear heater	a, λ	Rapeseed of varying moisture content	Moysey et al.,1977
Methods using external heater and analytical solution of the heat equation	Slab sample, temperature step applied to front surface, temperature on the insulated rear surface monitored	a	A-150 plastic whose thermal properties are equivalent to human tissue	Domen, 1980

Table 2.3: – continued

Method	*Experimental arrangement*	*Quantity measured*	*Foodstuff measured*	*Reference*
	Slab sample subjected to symmetrical step temperature rise on surface, temperature in mid-plane monitored	a	Coffee extract, avocado	Fito et al. 1974
	Temperature on the axis of cylindrical sample monitored after subjecting sample surface to temperature step	a	Spinach puree	Flambert, 1974
Direct use of temperature profiles to identify thermal properties	Slab sample asymmetrically heated; gradient and heat flux calculated from temperatures monitored at four points. λ obtained from the Fourier law	λ	Apples	Häckel, 1973
	Slab sample symmetrically heated; temperature monitored at 20 points. a obtained as ratio of partial derivatives of temperature field	a	Fish, ice, food models	Nesvadba, 1982
Temperature matching method	Temperature in the centre of a potato measured and matched with numerical solution of the heat equation	a	Whole potatoes	Matthews, 1966; Wadsworth and Spadaro, 1969
	Temperature distribution in slab samples matched with analytical solution using univariate function minimization	a	Agar solutions, mashed potatoes, peeled shrimp	Albin et al., 1979
	Temperature on axis of finite cylinder matched with analytical solution using tables	a	Soybean oil meal	Hougen, 1957
Fitch method	Temperature difference measured across a slab sample, heat flux estimated from warming-up of a bath	λ	Grapefruit, oranges Chicken breast muscle and skin	Bennet et al. 1962 Walters and May, 1963
	Temperature difference across slab. heat flux by special sensors	λ, c, H	Citric acid solution	Fedorov and Shubenko, 1975

Table 2.3: – continued

Method	*Experimental arrangement*	*Quantity measured*	*Foodstuff measured*	*Reference*
First method of regular phase (a-calorimeter)	Thermal regime of first kind (sample surface temperature varied stepwise by suddenly immersing the sample in a well-stirred water bath). Temperature monitored at one point in the sample. The slope of the linear portion of graph $\log(T_{bath} - T_{Sample})$ v. time is proportional to thermal diffusivity	a	Fresh and dry fish	Annamma and Rao, 1974
		a	Cod frozen in air and brine	Charm, 1963
		a	Tomato pulp	Bhowmik and Hayakawa, 1979
		a	Cylindrical vegetables	Chuma and Murata, 1969
		a	Beetroot	Movchan and Zhadan, 1968
		a	Meat products	Klein, 1970
		a	16 vegetables	Gegov and Elenkov, 1977
		a	Smoked sausages	Pelejev, 1963
		a	Canned products	Leonhardt and Dusse, 1975
		a	Cherries (individual and in bulk	Parker and Stout, 1967
		a	Tissue of fruits	Gane, 1936
		a	Minced smoked meats	Havliček and Adam, 1970
		a	Black caviar	Stefanovskij et al. 1968
		a	15 foodstuffs	Riedel, 1969
		a	Whole soybeans	Watts and Bilanski, 1973
Second method of regular phase (λ-calorimeter)	Thermal regime of the first kind. Temperature monitored at one interior point of the sample, the standard and the bath	λ	Fish minces and skinless sausages; standard = river sand	Budina and Gromov, 1976
		λ	Frozen sucrose solutions, standard = ice	Keppeler and Boose, 1970
Third method of regular phase (methods of two points	Thermal regime of first kind. Temperature monitored at two points in the sample. The slope and separation of the two $\log T$ v. t graphs yield a	a	Fish minces and skinless sausages	Budina and Gromov, 1976
	Thermal regime of second kind. (Sample surface temperature varied linearly.) Temperature at one surface and one interior point of sample monitored. The slope and separation of the two graphs of T v. t yield a	a	Chicken meat pieces in heavy sauce	Dickerson, 1965
		a	Frozen sucrose solutions	Keppeler and Boose, 1970
	Thermal regime of third kind. (Sample surface temperature varied periodically.) Temperatures monitored at two interior points of sample. The measured attenuation and/or phase shift of temperature oscillations yield a (the principle of Ångström's method (1861))	a	Apples and cherries	Häckel, 1973

In Table 2.3 the Fitch method needs an explanation. Fitch [70] places a thin slab of sample between two heat sinks. The temperature of one heat sink is kept constant. The other sink is heated and then allowed to cool. It is insulated, so the only way heat can leave the sink is through the sample. Since the sample is thin the temperature gradient is approximately constant. The thermal conductivity of the sample can then be calculated from (2.7) where C is the total heat capacity of the insulated sink, Δx is the thickness of the sample and T' is the temperature of the insulated sink. Both $T - T'$ and $\delta T'/\delta\tau$ can be measured by the same thermo-pile.

$$C\frac{\delta T'}{\delta\tau} = \frac{\lambda A\,(T - T')}{\Delta x} \tag{2.7}$$

2.1.4 Short description of the method used in this work

The method used for measurements here is a constant known heat flow added to an otherwise insulated sample and sample container. As will be shown in Section 2.2.3, after some time under these conditions a temperature profile will arise where dT/dr is independent of time. The thermal conductivity of the sample can then be found from the temperature difference between two simultaneous measurements at the top and bottom of the sample. The sample makes a large part of the insulated mass, and therefore the heat capacity can be measured simultaneously with the thermal conductivity by measuring $dT/d\tau$. It is also possible to measure the change in the thickness of the sample and thereby the change in density.

2.1.5 Reasons for the choice of method

The material of interest is food. Food can be corrosive, can be solid, liquid or partially liquid and have a limited shelf life. The sample must therefore be in a container of a material which is resistant, water proof and easily cleaned. The container must protect the rest of the instrument from the sample. The instrument itself must also be solid so it is not damaged if by accident food is spilled inside it. Food is seldom homogeneous so the sample size cannot be too small. Since the thermal properties are highly temperature dependent the method must somehow scan through a temperature interval before the sample decay. Many quick measurements at different temperatures can be a possibility, but the need of a sample of some size makes this difficult because the equilibrium time tends to be long. Both cooling and heating should be available since sub-cooling can be of interest. The sample container must also be designed to handle the relative large volume

change compared to other solid or liquid materials. Since the sample can be messy and difficult to prepare it is desirable that the method measures all the thermal properties simultaneously, and limits the handling of the sample to a minimum. Since the reproducibility of the samples can be limited this is more important than extreme accuracy.

The method for finding thermal properties described here is to expose the sample to a constant heat flux. The heat flux must be small, and the sample must be insulated from the surroundings. Heat capacity is found from the rate of temperature change, and the thermal conductivity is found from a simultaneous measurement of temperature at two points with different distances to the heat source. This method is chosen because by this makes it possible to design an instrument which satisfies all the demands above. No other method does this.

2.2 Materials and methods

This section describes the design of the thermal multimeter first, so the following parts have a visual foundation. The analytical mathematics which is the basis for the method is then described in detail, followed by numerical simulations which show at what heating rates the analytical equations are valid when the thermal properties of the sample are temperature dependent. The accuracy of the analytical equations are then tested against a numerical simulations of the thermal multimeter. It is then described how the instrument is calibrated and how the thermal properties are calculated from the log data.

2.2.1 Design of the thermal multimeter

A complete 3D AutoCAD drawing of the thermal multimeter is available from this thesis download page. Se page 155. Technical drawings of some important parts are in the appendix. Here pictures and computer generated cross-sections with dimensions of important parts are presented. Figure 2.2 is a picture of the whole thermal multimeter except the brine cooler.

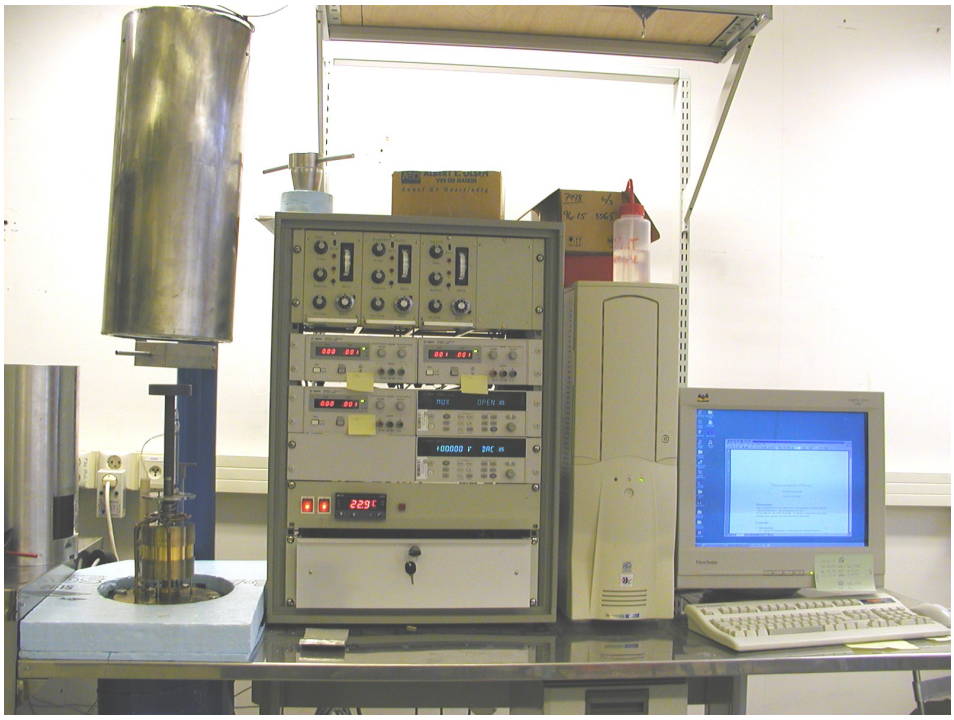

Figure 2.2: Picture of the whole thermal multimeter

Left in the picture is the thermal multimeter when it is open. It is shown closed in Figures 2.3 and 2.4. In the centre is the measuring and controlling hardware and to the right is the PC which is used for controlling, data acquisition and calculations.

Figures 2.3 and 2.4 show the important parts of the thermal multimeter. Note that Figure 2.4 is a close up of Figure 2.3.

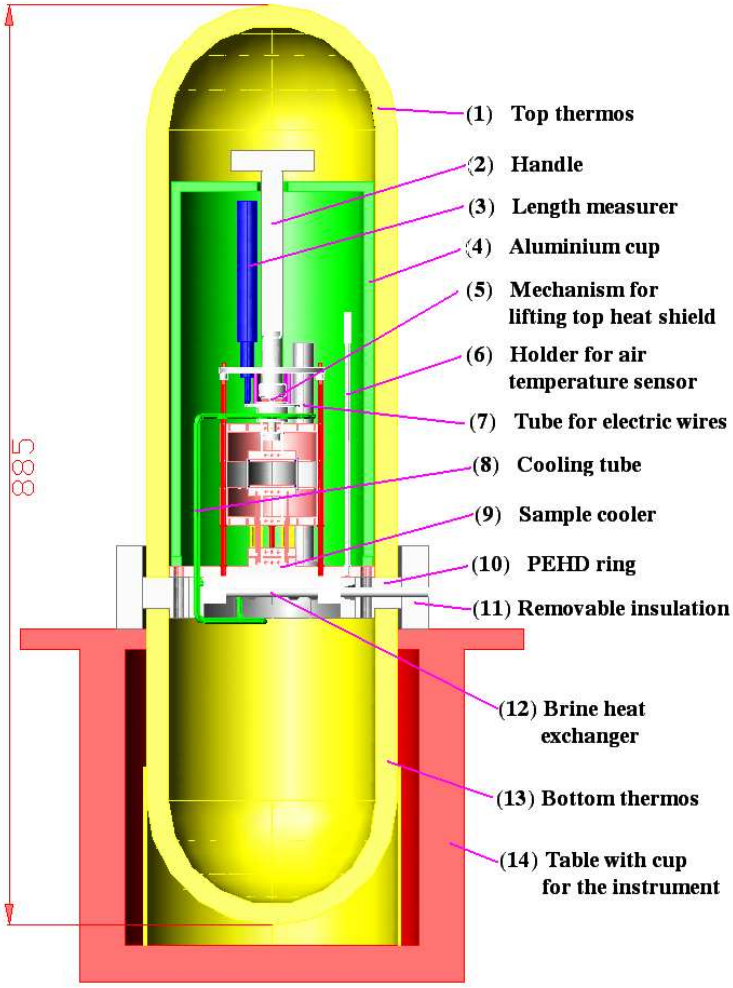

Figure 2.3: Cross-section of the thermal multimeter

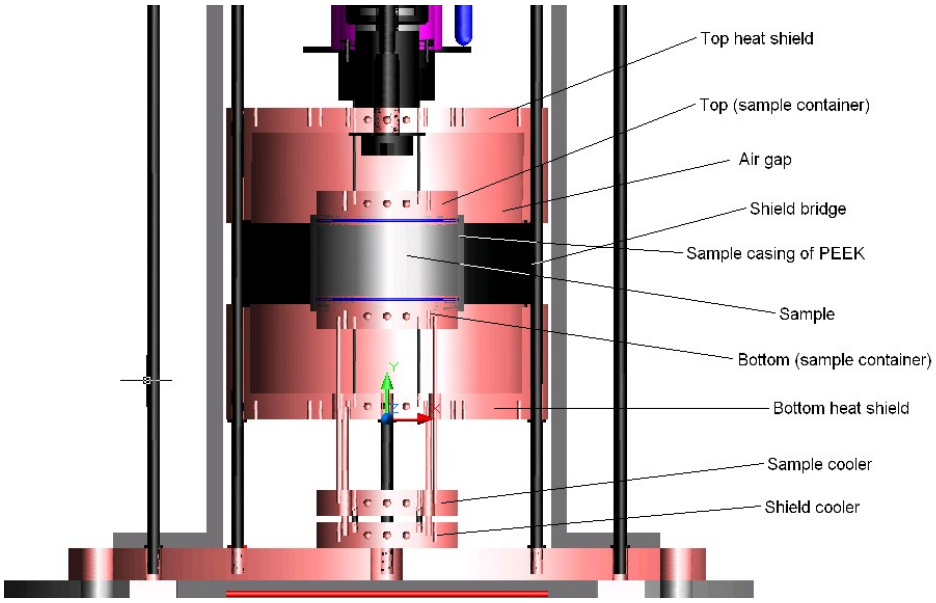

Figure 2.4: Cross-section of the thermal multimeter (Zoom)

Some of the parts in Figure 2.4 are given abbreviations. The abbreviations are often used.

Top heat shield = THS	Top of sample = TS	Sample cooler = SaC
Bottom heat shield = BHS	Bottom of sample = BS	Shield cooler = ShC

Figures 2.5 and 2.6 show the dimensions in Figures 2.3 and 2.4.

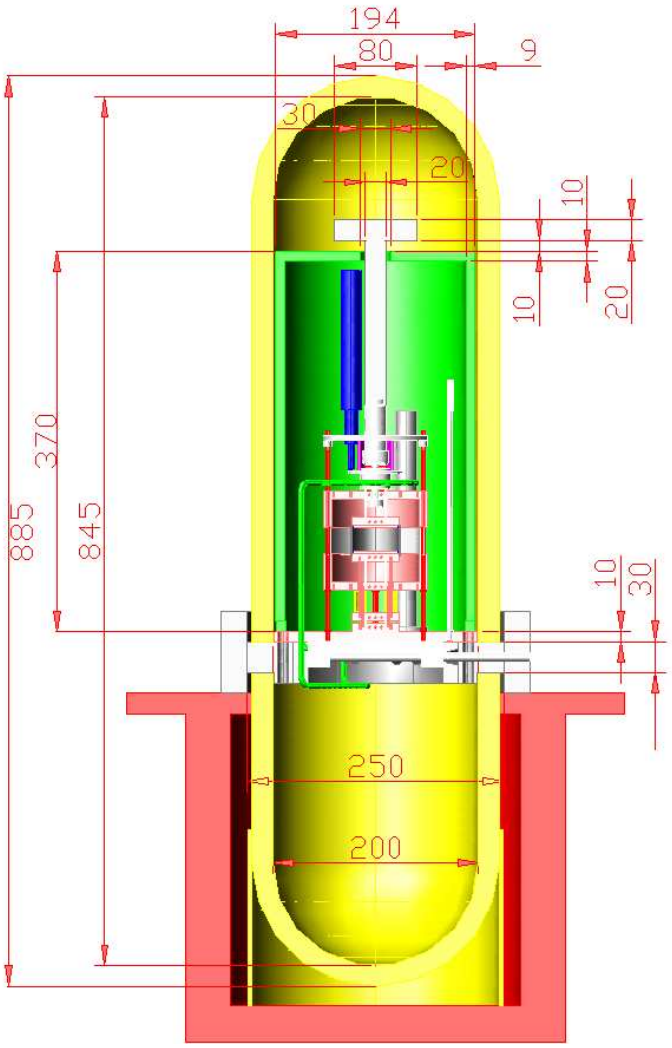

Figure 2.5: Cross-section of the thermal multimeter with dimensions

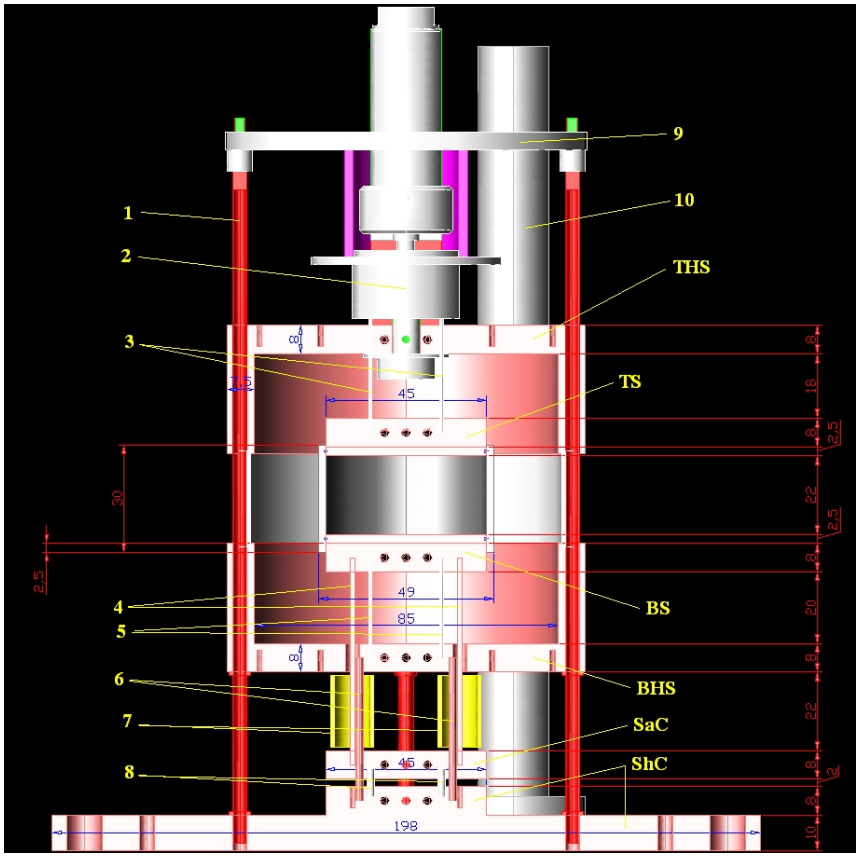

Figure 2.6: Cross-section with dimensions (Zoom)

1	*Steel tubes which hold the instrument together*	*6*	*Copper rods between BHS and ShC*
2	*Device for handling sample expansion*	*7*	*Insulation for 5*
3	*Steel tubes between 2 and TS*	*8*	*Steel rods between SaC and ShC*
4	*Steel tubes between BS and BHS*	*9*	*Support for opening device*
5	*Copper rods between BS and SaC*	*10*	*Tube for electric wires*

Tubes have the primary function to support parts. Rods have the primary function to conduct heat between parts.

Figure 2.7 shows the sample container.

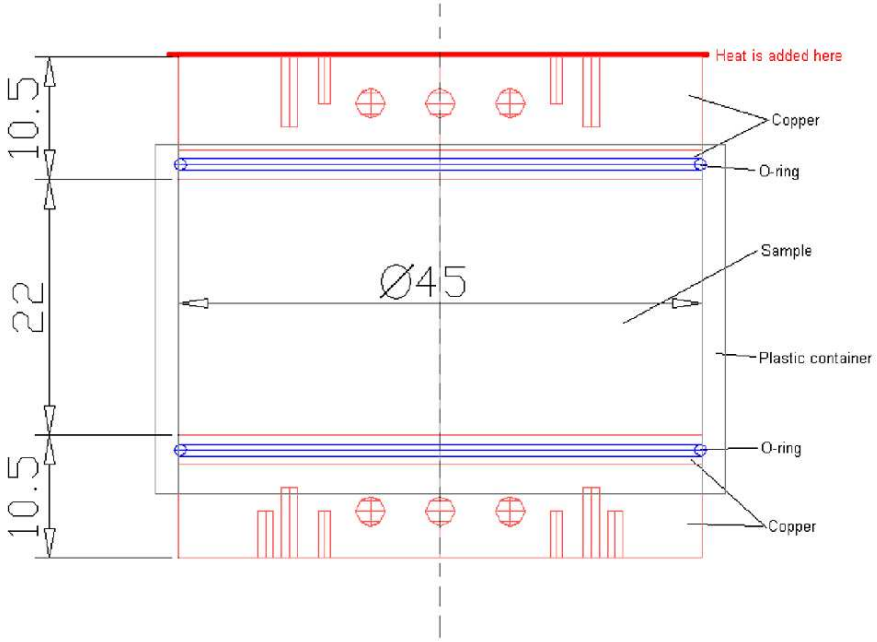

Figure 2.7: Sample container

Except for eight thin tubes of steel and two thin tubes of copper the sample container is surrounded by air which is the insulation between the sample and guard in the thermal multimeter. The two thin tubes of copper are connected to SaC. If SaC is colder than BS the sample is cooled. The heat removed is calculated from the temperature difference. The top copper part of the sample container is TS and the bottom copper part is BS. The parts in the sample container are assembled before each measurement, as shown in Figure 2.8.

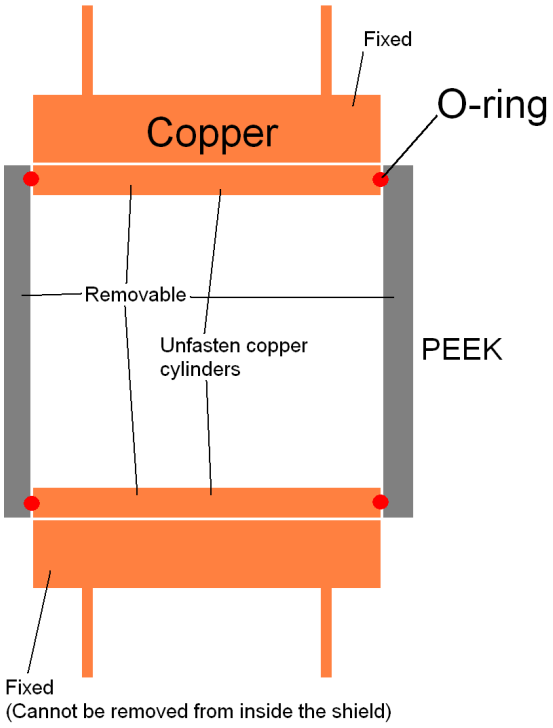

Figure 2.8: A cross-section of the sample container

The fixed parts are included in the sample container since they are a thermal part of it. This means that the top of the sample container consists of two plates.

The top of the sample container consists of two circular plates of copper. The upper of the two plates is fixed to the thermal multimeter, and holds TS-H, TS-Pt100, and the ends of TS-BS-TP and TS-THS-TP. The lower plate follows the sample in and out of the multimeter. It has a slot for an O-ring which closes against the inside PEEK cylinder shell. Together with the topmost cylinder of the bottom of the sample container it will close in a liquid sample. Outside the PEEK cylinder shell there is a cylinder shell of paper coated with leaf gold which is fitted outside the PEEK. The function of this paper is to reduce radiation. The two cylinders are gilded to avoid verdigris and other corrosion. The gilding also ensures good thermal contact between the two plates at the top of the sample container. The

bottom of the sample container is a mirror image of the top. The lowest of the plate hold BS-H, BS-Pt100 and the ends of TS-BS-TP and BS-BHS-TP.

Figure 2.9 shows the brine cooling system which is soldered to SaC. The brine temperature is regulated by a Julabo FP88-HP brine cooler which can regulate the temperature within 0.02 K accuracy.

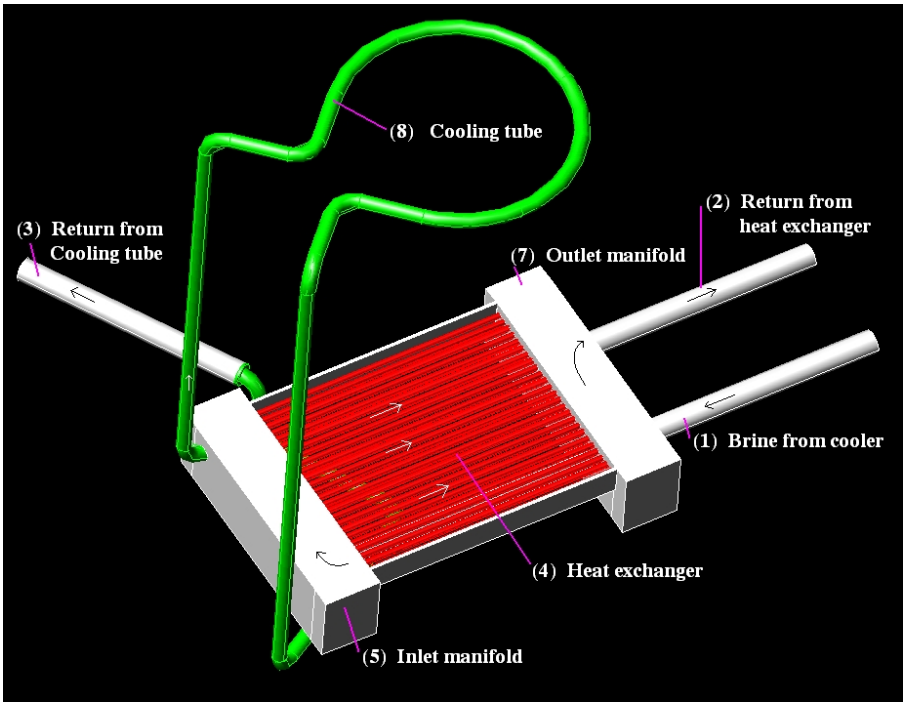

Figure 2.9: Brine heat exchanger

Figure 2.10 is a thermal illustration of the sample, shield and temperature controlling parts (SaC and ShC) in the thermal multimeter.

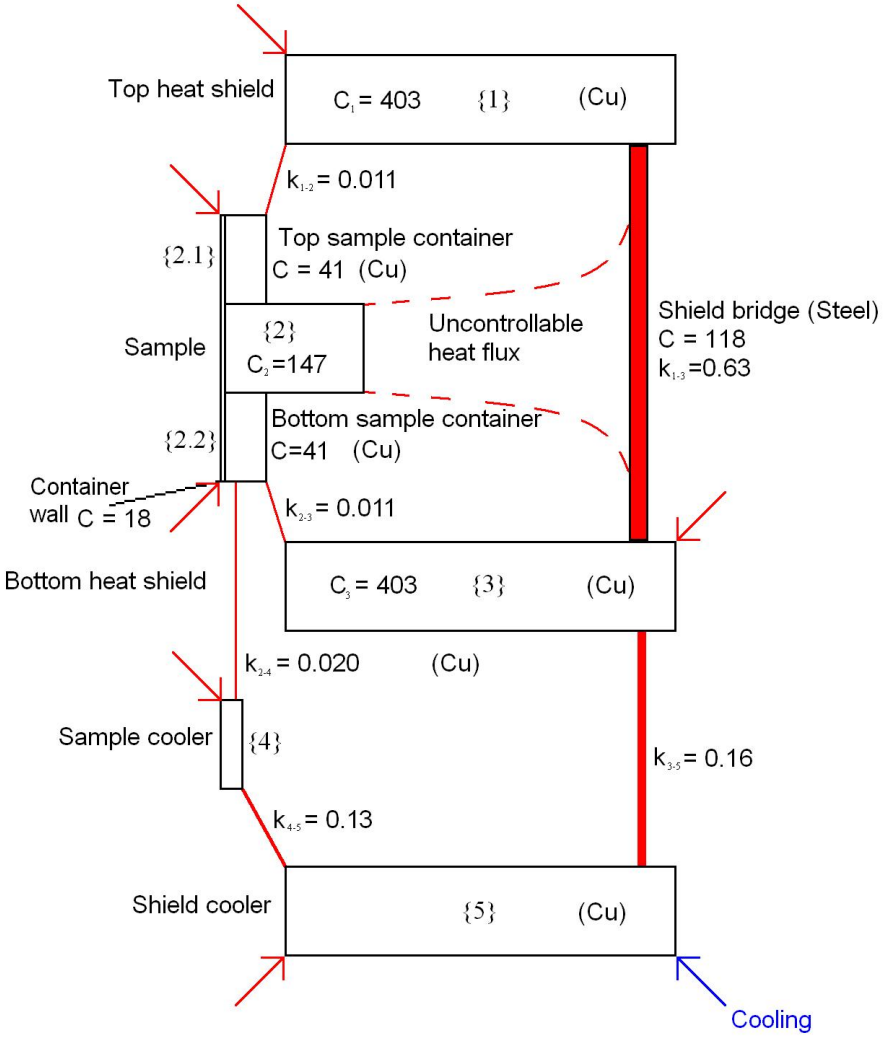

Figure 2.10: Sketch of the principle of the thermal multimeter

The boxes roughly give the heat capacity of each part. The parts are connected by heat bridges. The ability of the bridges to conduct heat is indicated by the red lines. C and k values are used to calculate heat flow between THS, BHS, SaC and ShC in the appendix.

2.2.2 The instrumentation of the thermal multimeter

There are several electric heaters, Pt100 temperature sensors and thermopiles in the instrument. They are denoted according to which part of the thermal multimeter they are connected to. The heater connected to TS is then denoted TS-H, the Pt100 sensor in BS is denoted BS-Pt100 and the thermopile between BS and BHS is denoted BS-BHS-TP. The Pt100 sensors are double. If both platinum wires in the sensor are used for measuring the temperature the wires are denoted Pt100-1 and Pt100-2.

Table 2.4: Sensors and heaters in the thermal multimeter

Sensor	Use
THS-Pt100	Used for safety purpose
TS-Pt100	Measuring accurate temperature in the top of the sample
BS-Pt100-1	Measuring accurate temperature in the bottom of the sample
BS-Pt100-2	Controlling the brine cooler
SaC-Pt100	Measuring accurate temperature in the sample cooler
SaC-Pt100	Measuring temperature in the shield cooler
Air-Pt100	Measuring the air temperature outside the shield
TS-THS-TP	Controlling THS temperature
TS-BS-TP	Accurate measurement of temperature difference between TS and BS
BS-BHS-TP	Controlling BHS temperature
BHS-SaC-TP	Controlling SaC temperature
Air-TE	Thermoelement. Measuring temperature outside the thermal multimeter
THS-H	Controlling THS temperature
TS-H	Heating of sample
BS-H	Used for calibration purpose
BHS-H	Controlling BHS temperature
SaC-H	Controlling SaC temperature

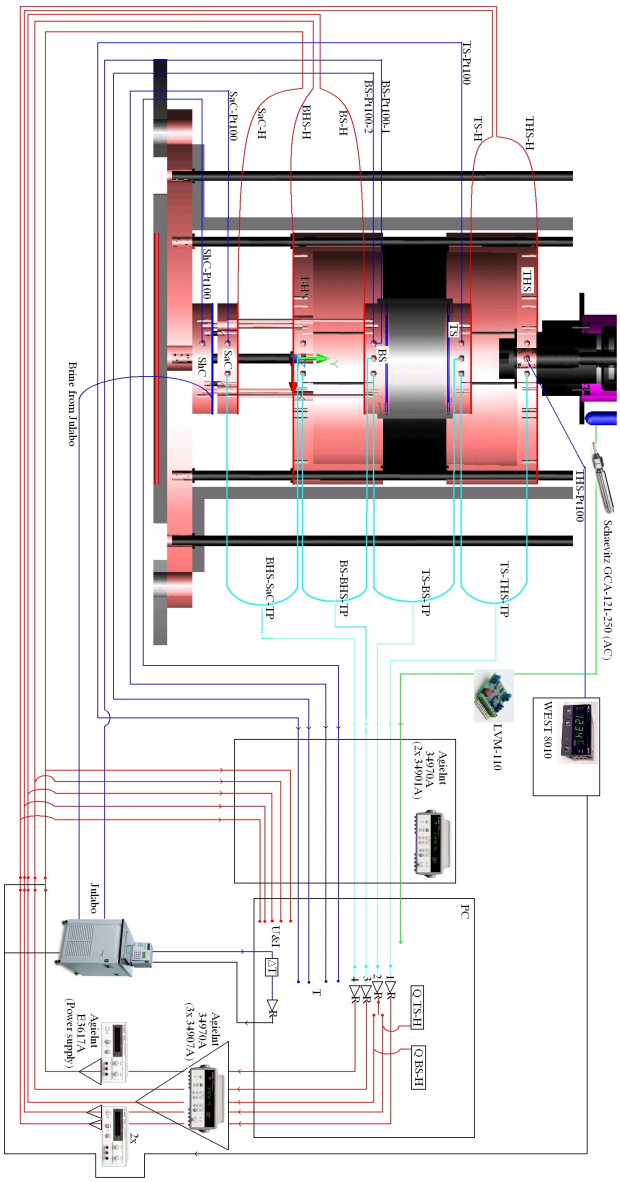

Figure 2.11: Logging and control system

Figure 2.11 shows the signal exchange in the thermal multimeter. The core in the system is two Agilent 34970A data switch units which communicate with a PC through RS-232. Signals from thermopiles, thermoelement, Pt100 elements and the LMV-110 AC/DC converter to the Schaevitz GCA-121-250 position sensor are measured by two 34901A 20 channel multiplexer (2/4-wire) modules in one 34970A unit. These signals are sent to the PC every 15 seconds where they are received by a Lab view data program. The signals from Pt100 Sensors are transferred as temperatures (indicated by T on the figure). Other signals are voltage signals. They are converted to the temperature difference, voltage, current, power and length by the program in real time if necessary or by a post processing program if not.

There are two signals which do not go through the 34970A units to the PC. That is the signal from and to the Julabo brine cooler. The brine cooler measures the temperature from the BS-Pt100-2 sensor which is sent to the PC, and the PC sets the temperature in the brine cooler bath. Because of the tubes for brine which transport heat from the thermal multimeter to the cooler, the temperature in the brine cooler bath is not the same as the temperature measured by the BS-Pt100-2 sensor. The manipulated variable from the cooler in the figure is the temperature in the brine pumped into the tubes.

The program stores data and sends signals to the other 34970A with three 34907A multifunction modules which can deliver up to 12V DC. The 34907A modules are used to power the heaters. THS, BHS and SaC requires more than 12 W so the signals are amplified by three Agilent E3617A power supplies which can deliver up to 60V. The program also sets the temperature in the brine cooler bath.

Five PID regulators for the heaters and the Julabo brine cooler are emulated in software, but they are not all used during a measurement. The regulator which can regulate the temperature in TS after BS or the other way round is only used for calibration purposes. Through a normal measurement the heat (Q TS-H and Q BS-H in the figure) to TS and BS is preset. This is indicated by a relay inside the PC. The regulator for the brine cooler controls the temperature in the bath so the difference (ΔT in the figure) between BS and ShC is a constant preset value. The bath absolute temperature can also be preset. The regulator for the SaC can also be programmed so there is a constant temperature difference between BS and SaC. (This facility is not used yet, and is therefore not indicated on the figure.)

The WEST 8010 1/8 DIN Panel Indicator measures the temperature in the THS-Pt100 sensor. It the temperature goes above the preset value the WEST 8010 unit sends a signal which cuts the power to the heaters and turns off the cooler. This is a safety feature which works independently of the PC. The voltage and current measurements are done with a measuring bridge as shown in Figure 2.12.

The heat supplied to the heaters is measured with a measuring bridge.

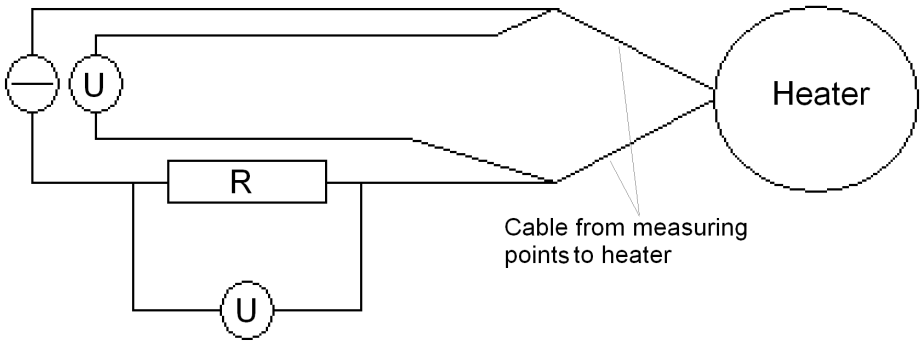

Figure 2.12: Measuring bridge for heaters

2.2.3 Mathematical description of method

The measuring method is based on the analytical solution for a single homogeneous rod of sample which is heated on one side and insulated elsewhere. To build a practical instrument the sample must be encapsulated in a sample container.

The analytical solution for such a rod is presented in this section. This solution is then extended to include a three-sectional rod accounting for the top and bottom of the sample container. It is also shown how heat capacity and thermal conductivity can be calculated if only the temperature is known as a function of time at top and bottom of the sample. In the end the unwanted heat flow around the sample is discussed. Terms to correct for this heat flow are included in the analytical equations.

Problem description for a single homogeneous rod

Mathematically, a single rod of homogeneous material with *temperature independent thermal properties* which is heated from one side and insulated elsewhere, is described by the one-dimensional Fourier heat equation

$$\rho c_p \frac{\partial T}{\partial \tau} = \lambda \frac{\partial^2 T}{\partial r^2} \tag{2.8}$$

and the boundary condition

$$\begin{aligned} \frac{\partial T(0,\tau)}{\partial r} &= -\frac{\dot{q}_0}{\lambda} \\ \frac{\partial T(L,\tau)}{\partial r} &= 0 \end{aligned} \tag{2.9}$$

An initial condition is uniform temperature described by

$$T(r,0) = T_0 \qquad r \in [0,L] \tag{2.10}$$

Figure 2.13 shows the problem. A solution of the problem was presented by Myers [71].

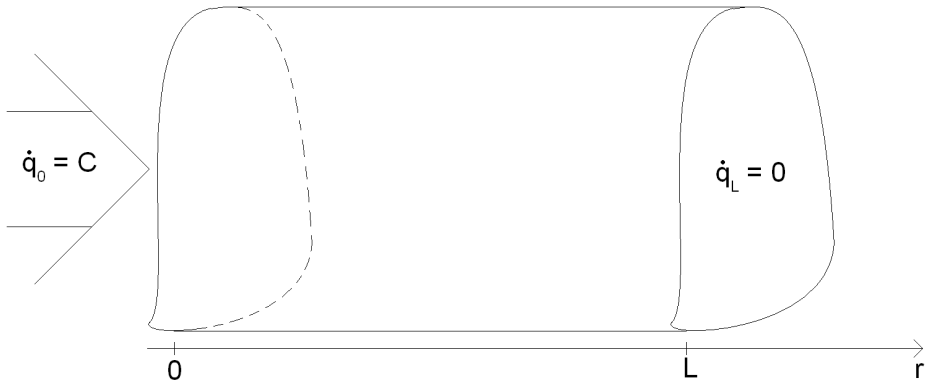

Figure 2.13: Heating from one side of a homogeneous insulated rod

General solution of the heat equation for single homogeneous rod

A general solution of (2.8) can be obtained by separation of variables. Using the product method $T(r,\tau)$ can be separated into two functions, where one is a function of time and the other of position. Myers uses the general solution to solve the problem by the variation in parameters. However, the solution is obtainable in a more direct way by assuming that when heat is added at a constant rate, and at the same place, to two or more substances with constant thermal properties which

are insulated from the surroundings, then the temperature profile will be

$$T\left(\vec{r},\tau+\Delta\tau\right)=T\left(\vec{r},\tau\right)+\frac{\dot{Q}}{C}\Delta\tau \qquad C=\sum_{\mathrm{i}=1}^{\mathrm{n}} m_i c_{p\,i} \tag{2.11}$$

as time goes towards infinity. Equation (2.11) is valid for all $\vec{r}$ inside the boundary and all $\Delta\tau$. C is the total heat capacity of the insulated volume, in this case between 0 and L in Figure 2.13, where heat is generated or added at a constant rate. Equation (2.11) claims that when τ approaches infinite the temperature rise at every point is equal to the average temperature rise.

The assumption is sensible since there is no reason that any kind of oscillation should be introduced to the system when the temperature rises. It is also in agreement with first and second laws of thermodynamics, and gives results which are solutions to the heat equation with given boundary conditions. The assumption in (2.11) is presented because it is a necessary tool to solve the same kind of problems when several rods of different materials are connected.

For this problem (2.11) can be rewritten as

$$\frac{\partial T\left(r,\tau\right)}{\partial\tau}=\frac{\dot{q}_0}{\rho c_p L} \tag{2.12}$$

If (2.11) is true, the constant heat profile $T\left(\vec{r}\right)$ must have a shape so that every part of the rod gets the amount of heat which causes $\partial T/\partial\tau$ to be constant everywhere. In this case

$$\lambda\frac{\partial T\left(r,\tau\right)}{\partial r}=\dot{q}_0\frac{r-L}{L} \tag{2.13}$$

Equation (2.13) is no more than a heat balance for every part of the rod. Equations (2.12) and (2.13) are first order linear equations which can easily be solved. It is further easy to show that the sum of the solutions of (2.12) and (2.13) satisfy Fourier heat equation, (2.8), with the actual boundary conditions described in (2.9).

The complete solution of the problem described in Figure 2.13 is according to Myer

$$\begin{aligned} T\left(r,\tau\right)=\dot{q}_0\Bigg[&\frac{1}{\lambda}\left(\frac{r^2}{2L}-r\right)+\frac{1}{\rho c_p L}\tau+\frac{1}{3}\frac{L}{\lambda}\\ &-\frac{L}{\lambda}\frac{2}{\pi^2}\sum_{n=1}^{\infty}\frac{1}{n^2}\cos\left(\frac{n\pi r}{L}\right)e^{-\left(\frac{n\pi}{L}\right)^2\frac{\lambda}{\rho c_p}\tau}\Bigg]+T_0 \end{aligned} \tag{2.14}$$

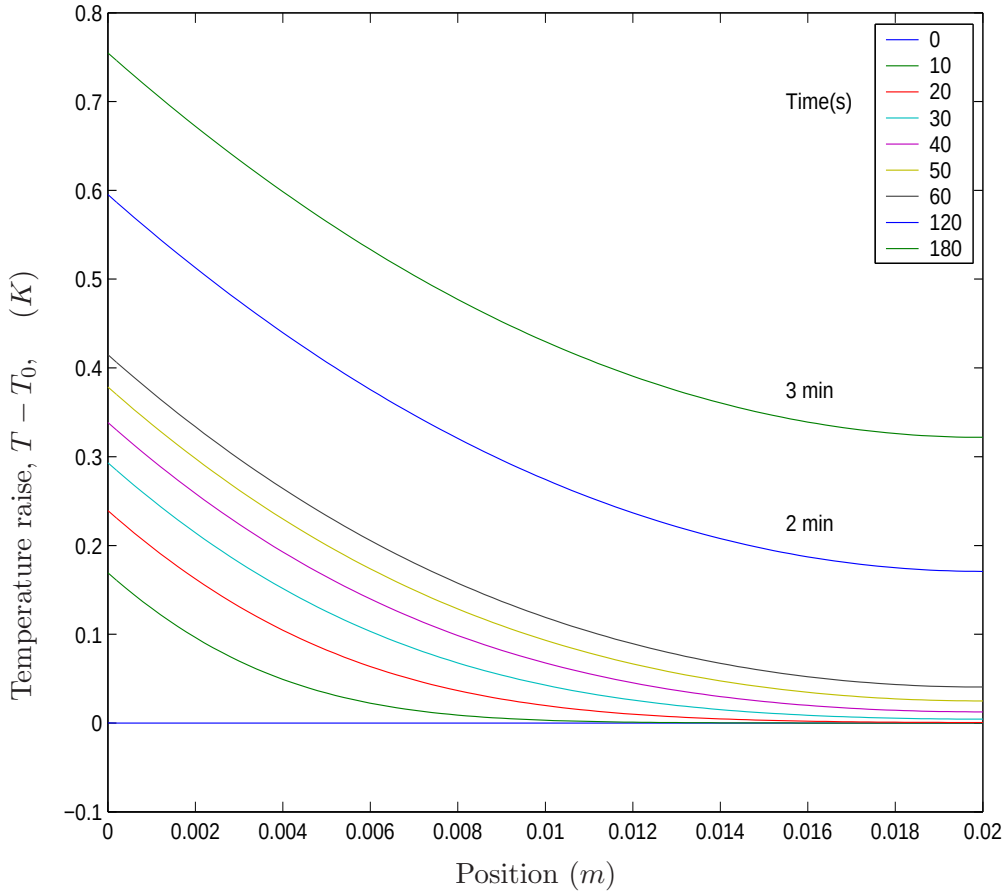

Figure 2.14: Temperature as the function of time and position

Equation (2.14) is plotted in this figure. The time for each line is given by the legend in the top right-hand corner of the figure. The first line is on the r-axis ($T = 0$). The chart shows how the temperature will rise in a material with thermal properties independent of the temperature. As input to (2.14) $L = 20\ mm$, $\dot{q} = 100\ W/m^2$ and the thermal properties of ice at 0 ℃ are used. The sum of the infinite series in (2.14) is approximated with the first 1000 terms.

It can be seen from Figure 2.14 that after some time the temperature profile does not change shape. It is only displaced parallel to the position-axis. As shown in Section 2.2.3 this behaviour makes it possible to calculate heat capacity from the temperature rise as a function of time and thermal conductivity as function of the temperature difference over the slab.

Finding thermal properties from measurements

It is assumed that it is possible to construct an instrument that can expose a sample to the boundary condition in (2.9). If the sample has constant but unknown thermal properties, the properties can be estimated by measuring the temperature at the boundaries.

As long as the thermal properties are constant the negative exponent causes the series in (2.14) to approach 0 when τ becomes large. With another initial condition than (2.10) the series will be different, but any series which describe an initial condition, will approach 0 when time goes to infinity. After some time

$$T(r,\tau) = \dot{q}_0 \left[\frac{1}{\lambda} \left(\frac{r^2}{2L} - r \right) + \frac{1}{\rho c_p L} \tau + \frac{1}{3} \frac{L}{\lambda} \right] + T_0 \tag{2.15}$$

will give a good approximation to the temperature profile. *Note that (2.15) is a specially case of (2.11).* If $T(0,\tau)$ and $T(L,\tau)$ are known and the thermal properties are unknown, a subtraction of $T(0,\tau) - T(L,\tau)$ gives a formula for estimating thermal conductivity. $\bar{T}$ is defined in (2.19).

$$\lambda\left(\bar{T}\right) = \frac{L}{2} \frac{\dot{q}_0}{(T(0,\tau) - T(L,\tau))} \tag{2.16}$$

If $T(0,\tau)$, $T(L,\tau)$, $T(0,\tau+\Delta\tau)$ and $T(L,\tau+\Delta\tau)$ are known a subtraction of $T(0,\tau+\Delta\tau) + T(L,\tau+\Delta\tau) - T(0,\tau) - T(L,\tau)$ gives a formula for estimating heat capacity. $\hat{T}$ is defined in (2.20)

$$c\left(\hat{T}\right) = \frac{2\dot{q}_0}{\left(T(0,\tau+\Delta\tau) + T(L,\tau+\Delta\tau) - T(0,\tau) - T(L,\tau)\right)\rho L} \Delta\tau \tag{2.17}$$

(The average of the two temperatures on the edges is used.)

These formulas for estimating heat capacity and thermal conductivity are only valid if the "series terms" in (2.14) has time to fade out. A criterion for how long time is needed can be found by assuming that the absolute value of $\frac{1}{\lambda}\left(\frac{r^2}{2L} - r\right)$

must be much smaller than $-\frac{1}{\lambda}\frac{2}{L}\left(\frac{L}{\pi}\right)^2\cos\left(\frac{\pi r}{L}\right)e^{-\left(\frac{\pi}{L}\right)^2\frac{\lambda}{\rho c_p}\tau}$ which is the term in the series that disappears last. $\left|\frac{1}{\lambda}\left(\frac{r^2}{2L}-r\right)\right|$ is largest when $r=L$ so the comparison takes place here.

$$\left|\frac{1}{\lambda}\left(\frac{L^2}{2L}-L\right)\right| >> \left|-\frac{1}{\lambda}\frac{2}{L}\left(\frac{L}{\pi}\right)^2\cos\frac{\pi L}{L}e^{-\left(\frac{\pi}{L}\right)^2\frac{\lambda}{\rho c_p}\tau}\right|$$

$$\frac{\pi^2}{4} >> e^{-\left(\frac{\pi}{L}\right)^2\frac{\lambda}{\rho c_p}\tau}$$

$$\tau <= -\ln\left(\frac{\pi^2}{4}\cdot 0.01\right)\frac{\rho c_p L^2}{\lambda\pi^2} \tag{2.18}$$

τ in (2.18) is time from $T(r,0)=T_0$ to the difference between (2.14) and (2.15) which is less than 1%. When (2.18) is true, the error in the estimate of heat capacity and thermal conductivity by (2.16) and (2.17) is also smaller than 1%. (2.18) gives an absolute worst estimate of the equilibrium time. The heat flux is not a part of (2.18). This is the basis for the discussion in Section 2.2.4.

Mean temperature in the sample under adiabatic boundary conditions

If the heating to the rod is suddenly turned off, the whole sample will reach the same temperature after a while. This temperature is found by the integral

$$\bar{T}(\tau) = T(L,\tau) - \frac{\int_0^L \frac{\dot{q}_0}{\lambda}\left(\frac{r^2}{2L}-r\right)dr}{L} = T(L,\tau)+\frac{\dot{q}_0 L}{3\lambda} \tag{2.19}$$

It seems right to use this temperature for which the thermal conductivity is calculated in (2.16). Another possibility is a simple mean. The choice of method for calculating this temperature can be important when the method is used on materials with temperature dependent on thermal properties. Similarly the temperature calculated by

$$\hat{T} = \frac{\bar{T}(\tau)+\bar{T}(\tau+\Delta\tau)}{2} \tag{2.20}$$

is likely to be the correct temperature for which the heat capacity is calculated in (2.17). Note that (2.20) is defined by the terms of (2.19).

Analytical solution for a three-layer rod

Food can be liquid or produce liquid. To measure the thermal properties by the method described, the food sample has to be placed in a container. In the thermal multimeter the sample container is as shown in Figure 2.7. If the plastic (PEEK, PTFE) container is thin walled and thermal conductivity and heat capacity is low, the error in ignoring it is small. It is also possible to adjust for the error as shown later in this section.

We then have a three-layer rod, where the temperature history has an analytical solution of the problem described by Figure 2.15 and (2.21), (2.22) and (2.23).

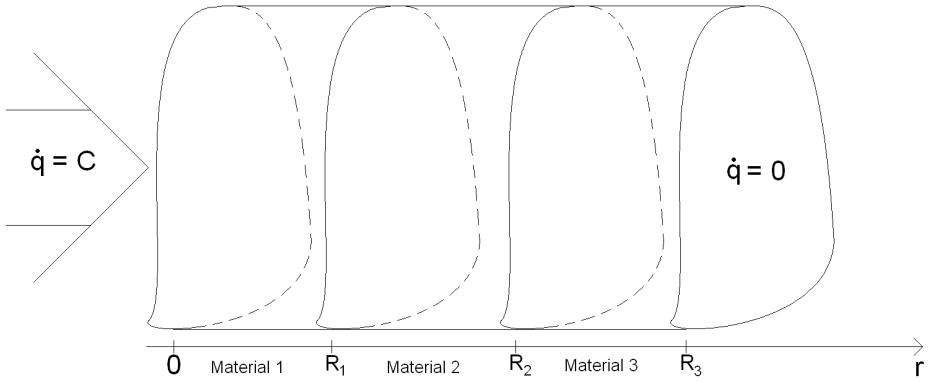

Figure 2.15: Heating of three-layer insulated rod

The rod is insulated on all sides except for the cross-section at $r = 0$ where the heat flux is constant. The set of equation to be solved is the one-dimensional Fourier heat equation for a three-layer rod

$$\frac{\partial T_n}{\partial \tau} = \left(\frac{\lambda}{\rho c_p}\right)_n \frac{\partial^2 T_n}{\partial r^2} \quad , \quad n \in \{1, 2, 3\} \tag{2.21}$$

with boundary conditions

$$\begin{array}{lllll} Material\ 1: & n=1 & r\in[0,R_1] & \frac{\partial T_1(0,\tau)}{\partial r}=-\frac{\dot{q}}{\lambda} \\ & & & T_1(R_1,\tau)=T_2(R_1,\tau) \\ Material\ 2: & n=2 & r\in[R_1,R_2] & T_1(R_1,\tau)=T_2(R_1,\tau) \\ & & & T_2(R_2,\tau)=T_3(R_2,\tau) \\ Material\ 3: & n=3 & r\in[R_2,R_3] & T_2(R_2,\tau)=T_3(R_2,\tau) \\ & & & \frac{\partial T_3(R_3,\tau)}{\partial r}=0 \end{array} \tag{2.22}$$

and initial conditions

$$T(r,0)=T_0 \qquad r\in[0,R_3] \tag{2.23}$$

Assuming (2.11) is true it can be rewritten as

$$\frac{\partial T(r,\tau)}{\partial \tau}=\frac{\dot{q}}{\rho_1 c1 R_1+\rho_2 c_2(R_2-R_1)+\rho_3 c_3(R_3-R_2)} \tag{2.24}$$

Again if (2.11) is true the constant heat profile $T(\vec{r})$ must have a shape so every part of the rod gets the amount of heat which causes $\partial T/\partial\tau$ to be constant everywhere. In this case if C_1,C_2,C_3 and C_{SaC}, are defined as in (2.25), (2.26) gives an expression for $\partial T/\partial r$.

$$\begin{array}{l} C_1=\rho_1 c_1 R_1 \\ C_2=\rho_2 c_2(R_2-R_1) \\ C_3=\rho_3 c_3(R_3-R_2) \\ C_{SaC}=C_1+C_2+C_3=\rho_1 c_1 R_1+\rho_2 c_2(R_2-R_1)+\rho_3 c_3(R_3-R_2) \end{array} \tag{2.25}$$

$$\begin{array}{lll} r\in[0,R_1] & -\lambda_1\frac{\partial T_1(r,\tau)}{\partial r}=\dot{q}\frac{\rho_1 c_1(R_1-r)+C_2+C_3}{C_{SaC}} \\ r\in[R_1,R_2] & -\lambda_2\frac{\partial T_2(r,\tau)}{\partial r}=\dot{q}\frac{\rho_2 c_2(R_2-r)+C_3}{C_{SaC}} \\ r\in[R_2,R_3] & -\lambda_3\frac{\partial T_3(r,\tau)}{\partial r}=\dot{q}\frac{\rho_3 c_3(R_3-r)}{C_{SaC}} \end{array} \tag{2.26}$$

(2.24) and (2.26) are then integrated and grouped, and the integration constants

are adjusted so the boundary condition is satisfied.

$$\begin{aligned}
T_1(r,\tau) &= \tfrac{\dot{q}}{C_{SaC}}\left\{-\tfrac{r}{\lambda_1}\left[\rho_1 c_1\left(R_1-\tfrac{r}{2}\right)+C_2+C_3\right]+\tau\right\}\\
T_2(r,\tau) &= \tfrac{\dot{q}}{C_{SaC}}\left\{-\tfrac{r}{\lambda_2}\left[\rho_2 c_2\left(R_2-\tfrac{r}{2}\right)+C_3\right]+\tau+\right.\\
&\left.\tfrac{R_1}{\lambda_2}\left[\rho_2 c_2\left(R_2-\tfrac{R_1}{2}\right)+C_3\right]-\tfrac{R_1}{\lambda_1}\left[\rho_1 c_1\tfrac{R_1}{2}+C_2+C_3\right]\right\}\\
T_3(r,\tau) &= \tfrac{\dot{q}}{C_{SaC}}\left\{-\tfrac{r}{\lambda_3}\rho_3 c_3\left(R_3-\tfrac{r}{2}\right)+\tau+\right.\\
&\tfrac{R_2}{\lambda_3}\rho_3 c_3\left(R_3-\tfrac{R_2}{2}\right)+\tfrac{R_2}{\lambda_2}\left[\rho_2 c_2\tfrac{R_2}{2}+C_3\right]+\\
&\left.\tfrac{R_1}{\lambda_2}\left[\rho_2 c_2\left(R_2-\tfrac{R_1}{2}\right)+C_3\right]+\tfrac{R_1}{\lambda_1}\left[\rho_1 c_1\tfrac{R_1}{2}+C_2+C_3\right]\right\}
\end{aligned} \tag{2.27}$$

(2.27) satisfies the heat equation and the boundary conditions. It does not satisfy the initial condition but the discussion in Sections 2.2.3 and 2.2.4 show that this is not important.

If the thermal conductivity material for 1 and 3 is very high compared with material 2, the equation set can be simplified to:

$$\begin{aligned}
T_1(r,\tau) &= T_2(R_1,\tau)\\
T_2(r,\tau) &= \tfrac{\dot{q}}{C_{SaC}}\left\{-\tfrac{r}{\lambda_2}\left[\rho_2 c_2\left(R_2-\tfrac{r}{2}\right)+C_3\right]+\right.\\
&\left.\tau+\tfrac{R_1}{\lambda_2}\left[\rho_2 c_2\left(R_2-\tfrac{R_1}{2}\right)+C_3\right]\right\}\\
T_3(r,\tau) &= T_2(R_2,\tau)
\end{aligned} \tag{2.28}$$

From (2.28) equations for the heat capacity and thermal conductivity of material 2, which would be the sample in a real instrument can be found, when the temperature is known.

$$c_2\left(\hat{T}\right) = \frac{\dot{q}\frac{2\Delta\tau}{T_2(R_1,\tau+\Delta\tau)+T_2(R_2,\tau+\Delta\tau)-T_2(R_1,\tau)-T_2(R_2,\tau)}-(C_1+C_3)}{\rho_2\left(R_2-R_1\right)} \tag{2.29}$$

$$\lambda_2 = \frac{\dot{q}\left(R_2-R_1\right)}{T_2\left(R_1,\tau\right)-T_2\left(R_2,\tau\right)}\cdot\frac{\frac{1}{2}C_2+C_3}{C_{SaC}} \tag{2.30}$$

(2.29) can also be deduced directly from the assumption in (2.27). Mark that C_1 to C_3 and C_{SaC} are still defined by (2.25) with unit $J/(m^2 kgK)$, but since they

are collected in one fraction they can be replaced by measured heat capacity with unit J/K of parts 1, 2 and 3 in Figure 2.15. Heat can be supplied anywhere in material 1 in Figure 2.15 because the thermal conductivity of this material is very high.

Adaptation of solution to a practical instrument

In a real instrument there must be a casing around the sample as shown in Figure 2.7. Some heat will also flow in the air surrounding the sample casing. It is unlikely that there will be perfect thermal contact between TS, the sample and BS, but this contact cannot be too poor if the instrument is to be suitable for measuring thermal conductivity, since heat is supplied to TS and the temperature is measured in TS and BS. It is now discussed how (2.29) and (2.30) can be modified to take this into consideration.

The heat capacity of the instrument can be measured by making a measurement on a known sample. The heat capacity of the whole container without the sample is then found by subtraction. This value will then be used to correct (2.29) to

$$c_{Sa} = c_2 = \frac{\dot{Q}\frac{2\Delta\tau}{T_2(R_1,\tau+\Delta\tau)+T_2(R_2,\tau+\Delta\tau)-T_2(R_1,\tau)-T_2(R_2,\tau)} - C_C}{\rho_2 \left(R_2 - R_1\right) A_{Sa}} \tag{2.31}$$

where $A_{Sa} = \frac{\pi}{4}d^2$, $d = 45\ mm$ and C_C is the heat capacity $J/(kgK)$ of the whole container. (See Fig. 2.7) The heat capacity is not influenced by imperfect thermal contact.

It is not this simple to modify (2.30) to include imperfect thermal contact and heat flowing through the sample casing and surrounding air. To make it possible three assumptions are made:

1 There is no temperature variation in the radial direction.
2 The heat flow around the sample is proportional to the temperature difference between top and bottom of the sample.
3 There is imperfect thermal contact only in two places. The thermal contact resistance at these places is equal and constant.

Assumption 1 is an approximation. If the PEEK has a higher conductivity than the sample, heat will flow along the PEEK before it enters the sample, causing a temperature gradient in radial direction, but as shown in Section 2.2.5 there is little radial heat flow.

Assumption 2 is almost correct. There will be convection and radiation in the air, and the heat flow caused by this is not linearly dependent on the temperature.

However the temperature difference between TS and BS is small. Then the non-linear effects can be assumed linear for a temperature interval. By introducing an artificial bypass thermal conductivity (λ_P) with an area (A_P) of the sample casing and air (2.30) can be corrected by (2.32).

$$\lambda_{Sa} = \lambda_2 - \frac{A_P \lambda_P}{A_{Sa}} \tag{2.32}$$

The result is

$$\lambda_{Sa} + \lambda_P = \frac{\left(\frac{\dot{Q}_{Sa}}{A_{Sa}} + \frac{\dot{Q}_P}{A_P}\right)(R_2 - R_1)}{T_2(R_1, \tau) - T_2(R_2, \tau)} \cdot \frac{\frac{1}{2}C_2 + C_3}{C_{SaC}} \tag{2.33}$$

Equation (2.32) is better than (2.30) because it adjusts for the heat flow along the wall in the plastic container. Again the heat flow represented by a bypass thermal conductivity ($A_P \lambda_P$) in (2.32) can be found by measuring on a known sample. It is not a problem that $A_P \lambda_P$ varies with temperature since it can be measured for all temperatures.

Assumption 3 is uncertain. The thermal resistance between two plates in imperfect contact is dependent on many factors, and can differ each time they are pressed against each other. The thermal contact resistance however should not differ that much when clean gold coated copper plates are put together.

If assumption 3 is correct there is a difference between $T_2(R_1, \tau)$ and T_1, and $T_2(R_2, \tau)$ and T_3 given by

$$\begin{aligned} T_2(R_1, \tau) &= T_1 - \frac{\dot{q}}{\alpha}\frac{C_2 + C_3}{C_{SaC}} \\ T_2(R_2, \tau) &= T_3 + \frac{\dot{q}}{\alpha}\frac{C_3}{C_{SaC}} \end{aligned} \tag{2.34}$$

(2.30) can then be modified to (2.35).

$$\lambda_2 = \frac{\dot{q}(R_2 - R_1)}{T_1 - T_3 - \frac{\dot{q}}{\alpha}\frac{C_2 + 2C_3}{C_{SaC}}} \cdot \frac{\frac{1}{2}C_2 + C_3}{C_{SaC}} \tag{2.35}$$

Similarly as for (2.16) and (2.17) when the thermal properties vary with temperature it is a question for which temperature the thermal properties calculated by (2.29) and (2.30) are valid. The introduction of a container complicates the problem a little, but it seems right to integrate (2.28) to find the equalizing temperature for the sample without the container. This equalizing temperature is the temperature which will occur if the sample suddenly was moved to a container of

perfectly insulating material. The expression for this temperature is

$$\bar{T}(\tau) = \frac{\int_{R_1}^{R_2} (T_2(r,\tau))dr}{R_2 - R_1}$$

which after some manipulation, becomes

$$\bar{T}(\tau) = T_2(R_1,\tau) - \frac{\dot{q}(R_2 - R_1)}{C_{SaC}\lambda_2}\left(\frac{1}{3}C_2 + \frac{1}{2}C_3\right) \tag{2.36}$$

$T_2(r,\tau)$ is defined in (2.28). C_{SaC} is here the heat capacity of the sample and the sample container. Equation (2.36) depends on perfect contact between the sample, TS and BS.

2.2.4 Temperature dependent thermal properties

The effect of infinitesimal low heat rate on a sample

So far all equations have assumed constant thermal properties and the equations have been analytical. Now the question is if the equations can be used as a basis for an instrument that measures thermal properties as a function of temperature. If heat is added at infinitesimal low rate to a sample with thermal properties which vary with temperature, and with the same boundary condition as in (2.9), the thermal properties will need such a long time to change that they can be considered constant. This is because the temperature rises infinitely slowly. Then the temperature profile will be close to (2.15), and (2.16) and (2.17) and can be used to estimate the thermal properties. An infinitesimal low heat rate gives a temperature difference that cannot be measured. It will also take an infinitely long time to measure heat capacity and thermal conductivity for all temperatures in a range.

The effect of a measurable heat flux on the sample

The question is now, how high can the heat flux become, before the equations become too inaccurate? Since no analytical expressions for the inaccuracy of (2.16) and (2.17) for different heat fluxes and thermal properties which vary with temperature are available, numerical simulations are used to estimate the uncertainty.

To verify (2.16) and (2.17), estimate their accuracy at different heat fluxes, and find out if they are suitable as a basis for a real instrument, some one-dimensional numerical simulations were carried out. The thermal properties of pork meat was used as input to the simulation. A 40-element one-dimensional finite element model (FEM) of Figure 2.13 was implemented in the simulation program ALGOR (see www.algor.com). The thermal properties of pork meat was estimated from composition data by Viðar Harðarson. Theories presented in the COST90 [9] project originated from Schwartzberg [72] were used. The length of the rod was $L = 20\ mm$. Simulations were run for values of $\dot{q}$ of 10 W/m^2, 100 W/m^2 and 1000 W/m^2 It would take 250, 25 and 2.5 hours respectively to raise the temperature from -40 to +45 ℃. The simulation was carried out with time steps of one minute and the temperatures $T(0,\tau)$ and $T(L,\tau)$ were recorded. In numerical simulations of transient heat transfer with varying thermal properties the result will be inaccurate if the time step size becomes too large. To ensure that the time step size was short enough, a simulation with larger time step size was also carried out. No difference in the resulting data was observed. These data were later used in (2.16) and (2.17) to calculate the thermal properties. To show the accuracy of thermal properties estimated by (2.16) and (2.17) at different heat flux, the error between "input" and "output" data is plotted in Figures 2.16 and 2.17. The maximum error at each temperature gives an estimate of the variance.

The graphs in Figures 2.18 and 2.19 plot the percentage errors for heat capacity and thermal conductivity respectively against temperature. The variance is largest for a heat flux of $\dot{q} = 1000\ W/m^2$ and smallest for $\dot{q} = 10\ W/m^2$.

The variance charts clearly show that for pork meat a heat flux larger than $\dot{q} = 100\ W/m^2$ will give poor results. It is worth noting that there is an increase in the error where the knuckle points in the implemented data occur. (Compare Figures 2.17 and 2.19.) Smoothing the implemented data, so that they match the real products better, will improve the result.

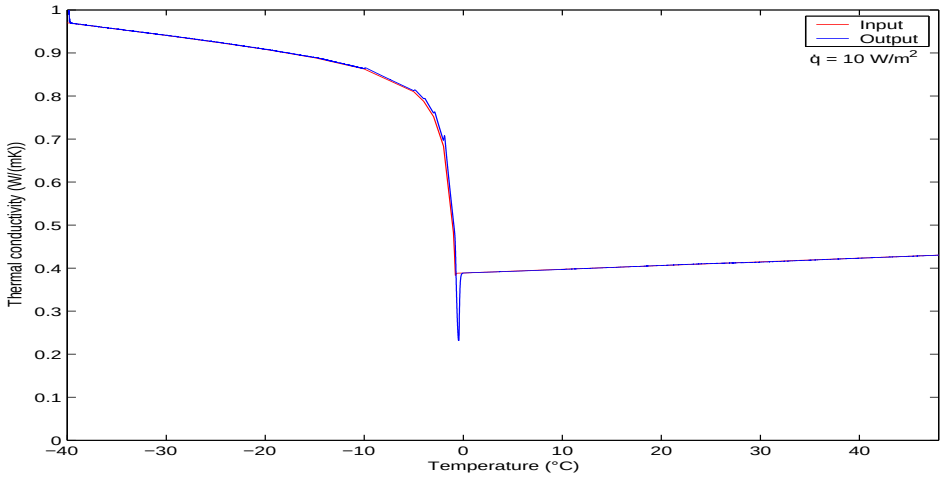

Figure 2.16: Thermal conductivity calculated by (2.16)

A comparison between λ used as input to simulation and λ calculated from the output by (2.16).

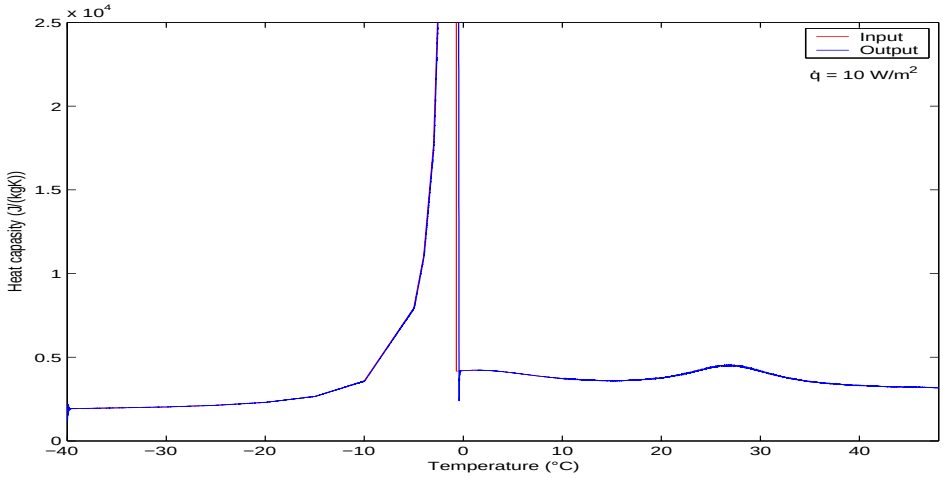

Figure 2.17: Heat capacity calculated by (2.17)

A comparison between c_p used as input to simulation and c_p calculated from the output by (2.17).

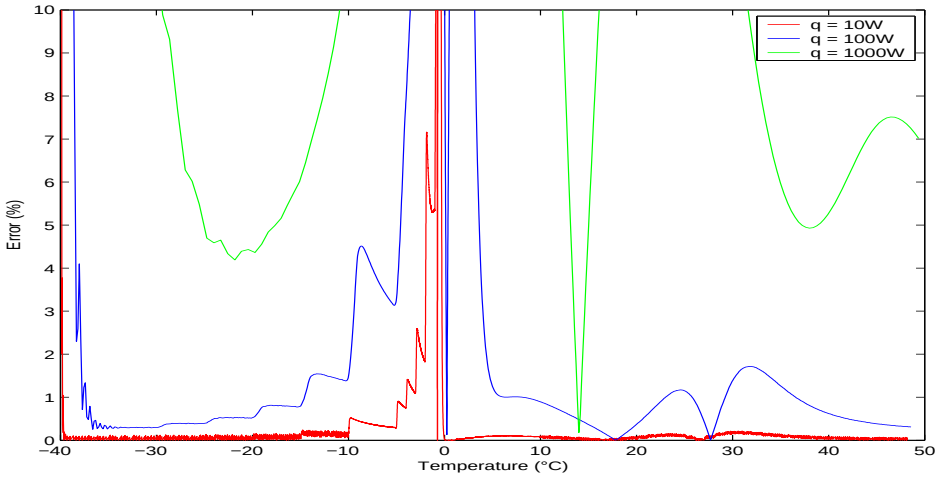

Figure 2.18: Error, thermal conductivity

The difference between λ_{input} and λ_{output} in % for where $\dot{q}$ is 10, 100 and 1000 W/m^2

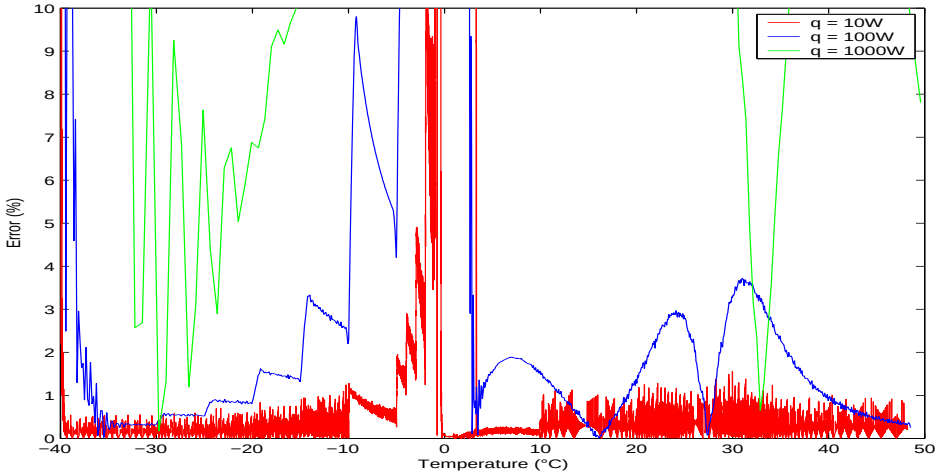

Figure 2.19: Error, heat capacity

The difference between $c_{p\ input}$ and $c_{p\ output}$ in % for where $\dot{q}$ is 10, 100 and 1000 W/m^2

2.2.5 Numerical simulations of the thermal multimeter

Numerical simulations are a valuable tool to increase the understanding of a system. In a simulation all properties are absolutely determined as input to the simulation. The simulation will also produce the same result with high accuracy. It is also possible to test conditions which cannot be archived in a real experiment and find values which cannot be measured in a real experiment. This can unmask effects which otherwise would be impossible to detect. It is of course important to remember that a simulation is not the real system.

To make a better prediction of expected accuracy, a numerical simulation of the instrument including the sample was done. Due to the symmetry of the instrument the simulation can be done in 2D, but a transient simulation of several hours, even in 2D, demands a lot of CPU time.

Description simulation method

Since the temperature control shown in Figure 2.20 is a boundary condition not available in commercial simulation programs, a program was written in Fortran. The code can be downloaded from this theses download page. (Se page 155.)

In the simulation the Forward Euler method (Named after Leonhard Euler (1707-1783)) described by Iserles [73] among others, was used. This method is easy to understand and program, and gives good results, but the time steps must be small to ensure numerically stability. Forward Euler is stone age in computer simulation and a lot of CPU time could have been saved by using another method. A mainframe computer was however available and in this numerical simulation the result was of interest, and not the method.

Figure 2.20 shows temperature controlling, edge conditions and materials for the different parts of the multimeter. The multimeter is cylindrically symmetric. The r-axis on the figure shows the radius and the z-axis shows the height. The heat conduction equation is solved in 2D cylindrical co-ordinates. The part numbers are the same as in Figure 2.10. The temperature at the top of the shield is set equal to the temperature in the copper above. The same applies to the bottom of the sample and the lower shield. Where the temperatures are measured and controlled in TS, BS, THS etc. does not really matter, because the high thermal conductivity of copper causes the temperature to be almost the same in the whole copper part.

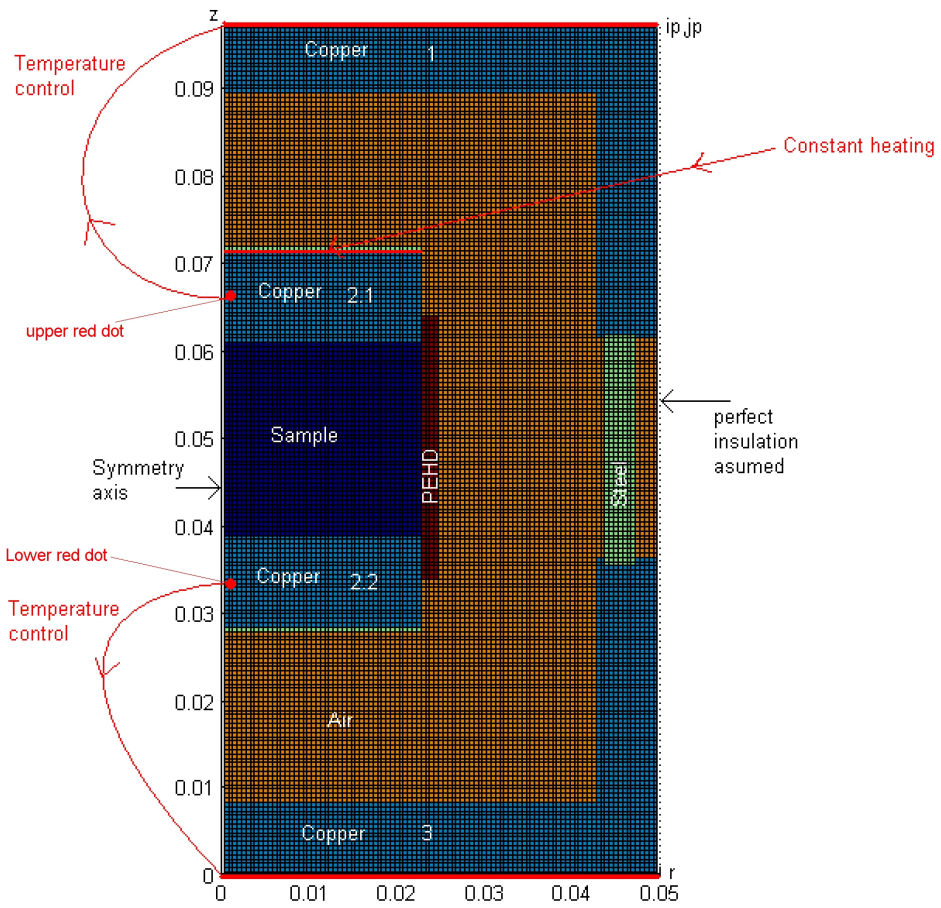

Figure 2.20: Materials in the thermal multimeter

The colour code for material is as follows. Dark blue represents the sample, light blue represents the copper, orange represents the air, green represents the steel and brown represents the plastic. The part numbers are the same as in Figure 2.10. The temperature at the top of the shield is set similar to the temperature in the copper above. The same applies to the bottom of the sample and the lower shield. ip =100 and jp = 194 refer to the grid.

The edge condition on the right hand side is perfect insulation because the whole calorimeter is surrounded by air with almost the same temperature. Smaller details such as steel and copper pipes, holes, screws and Pt100 elements are ignored, since the effect of them is small. The conduction through the steel and copper pipes is small because they connects parts which have the same temperature during a measurement. Steel screws, holes etc. are fitted in copper which has high thermal conductivity. Therefore the heat will then find another path around such small details without altering the temperature field significant. Conduction through air is the main transport path for heat leakage between the shield and the sample. Since the temperature in the thermal multimeter increases with the height, heat leakage by convection in the air is assumed to be small and is ignored. Radiation is also ignored. If both the sample and the shield are assumed to radiate like black bodies almost four times as much heat would be transported by radiation as by conduction through the air, but according to Siegel [74] and Palik [75] the emissivity from electrical conductors is very small at low temperatures. Emissivity of polished gold can is as low as 0.02. The parts in the thermal multimeter are copper coated with gold. The emissivity is not measured, but if it is this low, conduction account for over 90% of the heat flow through the air. This is estimated by inspection of the ratio

$$\frac{\sigma\varepsilon\left((T+\Delta T)^4-T^4\right)}{k_{Air}\Delta T\Delta r^{-}1}=\frac{5.67\cdot10^{-8}(W/m^2K)\cdot0.02\left((273\ K+\Delta T)^4-273\ K^4\right)}{0.0241(W/mK)\cdot\Delta T\cdot(0.02\ m)^{-1}}=0.08$$

The emissivity is probably higher than 0.02. To include radiation would complicate the calculations. The simulations therefore cannot be used to calibrate the real instrument, but they are useful for estimating the magnitude of heat leakages and testing the modified equations for finding the thermal properties presented in Section 2.2.3.

The thermal properties in the simulation are temperature independent. Furthermore, perfect contact is assumed between all materials. With these assumptions the temperature in the next time step is based on the current temperature as described by the explicit algorithm

$$T_{i,j}\left(\tau+\Delta\tau\right)=\left[\begin{array}{l}+\left(\frac{1}{\Delta r^2}+\frac{1}{2r\Delta r}\right)\frac{2\lambda_{i+1,j}\lambda}{\lambda_{i+1,j}+\lambda}\left(T_{i+1,j}-T_{i,j}\right)\\+\left(\frac{-1}{\Delta r^2}+\frac{1}{2r\Delta r}\right)\frac{2\lambda_{i-1,j}\lambda}{\lambda_{i-1,j}+\lambda}\left(T_{i,j}-T_{i-1,j}\right)\\+\frac{1}{\Delta z^2}\frac{2\lambda_{i,j+1}\lambda}{\lambda_{i,j+1}+\lambda}\left(T_{i,j+1}-T_{i,j}\right)\\-\frac{1}{\Delta z^2}\frac{2\lambda_{i,j-1}\lambda}{\lambda_{i,j-1}+\lambda}\left(T_{i,j}-T_{i,j-1}\right)\\+\frac{\dot{q}}{\Delta z}\end{array}\right]\frac{\Delta\tau}{\rho c_p}+T_{i,j}\left(\tau\right)\quad(2.37)$$

where edge and heating conditions are covered by the following corrections to (2.37).
$\left(\frac{1}{\Delta r^2} + \frac{1}{2r\Delta r}\right) \frac{2\lambda_{i+1,j}\lambda}{\lambda_{i+1,j}+\lambda} (T_{i+1,j} - T_{i,j}) = 0$ for $i = ip$
$\left(\frac{-1}{\Delta r^2} + \frac{1}{2r\Delta r}\right) \frac{2\lambda_{i-1,j}\lambda}{\lambda_{i-1,j}+\lambda} (T_{i,j} - T_{i-1,j}) = 0$ for $i = 1$
$T_{i,j} = T_{At\ upper\ red\ dot}$ for $j = jp \quad , \quad T_{i,j} = T_{At\ lower\ red\ dot}$ for $j = 1$
$\frac{\dot{q}}{\Delta z} = 0$ everywhere except where heat is added to the sample.
The indices i and j refer to the r-axis and y-axis respectively. ip and jp are the highest i and j values. ip and jp will be in top right-hand corner of Figure 2.20. For 0.5 mm grid with $ip = 100$ and $jp = 194$ the control temperatures become $T_{At\ upper\ red\ dot} = T_{1,134}$ and $T_{At\ lower\ red\ dot} = T_{1,64}$. See Figure 2.20 for the positions of the red dots. Heat is added, and $\frac{\dot{q}}{\Delta z} \neq 0$, for $T_{1-45,142}$. The method is stable if the Fourier number , $\frac{\lambda}{\rho c_p} \frac{\tau}{(\Delta r)^2}$, is smaller than 0.5 which gives a maximum time step size of $0.00109s$ (Iserles [73]). The limiting factor for stability is copper.

Simulation results

The result from the simulation is the temperature distribution in the thermal multimeter when the heat flux function is no longer time dependent. The heat flow can also be calculated from the temperatures. Figure 2.21 illustrates the temperature in the cross-section of Figure 2.20. The colours represent the temperature difference in Kelvin related to the initial temperature. As predicted, the temperature profile goes against the limit presented in (2.27). Figure 2.21 shows the temperatures for a sample with the properties of ice at 0 ℃ when the temperature profiles have been established. The heat flux is 100 W/m^2. The thermal properties is presented in Table 2.6.

The remaining figures shows the heat flux field. Figure 2.22 show the total magnitude of the flux whereas Figures 2.23 and 2.24 illustrate the results for the r and z component respectively. Negative heat flux indicates that the heat flow is against the direction of the axis. In Figures 2.25, 2.26 and 2.27, the values for the heat flux in the the shield and the sample are set to 0. Then the relatively small flux in the air gap becomes visible on the figures. Figure 2.25 shows the total heat, 2.26 the r component and 2.27 the z component. The heat flow in the air gap is of interest to estimate the heat leakage between the shield and the sample.

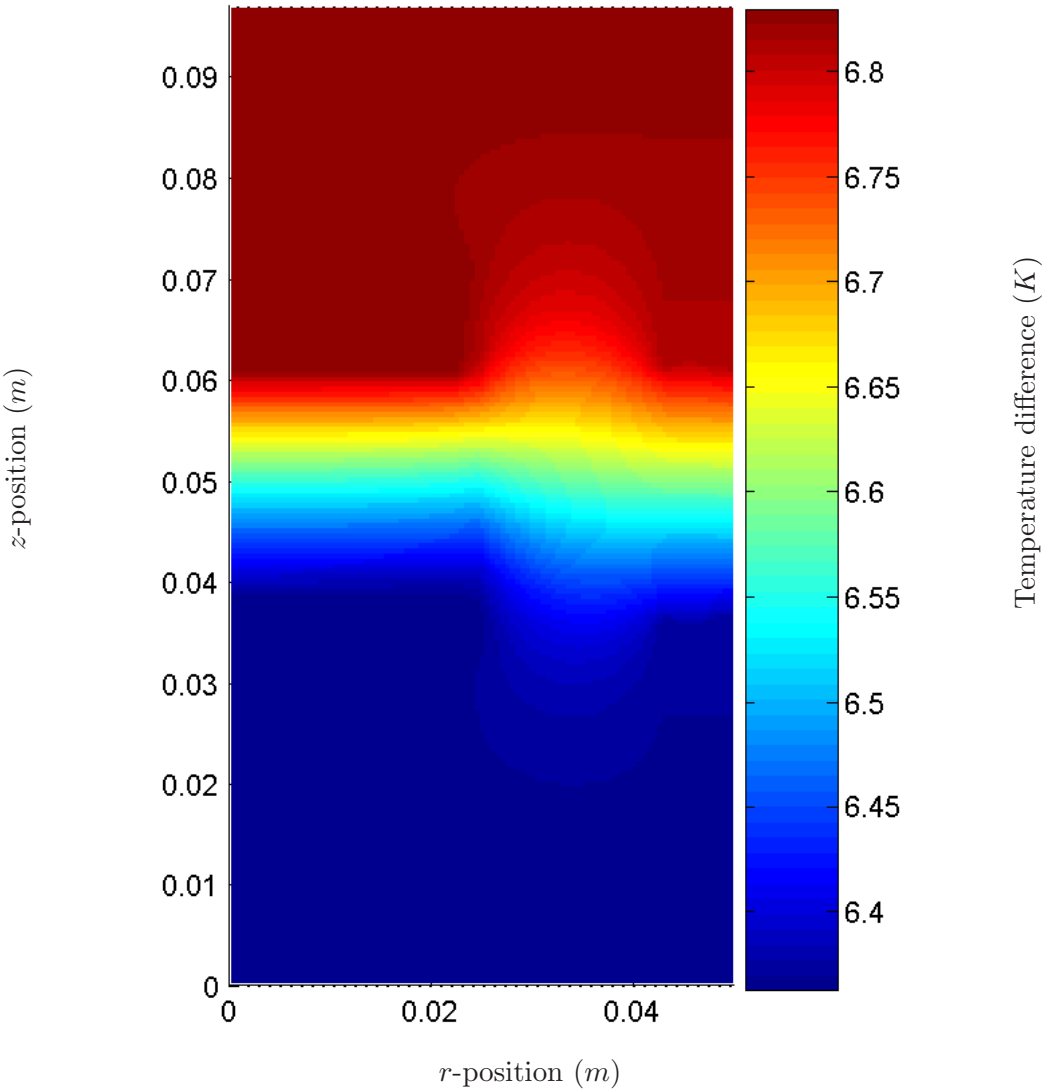

Figure 2.21: Temperatures in the thermal multimeter

Both axes indicate the position in the thermal multimeter in metres. The colours give the temperature difference compared to initial temperature ($T - T_0$).

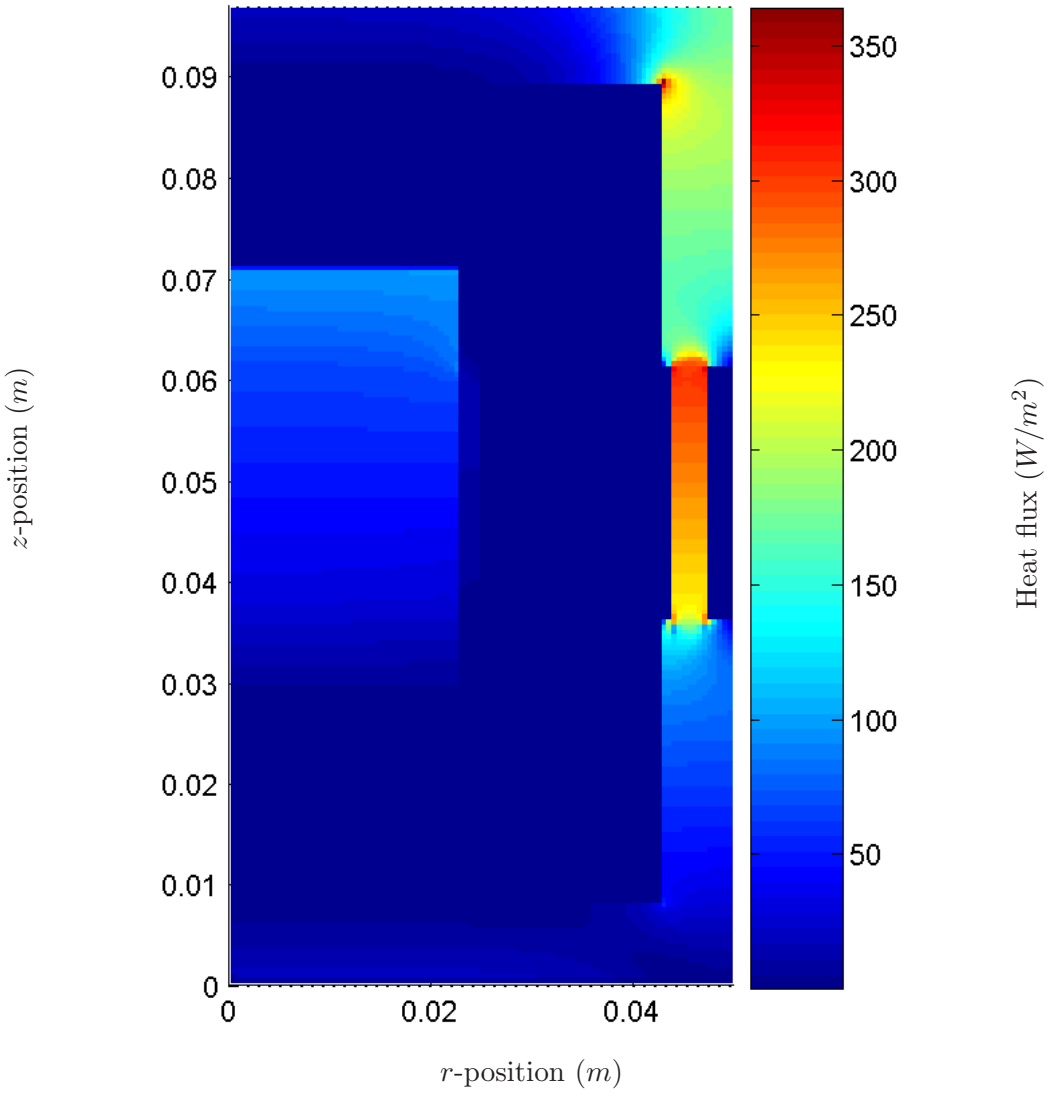

Figure 2.22: Heat flux magnitude in the thermal multimeter

Both axes indicate the position in the thermal multimeter in metres. The colours give the heat flux in W/m^2.

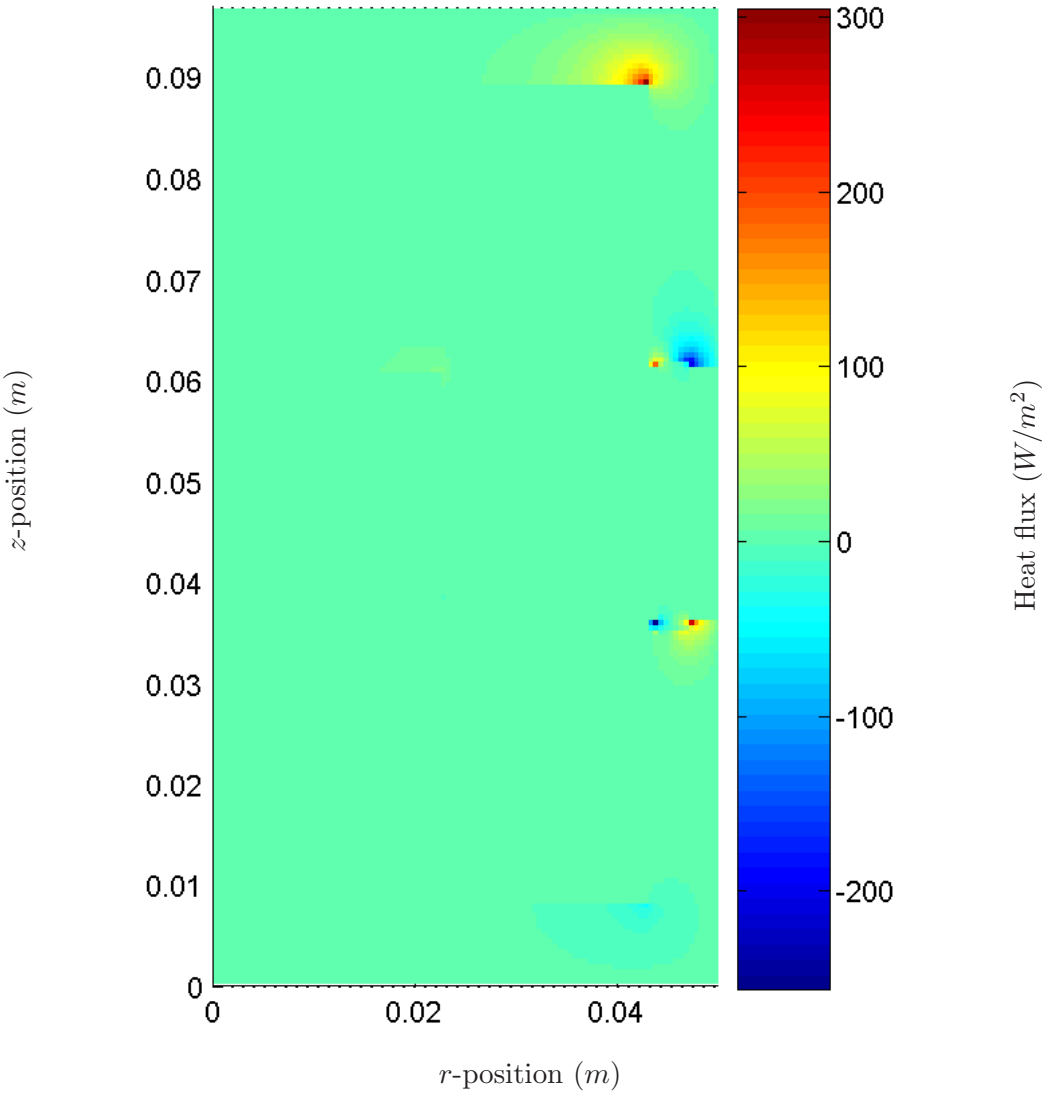

Figure 2.23: r component of heat flux in the thermal multimeter

Both axes indicate the position in the thermal multimeter in metres. The colours give the r component of heat flux in W/m^2.

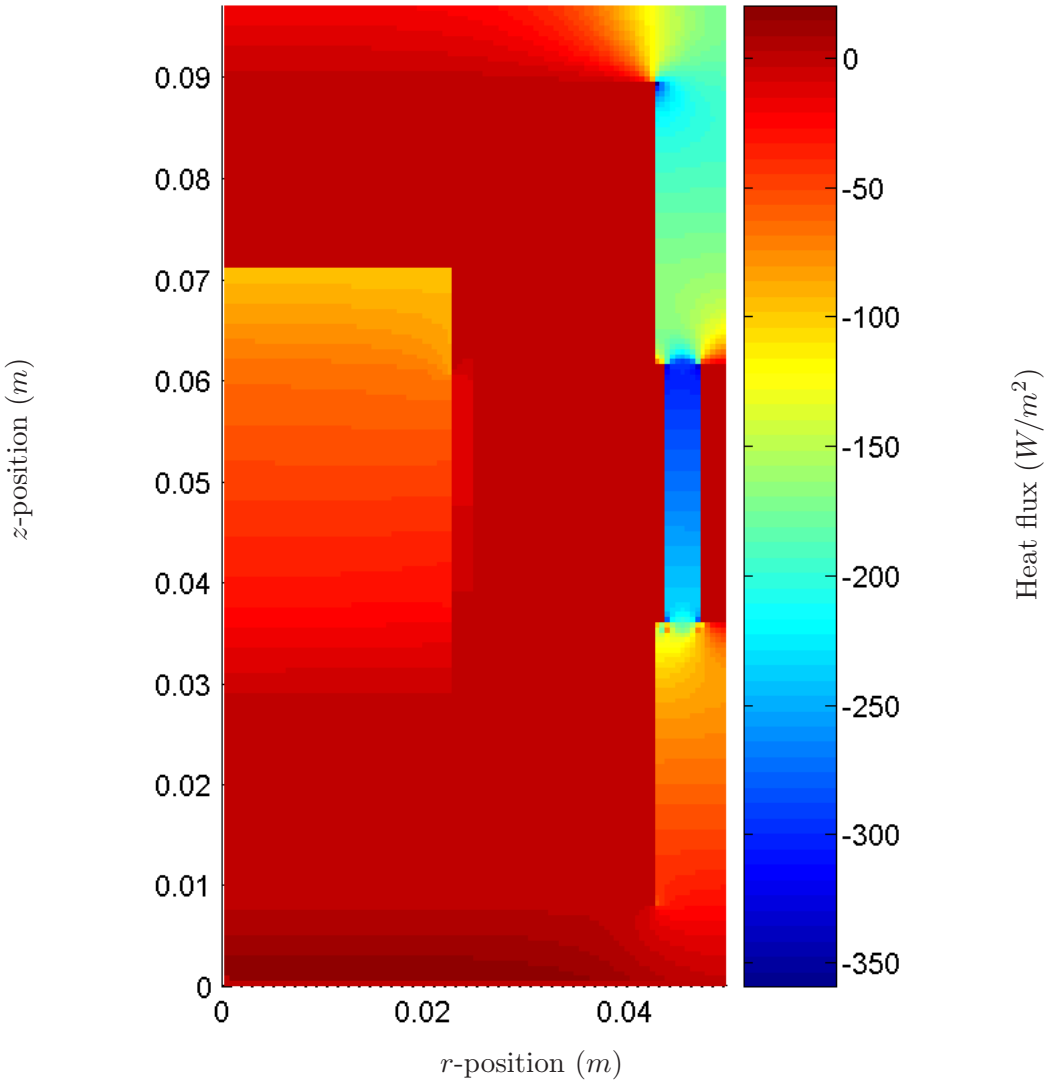

Figure 2.24: z component of heat flux in the thermal multimeter

Both axes indicate the position in the thermal multimeter in metres. The colours give the z component of heat flux in W/m^2.

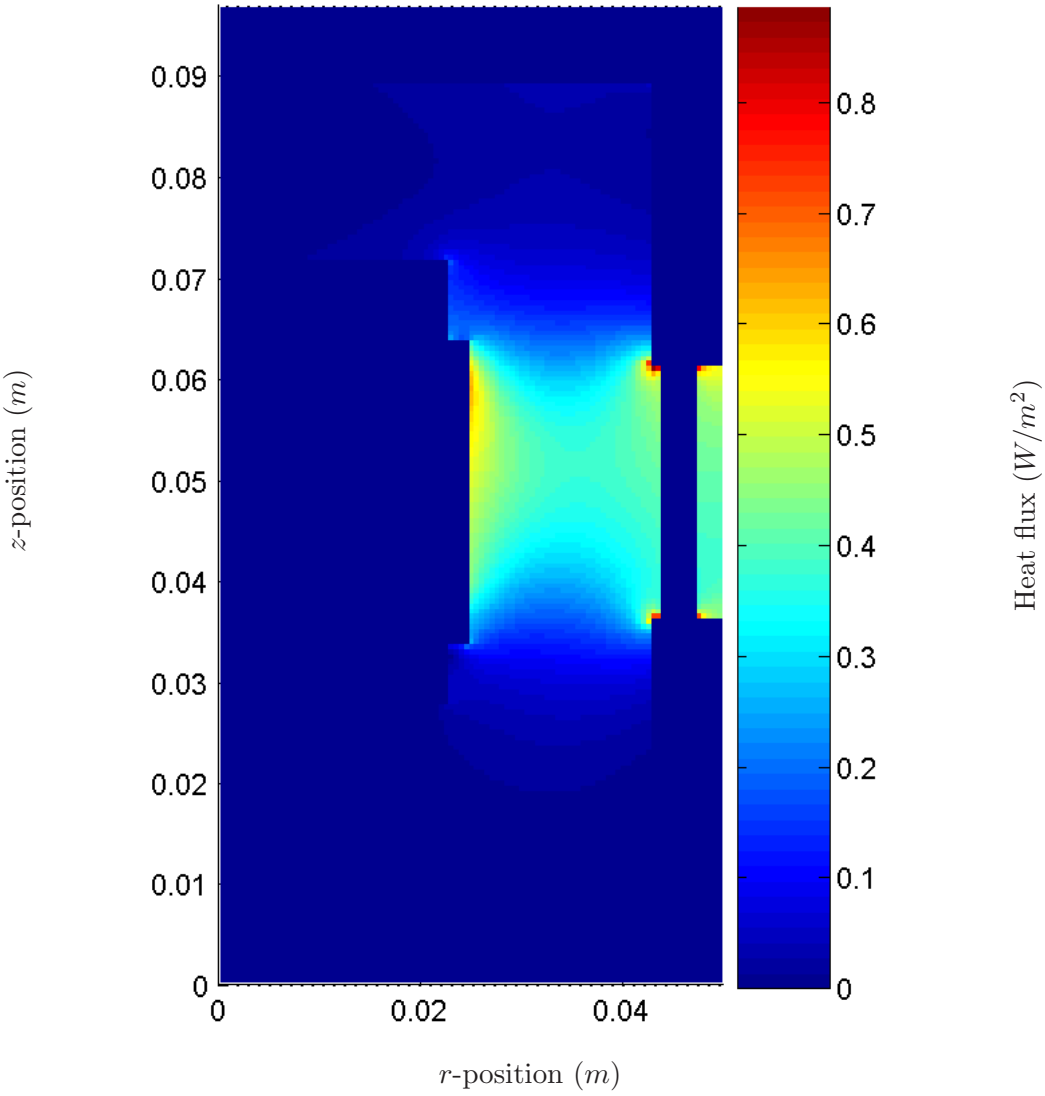

Figure 2.25: Heat flux in air gap in the thermal multimeter

This figure shows the heat flux in the air gap which is so small that it is invisible in Figure 2.22. Note that the largest heat flux in the gap is 0.9 W/m^2 while the heat flux through the sample is 100 W/m^2. Both axes indicate the position in the thermal multimeter in metres. The colours give the heat flux in W/m^2.

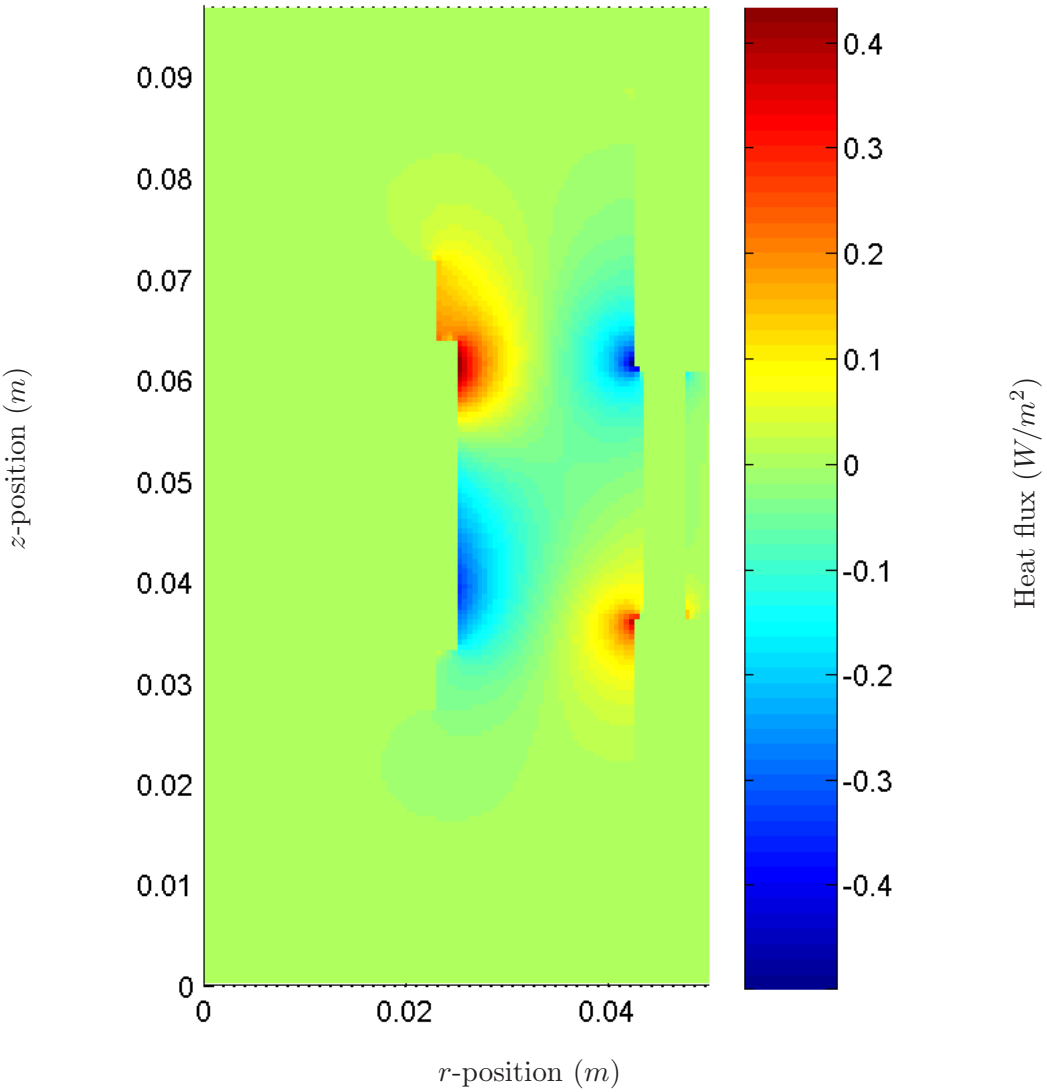

Figure 2.26: r component of heat flux in air in the thermal multimeter

Both axes indicate the position in the thermal multimeter in metres. The colours give the r component of heat flux in W/m^2.

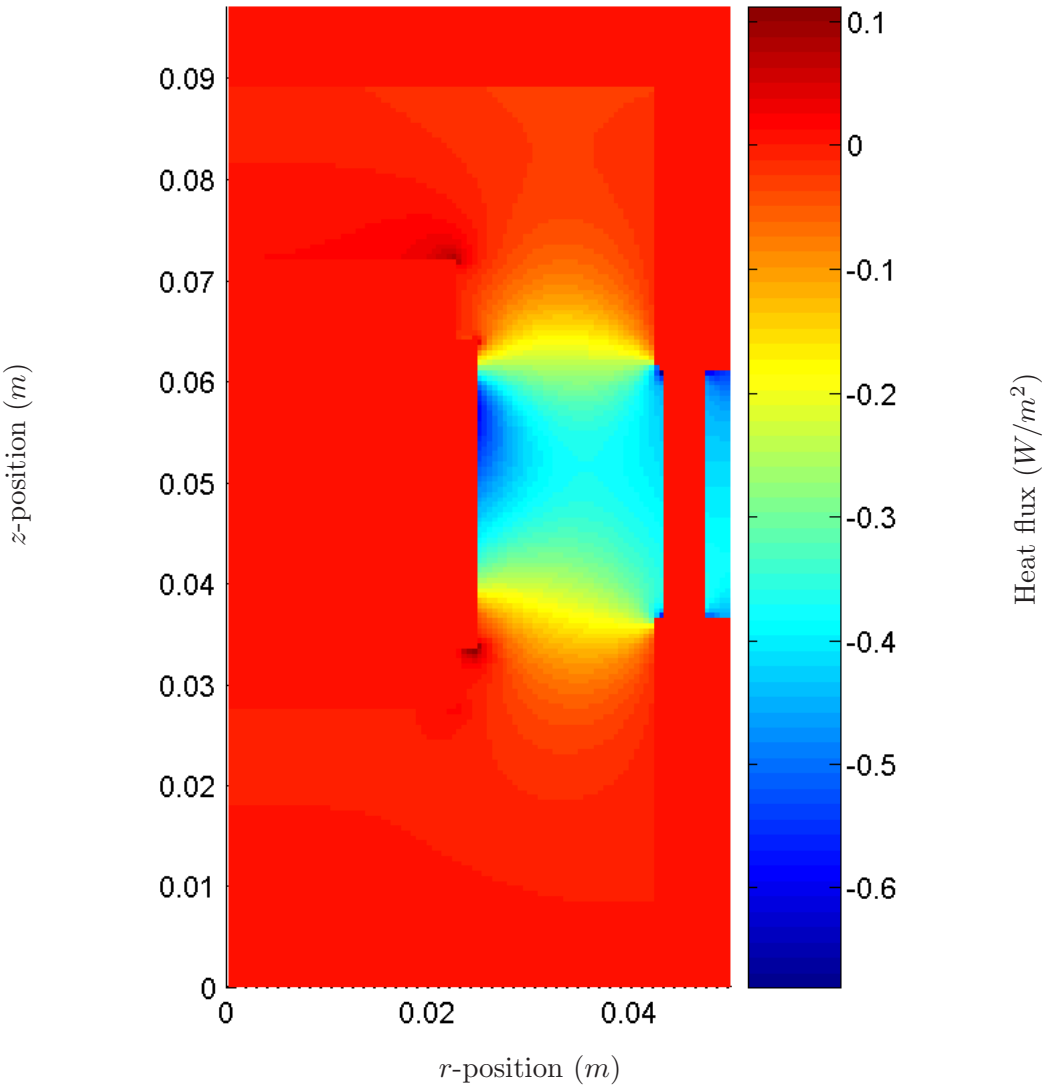

Figure 2.27: z component of heat flux in air in the thermal multimeter

Both axes indicate the position in the thermal multimeter in metres. The colours give the z component of heat flux in W/m^2.

Figure 2.25-2.27 indicate that heat is conducted into the air at the hot part of the sample, then the heat is conducted down through the air to the cold part, where it goes back into the sample. The simulation program was ran several times with different samples to see how the thermal properties of the sample influence the accuracy of the measurement.

2.2.6 Comparison of the numerical and analytical solutions

When a problem can be solved both analytically and numerically the solution can be compared to validate the calculations. Temperature values for the top and bottom of the sample can also be used in (2.31) and (2.32) to calculate heat capacity and thermal conductivity. Then the "measured" values can be compared with the values used as input to the simulation. The difference will give an indication of what accuracy can be expected from real measurements in the thermal multimeter.

In Table 2.5 the thermal conductivity and heat capacity are calculated by (2.31) and (2.32) from simulated measurements. The thermal multimeter is not made for measuring the thermal conductivity of air, and if an attempt is made to do this, the uncertainty will be very high. The simulation is included because such a measurement can be useful for calibration purposes.

Table 2.5: Error in estimate of thermal properties

Values used in numerical simulation					Values calculated by (2.31) and (2.32)				99% stable after	
Heat flux and sample properties					c_p		λ		Time	Temp change
Sample material	$\dot{q}$	ρ	c_p	λ	(2.31)	%Error	(2.32)	%Error	Time(s)	$\Delta T(K)$
Air*	57.5	1.293	1004	0.0241	-	-	0.0243	+0.67	24600	17.7
Timber	10	400	1600	0.15	1451	-10.3	0.147	-1.88	8500	0.85
Timber	100	400	1600	0.15	1451	-10.3	0.147	-1.88	8500	8.54
TDF*	57.5	790	1874	0.187	1770	-5.83	0.189	+0.83	9600	4.88
GA*	57.5	742.5	1600	0.192	1505	-6.33	0.194	+0.82	9000	4.84
Turbonitt*	57.5	1362	1274	0.304	1229	-3.63	0.306	+0.56	6600	3.19
Water	100	1000	4180	0.61	4119	-1.47	0.608	-0.30	4000	2.26
Water*	57.5	1000	4180	0.61	4117	-1.52	0.612	+0.28	4200	1.40
Ice	100	920	2100	2.3	2094	-0.29	2.291	-0.38	1500	1.16
Steel	100	7900	500	16	500.5	+0.10	15.63	-2.375**	500	0.29

* *These simulations have PEEK as casing. The others have PEHD.*

** *This figure appears because the thermal conductivity of steel is so large that copper no longer can be assumed to have infinite conductivity.*

The four first columns show the heat flux into the sample and the thermal properties used as input to the simulation. The table is sorted after λ. The four

next columns show the thermal properties calculated by (2.31) and (2.32), The %Error columns show the % difference between input in the simulation and the calculated thermal properties from the simulation result. The second-last column shows the simulated time before the temperature difference between TS and BS reaches 99% of its final value. This time is calculated from the simulation and has nothing to do with (2.18). The two simulations on timber, where the heat flux through the sample is different, show that this time is independent of the heat flux through the sample. The last column shows the final temperature difference between TS and BS.

There are two kinds of simulations. The first which includes timber, water, ice and steel was done before the instrument was built. Here the material the plastic sample casing was high density poly-ethylene (PEHD). The second which includes Air, GA, TDF, turbonitt and water was done after some calibration of the thermal multimeter. Since PEHD was unsuitable as sample casing it was replaced with poly-ether-ether-ketone (PEEK). PEEK has different thermal properties than PEHD. The heat capacity of TS and BS in the second numerical simulation was also corrected after what was measured in the thermal multimeter. Since the simulations took up to 10 days to finish, the first simulations were not repeated with adjusted thermal properties, but they are included since the adjusted properties are fairly similar to the initial. The simulation results in Table 2.5 are marked with '*' the adjusted properties given in Table 2.7 are used as input. Input for simulations that are not marked is given in Table 2.6.

Table 2.6: Thermal properties

	$\rho\ [kg/m^3]$	$c_p\ [J/(kg \cdot K)]$	$\lambda[J/(kg \cdot K)]$
Air	1.293	1004	0.0241
copper	8960	380	390
PEHD	965	2100	0.52
Ice	920	2100	2.3
Steel	7900	500	16

Table 2.7: Thermal properties *

	$\rho\ [kg/m^3]$	$c_p\ [J/(kg \cdot K)]$	$\lambda[J/(kg \cdot K)]$
Air	1.293	1004	0.0241
copper	8960	382.77	390
PEEK	1320	855.12	0.25
Steel	7900	500	16

The bypass thermal conductivity ($A_P\lambda_P$) in (2.32) was set to be equivalent to the casing with thermal properties of PEHD or PEEK depending on the measurement and the air from the sample, half the way to the shield. This because it is a reasonable estimate of $A_P\lambda_P$. A correction factor of 0.013 was included in the thermal conductivity.

$$\begin{aligned} \lambda_{Sa} = \lambda_2 - \frac{A_{PEHD\ or\ PEEK}}{A_{Sa}k_{PEHD\ or\ PEEK}} - \frac{A_{Air}}{A_{Sa}k_{Air}} + 0.013; \\ A_{PEHD\ or\ PEEK} = \pi\left(24.5e-3^2 - 22.5e-2^2\right) \\ A_{Air} = \pi\left(24.5e-3^2 - 33.5^2e-2^2\right) \end{aligned} \tag{2.38}$$

The correction factor is the factor which minimize the error in calculating thermal conductivity in (2.38). It is included because in calibration of the real instrument the whole term $-\frac{(A_{PEHD\ or\ PEEK})}{(A_{Sa})k_{PEHD\ or\ PEEK}} - \frac{(A_{Air})}{(A_{Sa})k_{Air}} + 0.013$; in (2.38) will be found when measuring a known sample. It is amazing how small the difference between the thermal conductivity used as input to simulations is compared with the thermal conductivity calculated by (2.32). This shows that the thermal multimeter can be an excellent instrument for measuring thermal conductivity.

It will be important to measure the bypass thermal conductivity. In Table 2.2.6 the correction factor in (2.38) is skipped. The influence is greatest on materials with low thermal conductivity. A reasonable degree of accuracy cannot be expected for materials with lower thermal conductivity than timber.

Table 2.8: Error in estimate of thermal properties (Continuation of Table 2.5)

Values used in numerical simulation				Calculated by (2.32)			Calculated by (2.42)	
Heat flux and thermal properties				λ			c_p	
Sample material	$\dot{q}$	c_p	λ	(2.32)	%Error	(2.39)	(2.42)	%Error
Timber	10	1600	0.15	0.134	-11.8	-0.30	1617	1.08
Timber	100	1600	0.15	0.134	-11.8	-0.30	1617	1.08
TDF*	57.5	1874	0.187	0.176	-6.50	-0.36	1869	-0.25
GA*	57.5	1600	0.192	0.181	-6.31	-0.33	1602	0.12
Turbonitt*	57.5	1274	0.304	0.293	-3.81	-0.37	1270	-0.29
Water	100	4180	0.61	0.595	-2.49	-0.49	4162	-0.44
Water*	57.5	4180	0.61	0.599	-1.88	-0.48	4161	-0.45
Ice	100	2100	2.3	2.278	-0.95	-0.20	2104	0.18
Steel	100	500	16	15.62	-2.46**	+0.71	500.7	0.15

*The values in this table are calculated the same way as the values in Table 2.5 except that the correction factor of 0.013 is skipped. See comments to Table 2.5 for * and **.*

A cylinder shell of steel connects THS and BHS. This shell has a small total heat capacity compared with THS and BHS, and relative much heat is conducted through the shell. The temperature profile of the steel shell is therefore almost linear. The temperature profile in the sample is described by (2.28). Higher heat capacity of the sample means more curvature than the curvature shown in Figure 2.14 as worst case. This means there can be a temperature difference between the sample and the shield, which can cause a net heat leakage from the shield to the sample. This will lead to a too low measured heat capacity as shown in Table 2.5.

There are two exceptions. First, if the thermal conductivity of the sample is high TS and BS will have almost the same temperature. The curvature of the temperature profile in the sample will then cause very little temperature difference between the shield and the sample, and therefore no heat leakage and suitable accuracy in measured heat capacity. Second, if the total heat capacity of the sample is small, the profile will be almost a straight line. Since the profiles in the sample and the steel shell are almost equal the heat leakage will be reduced. Normally this will not increase accuracy of measured heat capacity because the heat capacity of good insulators is generally very low and will be neglible compared with the heat capacity of the sample container.

Because of this profile which depends on the heat capacity of the sample it is not easy to find a way to correct for the heat leakage to the sample which can be included in the calibration routines for the thermal multimeter. One attempt is presented in Table 2.2.6 where the ratio

$$\frac{C_{va} \cdot \dot{q}}{C_{total} \cdot T_{diff}} \tag{2.39}$$

is presented. C_{va} in (2.39) is the difference between "measured" (calculated by (2.31)) and real (input to the simulation) total heat capacity of the sample and the sample container, $\dot{q}$ is the heat flux in the simulation, C_{total} is the heat capacity of the sample and the sample container and T_{diff} is the temperature difference over the sample. Here it is assumed that the heat leakage is only proportional with the temperature difference over the sample and that the effects of the heat profile can be ignored. The % variation in the ratio tells how good this assumption is. As Table 2.2.6 (column marked (2.39)) shows this is not a poor assumption, although the extreme high heat capacity for water causes considerable span. Steel can be ignored since the thermal conductivity is so high. Adding C_{va} given by (2.40) to the total measured heat capacity of the sample and sample container before the heat capacity of the sample is calculated will improve (2.31). The constant K_a in (2.40) can be found by measurements of known materials.

$$C_{va} = K_a \frac{C_{total} \cdot T_{diff}}{\dot{q}} \tag{2.40}$$

Assuming that C_{total} is almost equal measured C_{total}, (2.40) can be reformulated to (2.41).

$$C_{va} = K_a \frac{\Delta\tau(T_2(R_1,\tau+\Delta\tau)-T_2(R_2,\tau+\Delta\tau)+T_2(R_1,\tau)-T_2(R_2,\tau))}{T_2(R_1,\tau+\Delta\tau)+T_2(R_2,\tau+\Delta\tau)-T_2(R_1,\tau)-T_2(R_2,\tau)} \tag{2.41}$$

By using an average from all simulation except steel $K_a = 0.00054$. Inserting (2.41) into (2.31) gives (2.42).

$$c_{Sa} = \frac{\dot{Q}\frac{2\Delta\tau}{T_2(R_1,\tau+\Delta\tau)+T_2(R_2,\tau+\Delta\tau)-T_2(R_1,\tau)-T_2(R_2,\tau)} + C_{va} - C_C}{\rho_2 \left(R_2 - R_1\right) A_{Sa}} \tag{2.42}$$

(2.42) is used to calculate the heat capacity in the column marked (2.42) in Table 2.2.6. As seen from the table the agreement between input heat capacity to the simulation and the heat capacity calculated by (2.42) is considerably better than the heat capacity calculated by (2.42). By using the same assumptions as for (2.41) a K_a for the real instrument can be measured.

2.3 Results

This section gives the results from calibration and measurements done with the thermal multimeter.

2.3.1 Calibration

Since the instrument can measure thermal conductivity, heat capacity and density it must be calibrated for all three properties. This calibration is done in several steps.

Calibration of the instrument includes:
Calibration of temperature- and the length measurement sensor
Measurements of heat capacity of TS, BS and PEEK casing
A measurement of a known material where thermal contact is optimized to find K_a and to find the heat flow around the sample
A measurement of a known material under normal conditions to estimate the effect of imperfect thermal contact

Accuracy of the temperature measurement equipment

All measurements were done with two Agielnt 34970A switch units. The resistance of the Pt100 elements when placed in a water triple cell was for BS-Pt100-1 = 100.00444Ω, TS-Pt100 = 99.95964Ω and for SaC-Pt100 = 100.00414Ω. For the other Pt100 sensors no extreme accuracy is needed, and they were not calibrated. It was assumed that the temperature dependent resistance followed the standard curve for Pt100 elements. According to the specification for the Agielnt 34970A the accuracy of the temperature measurements with Pt100 is $\pm 0.06\ K$.

To study the stability of the Pt100 elements the heat supplied to the bottom sample container was controlled so the temperature difference between the top and bottom sample container became as small as possible. The temperature difference between the top and bottom sample measured by the Pt100 sensor TS-Pt100 and BS-Pt100-1 for five runs are plotted in Figure 2.28.

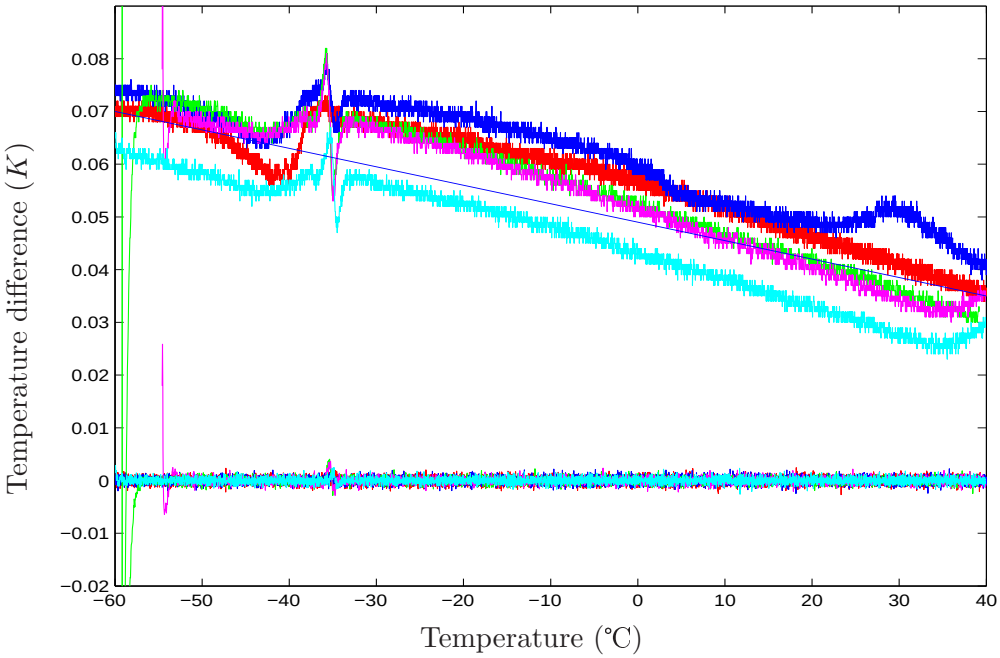

Figure 2.28: Stability of TS-Pt100 and BS-Pt100-1

The lines on the x-axis (x=0) are the temperature difference between TS and BS measured by the thermopiles, and the other lines are the temperature difference measured by Pt100 elements. The noise at about -36 ℃ may be caused by a phase transition in the grease used to ensure good thermal contact between the Pt100 element and copper.

The charts show that the accuracy can be improved above the specification of $\pm 0.06\ K$ by careful calibration. More important, this proves that a measurement is not random within the accuracy specification. The temperature change between two measurements done within $900s$ are accurate down to $\pm 0.01\ K$ during these measurements. This can be seen from Figure 2.28 since the shortest measurement took 13 hours and the temperature difference varies less than $\pm 0.01\ K$ on every 1/50 part on the curve.

The temperature difference between the sample and the shields, and over the sample was measured with 10 point thermopiles of type T. According to the specification of the Agielnt 34970A the accuracy of the voltage reading is $3.5\mu V$ close to $0V$. This corresponds to an uncertainty of $\pm 0.01\ K$ in the temperature difference

measurements done with a ten point thermopile. The temperature difference over the sample, used in the calculation of thermal conductivity, was calculated after the IEC standard using all 14 coefficients in the compound quantity.

For a thermopile, zero measured voltage over the pile means zero temperature difference unless there is a short circuit somewhere, or there is something wrong with the voltmeter. The alloy in the constantan thread used here, can differ from the defined standard constantan thread used in thermoelments of type T. If so, the gradient of the voltage temperature graph will differ from the standard. This causes an error for larger temperature differences, but as long the temperature difference is small the accuracy of the measured temperature difference is limited by the accuracy of the voltage measurement. At larger temperature differences the temperature difference measured by the thermopile can be compared with the temperatures measured by the Pt100 elements.

To show the typical performance of the shields, the temperature difference between different parts in the thermal multimeter when the shields are operating is presented in Figure 2.29.

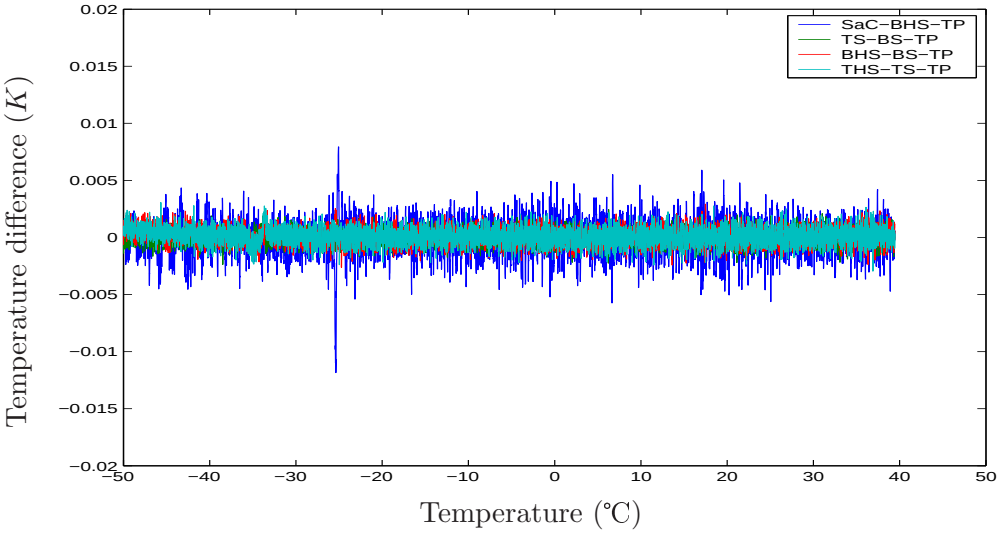

Figure 2.29: The performance the shields during calibration of the bottom sample

From the chart it is clear that the temperature of the shields follows the tem-

perature of the sample within $\pm 0.01\ K$. This can be improved slightly by choosing a better regulation algorithm.

The measurement of the power was done with the measuring bridge shown in Figure 2.12. The voltage measurement should have been done directly on the heater to avoid any measuring power loss in the cable. For practical reasons there is only two wires from the heaters. The bridge is attached to these wires about 40 cm from the heaters. Because of this the measured power is higher than the actual power in the heaters. An estimate of the resistance in the cable is 2Ω. The resistance in TS-H is 456Ω and the resistance in BS-H is 465Ω including the cable, which indicates that the error is less the 0.5%. This uncertainty dominates the power measurement accuracy.

The length sensor gives a voltage signal where changes in the signal are proportional to displacement. Calibration of the sensor is done by placing two samples of known and different lengths into the instrument. The connection between the voltage and the length of the sample can then be calculated. The user of the instrument must decide before each measurement if the sample expansion will be limited by the PEEK ring, or if the sample expands in three directions. In general the change in density can only be measured for non-porous materials which freeze. In the measurements done on solid materials with small thermal expansion (e.g. steel) the length measurement is replaced with the length measured with a slide caliper before the sample is placed in the instrument. Samples of food and other liquids are prepared so that the length is about 22 mm. The density of the sample is calculated from the length measured multiplied by the area of the sample.

Internal heat capacities

The heat capacity of TS, BS and the PEEK was measured in order to calculate the heat capacity and thermal conductivity of the sample. The heat capacity of the parts of the sample container was found in several steps.

First the heat capacity of the fixed part of the top sample was found during constant heating. The loose part of the sample container was then removed. The temperature in the bottom sample container and the shields was maintained at the same temperature as the top sample to ensure that there was no temperature gradient in the air surrounding the fixed part of the top sample container. Then no heat should be leaking from the fixed part of top sample container.

The process was repeated for the fixed part of the bottom sample with and without the two unfastened copper cylinders on top. Then measurements were done of a sample of copper with and without the cylinder shell of PEEK. Since

the thermal conductivity of copper is very high there was no temperature gradient in the air to cause a heat leakage. The heat capacity and thermal conductivity of the paper surrounding the sample container is included in the PEEK.

The heat capacity in all the measurement was found by the formula

$$C = \frac{\dot{Q}\Delta\tau}{\Delta T} \tag{2.43}$$

Then the heat capacity of the different parts was found by simple arithmetic. The logging interval was $15s$ in all measurements, but $\Delta\tau = 900s$. This because $\Delta\tau = 15s$ will cause large noise since ΔT then will be very small. With $\Delta\tau = 900s$ no filtering of the data is necessary. For the measured heat capacity a sliding mean of 60 measurements to smoothen the curve is used. This is done with almost no loss in accuracy of variable heat capacity since the values used for averaging is inside the interval of $\Delta\tau = 900s$.

The heat capacity of the parts as function of temperature is presented in Figure 2.30. The small tops at about -34 ℃ in the lines for the top and bottom sample container are caused by a phase transition in a silicon grease used to ensure good thermal contact between the copper and the temperature censors. The noise at +35 ℃ has something to do with the Agielnt 34970A switch units. Both phenomena can be seen in almost all measurements.

In Figure 2.31 the heat capacities of each part measured separately are summarized. The sum is compared with a measurement of heat capacity of all parts in the sample container where heat was supplied to both TS and BS. A heat leakage during the measurement of each part should have added up and caused a difference between the summarized total heat capacity and the measured heat capacity of the parts in the sample container. Since there is almost no difference it can be concluded that any heat leakage is small when heat is added to both TS and BS in such a way that the temperature in TS and BS are equal and the shields function properly.

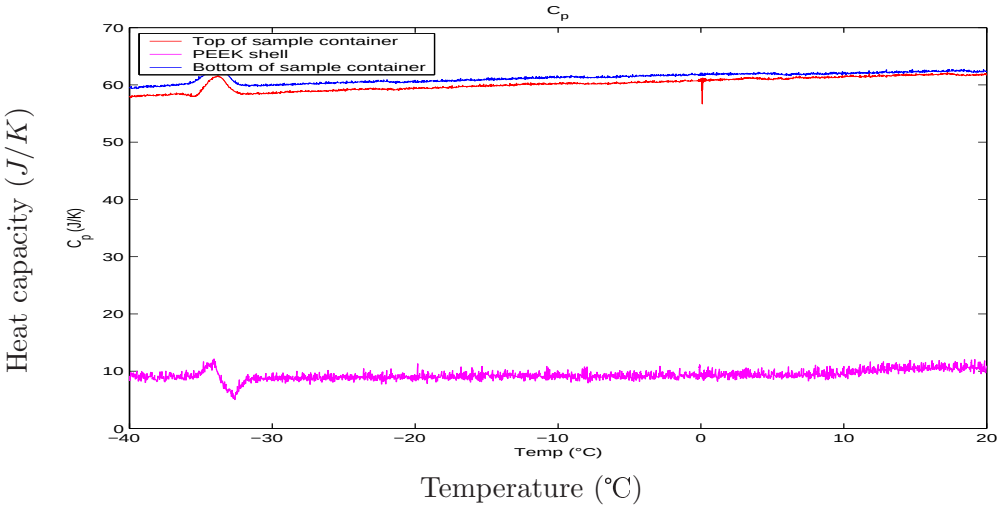

Figure 2.30: Heat capacity of different parts of the sample container

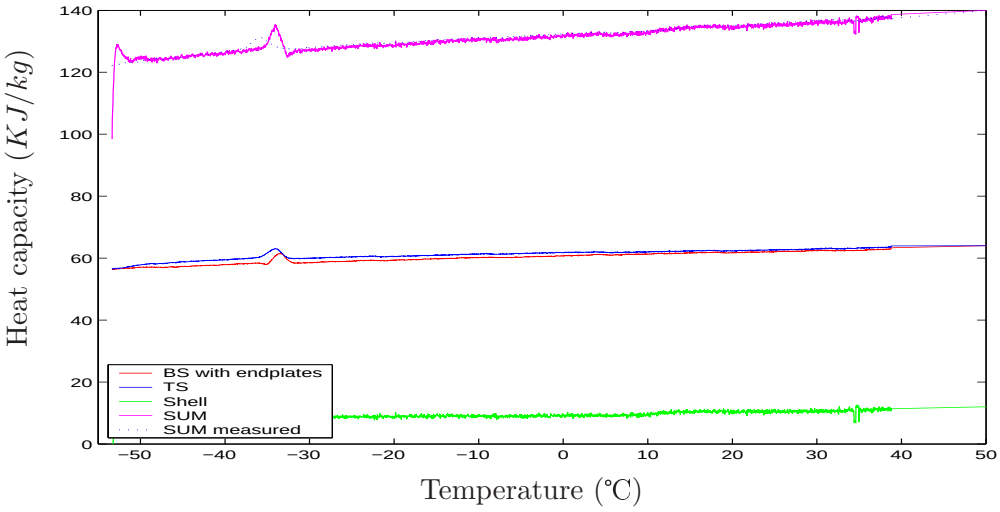

Figure 2.31: Sum of heat capacity of the sample container

Calibration of thermal conductivity against a known sample

The heat flow around the sample (2.32) was found by doing measurements on duran, also known as Pyrex. The thermal conductivity of Pyrex is certificated by BCR [76]. Duran is chosen as a reference material since the thermal conductivity has the same magnitude as food (water, meat and fish). The sample of duran is shown in Figure 2.32 was 22.4 mm thick and had a diameter of 45.0 mm.

Figure 2.32: The sample of duran

To ensure good thermal contact the surfaces of the two copper disks can be covered with silicon grease. These disks are parts of TS and BS and can be removed from the instrument (see Figure 2.8). Unfortunately this grease causes a large adhesion force which can damage the instrument when the sample is removed, and is therefore used only in three experiments on a sample of Pyrex. The average thermal conductivity for the three experiments is then calculated by (2.30) and compared with the thermal conductivity of Pyrex certificated by BCR (CRM039). The result is shown in Figure 2.33

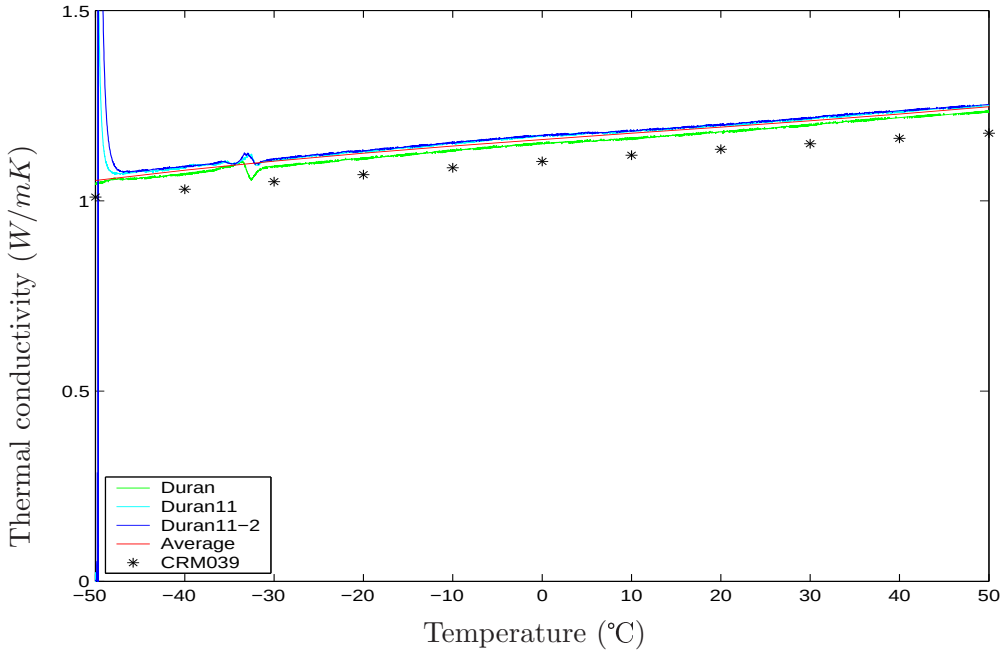

Figure 2.33: Average thermal conductivity of duran by (2.30)

The measurements Duran11 and Duran11-2 are done without taking the sample out of the instrument between the measurements. CRM039 is thermal conductivity of Pyrex certificated by BCR.

From this the correction in (2.30) was estimated to

$$\frac{A_P \lambda_P}{A_{Sa}} = 0.0575 + 1.107 \cdot 10^{-5} T - 3.054 \cdot 10^{-7} T^2 + 1.006 \cdot 10^{-7} T^3 \qquad (2.44)$$

where T is the temperature of the sample in ℃.

Thermal contact

Several measurements were done on Pyrex where the copper-copper surfaces in TS and BS were not covered with silicon grease. This was done to estimate the effect of imperfect thermal contact, and to say something about the repeatability of the instrument because of this imperfect thermal contact. This measurement where thermal conductivity is calculated by (2.32) with the correction given in (2.44) is shown in Figure 2.34.

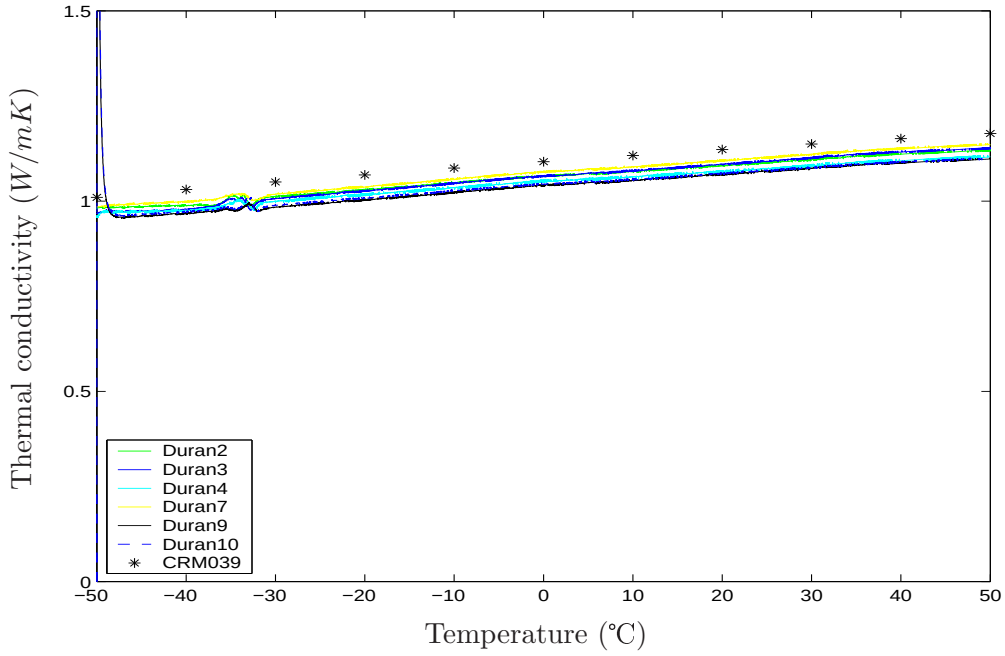

Figure 2.34: Thermal conductivity of duran by (2.32)

CRM039 is thermal conductivity of Pyrex certificated by BCR.

The thermal contact coefficient in (2.35) was from 2.34 estimated to $2200(W/m^2K)$. Calculated thermal conductivity from (2.35) for Pyrex is shown in Figure 2.35.

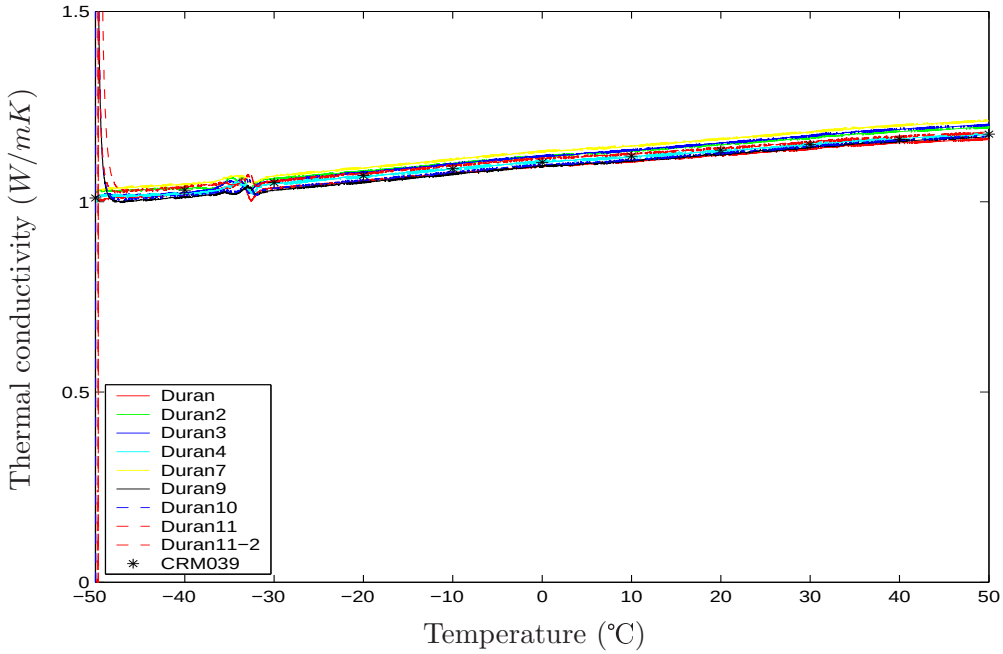

Figure 2.35: Thermal conductivity of duran by (2.35)

CRM039 is thermal conductivity of Pyrex certificated by BCR.

Figure 2.35 indicates a repeatability of 3.6%. The accuracy is found by measuring the thermal conductivity of other known materials with this calibration.

Calibration of heat capacity to correct for heat leakage.

As shown in the numerical simulation there is likely to be a heat leakage from the sample caused by the temperature difference between TS and BS. From the measurements done on duran K_a in (2.42) is $0.075 + 3 \cdot 10^{-5} \cdot T$ where T is the temperature of the sample in ℃. K_a is slightly dependent of the temperature which can be explained by radiation.

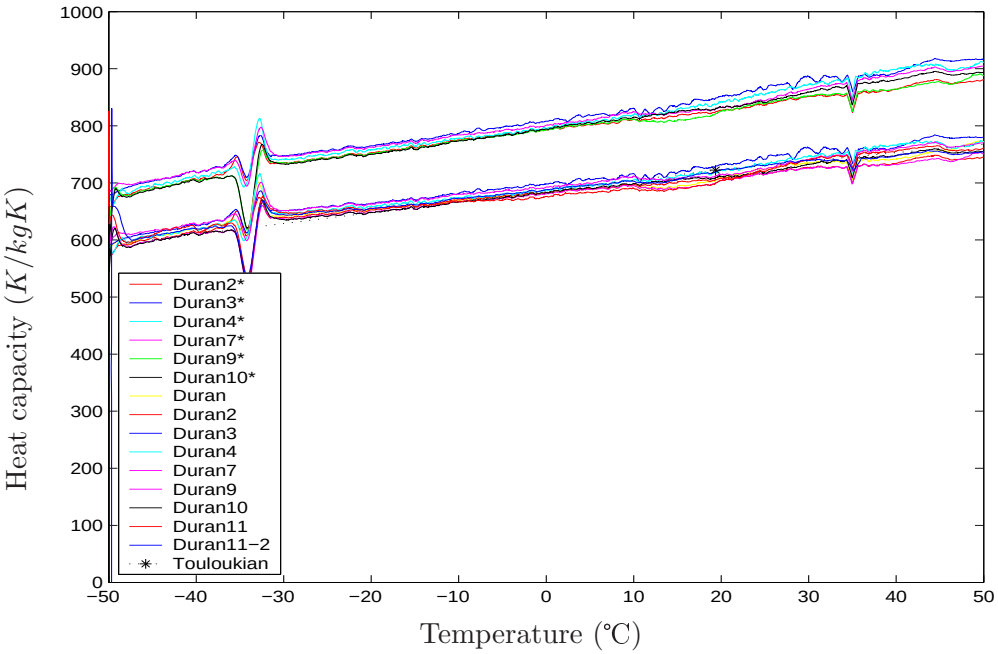

Figure 2.36: Heat capacity of duran by (2.31) and (2.42)

Heat capacity of duran calculated by (2.31) is marked with '*'. The heat capacity calculated by (2.42) is compared with the values given in the handbook "Thermophysical properties of high temperature solid materials" edited by Touloukian [77]

2.3.2 Measurement procedure

The sample is placed inside the PEEK ring with the two loose copper plates an each side. A tool is developed to do this. The tool ensures that the sample is 22 mm thick if the sample is liquid. The O-rings on the copper plates are greased with silicon to ensure that no liquid leaks from the sample. A picture of the tool is shown in Figure 2.37.

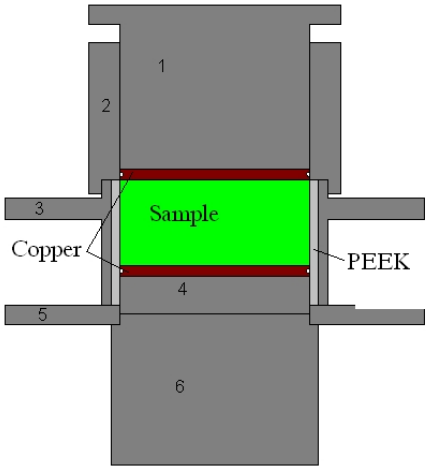

Figure 2.37: Tool for preparing the sample

The top and bottom surfaces of a solid sample are cowered by silicon grease to ensure good contact against the copper plates. This silicon influences the measured heat capacity. The other side of the copper plates and the fixed parts of the sample container are cleaned with ethanol. This ensures that the thermal contact resistance of these surfaces are almost equal in all experiments.

The weight of the sample is found by measuring the weight of the PEEK ring and copper plates before and after the sample is placed inside. The sample and the loose part of the sample container are placed inside the instrument. The sample is then strapped down between TS and BS by screwing a handle. Several parameters are then given to the control program in the thermal multimeter. The parameters are the name of the sample, the name of the instrument operator, the weight of the sample, the start temperature, the length of the pause before the measurement starts, the power to the sample heater and the stop temperature for the measurement. The operator must also decide how the sample expands, and at which temperature the enthalpy is to be zero. The experiment is then started and the controlling program does the rest.

The program starts the brine cooler and the sample is cooled to the start temperature. Then there is a pause before the heating starts. During heating the values of all sensors are logged and stored every 15 seconds. The program controls the shields and the temperature in the brine. When the sample is heated to the

stop temperature the controlling program stops the experiment, starts Matlab and terminates. A Matlab script calculates the thermal properties after the equations given in previous sections. This script is extensive since it converts data to Matlab format, imports data for the heat capacity of TS, PEEK and BS. These data must be interpolated so they can be used in the equations. Then the thermal properties are calculated. Charts are then made from the data and a report from the experiment is generated.

2.3.3 Results from measurements of reference materials

The performance of the thermal multimeter is estimated by doing measurements on materials where the thermal properties are known from the literature or measurements done in NTNU's plate apparatus. The reference materials were water, tylose and turbonitt.

A measurement was also done on an empty sample container. The instrument is not made for measuring thermal conductivity or heat capacity to air with any reasonable accuracy, but if the absolute value of measured thermal conductivity is far from 0.0241 W/mK which is the thermal conductivity of air at 0 ℃ and 1 atm., it is a strong indication that the instrument measures incorrectly.

Tylose (methyl cellulose) is according to Riedel [78] used as a thickener, agglutinant and emulsifier. It has become a reference material in food science since. Tylose with 77% water and enough salt to reduce the initial freezing point to -1 ℃ is known as "Karlsruhe test substance" and has very similar thermal properties as lean beef with 74% water content.

The sample of tylose was frozen and thawed twice and kneaded between each freezing before the measurement was done, to get rid of air bubbles and to ensure a homogeneous material. Still the tylose becomes more transparent during the measurement. Turbonit is also known as bakelite and is a fibrous plastic material widely used some decades ago as electric insulation in electric outlets.

Thermal conductivity

The thermal conductivity of water, tylose, turbonitt and the empty sample container are presented together with literature data or independent measurements.

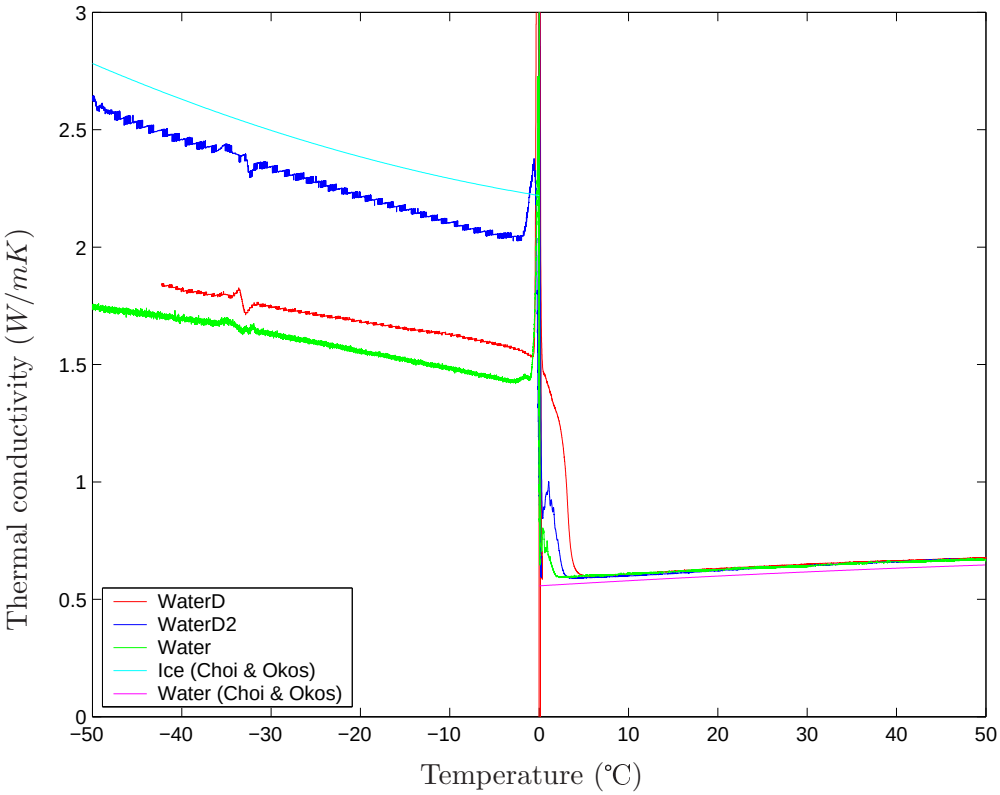

Figure 2.38: Thermal conductivity of water

Above freezing point, the measured thermal conductivity of water is 0.03 W/mK or 5% too high compared with Choi & Okos [60]. Below freezing point, the thermal conductivity of ice varies widely. This shows that the sample must be frozen in a controlled way, probably outside the sample container, to get a sample that is free of cracks and which has a flat surface against the copper plates.

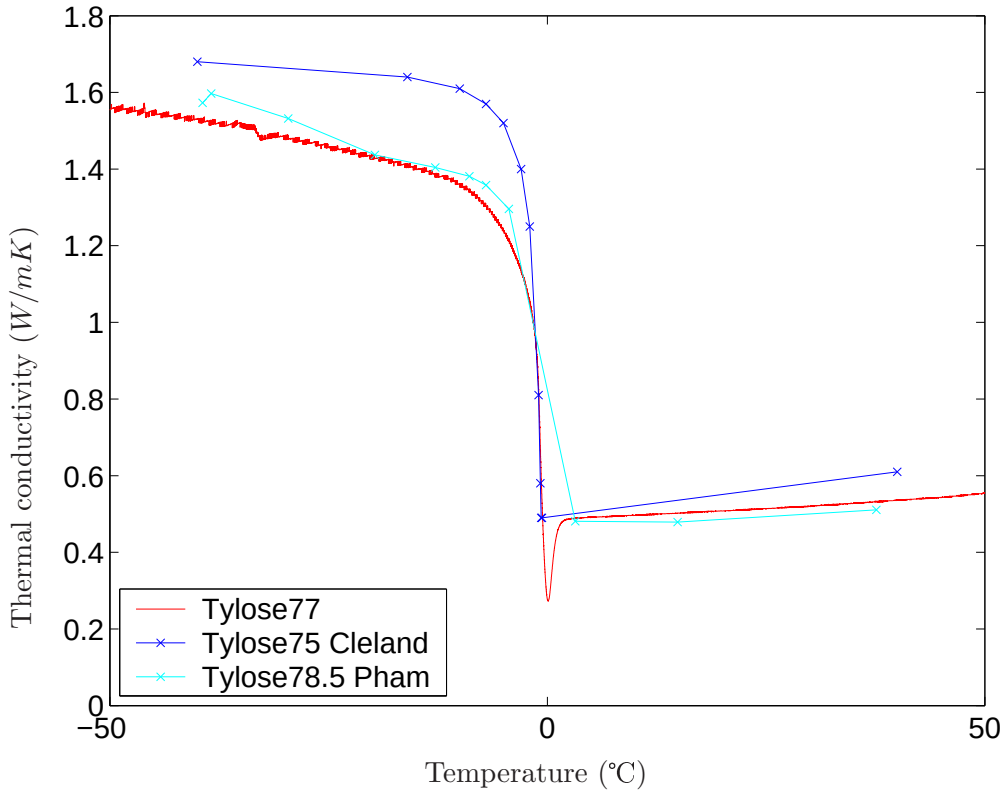

Figure 2.39: Thermal conductivity of tylose with 77% water

There was no literature data for thermal conductivity of tylose with 77% water. The measurement is compared with measurements done by Cleland & Earle [32] and Pham & Willix [79] who have done measurements of tylose with respectively 75% and 78.5% water. It should be expected that thermal conductivity should increase with increased water content. Here it is opposite, indicating that one or both of the literature measurements should be done again. Above freezing point the measured thermal conductivity of water is 0.08 W/mK or 14% too low compared with Cleland & Earle and 0.02 W/mK or 4% too high compared with Pham & Willix. Below freezing point the measurements are fairly close to the measurements done by Pham & Willix, but there is an open question if the freezing has caused cracks in the tylose which causes the measured thermal conductivity to be too low.

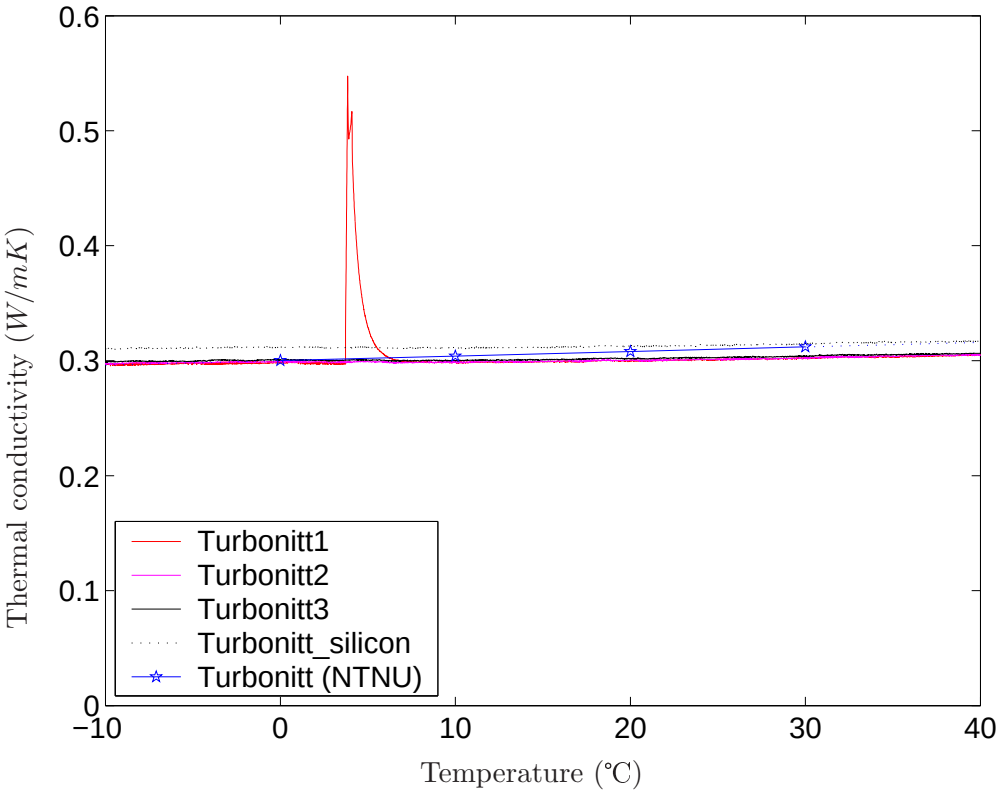

Figure 2.40: Thermal conductivity of turbonitt

Thermal conductivity is measured for turbonit with the plate apparatus at NTNU by Helge Jan Johansen. The measurements done in the thermal multimeter was done on the same sample. Brendeng & Frivik [80] has compared NTNU's instrument with other instruments in a test where the same material was measured by two other laboratories. The difference between the laboratories was 1.8% and 2.4%. Turbonit 1, 2 and 3 are three measurements on the same sample. In Turbonit_silicon the surfaces of the turbonitt are covered with silicon grease to get better contact between sample and copper. The difference between the measurements done in the plate apparatus (Turbonitt (NTNU) and the measurement done in the thermal multimeter is less than 0.01 W/mK or 3%. The peak at about 5 °C for Turbonitt1 is caused by a changed in supplied heat caused by the operator to show that measured thermal conductivity is independent of the supplied heat.

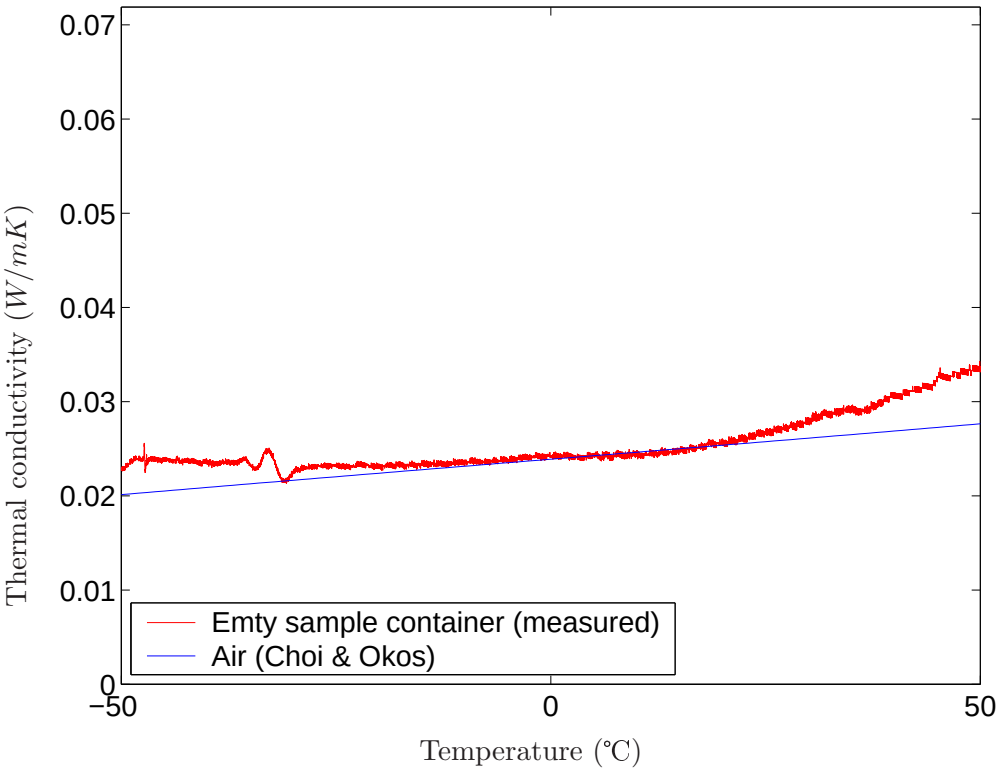

Figure 2.41: Measured thermal conductivity of empty sample container

There is good correspondence in the absolute measured value of thermal conductivity of air, and literature data of thermal conductivity of air. The calculated thermal conductivity for the other materials is therefore more likely to be correct. The relative error is 20% since the thermal conductivity is so low.

Heat capacity and enthalpy

Heat capacity and enthalpy are measured and compared with literature values for water, tylose and copper. The measurement of copper is the most accurate one since the high thermal conductivity of copper gives almost no temperature difference between TS and BS. Then there is little temperature difference between any part of the sample and the shield.

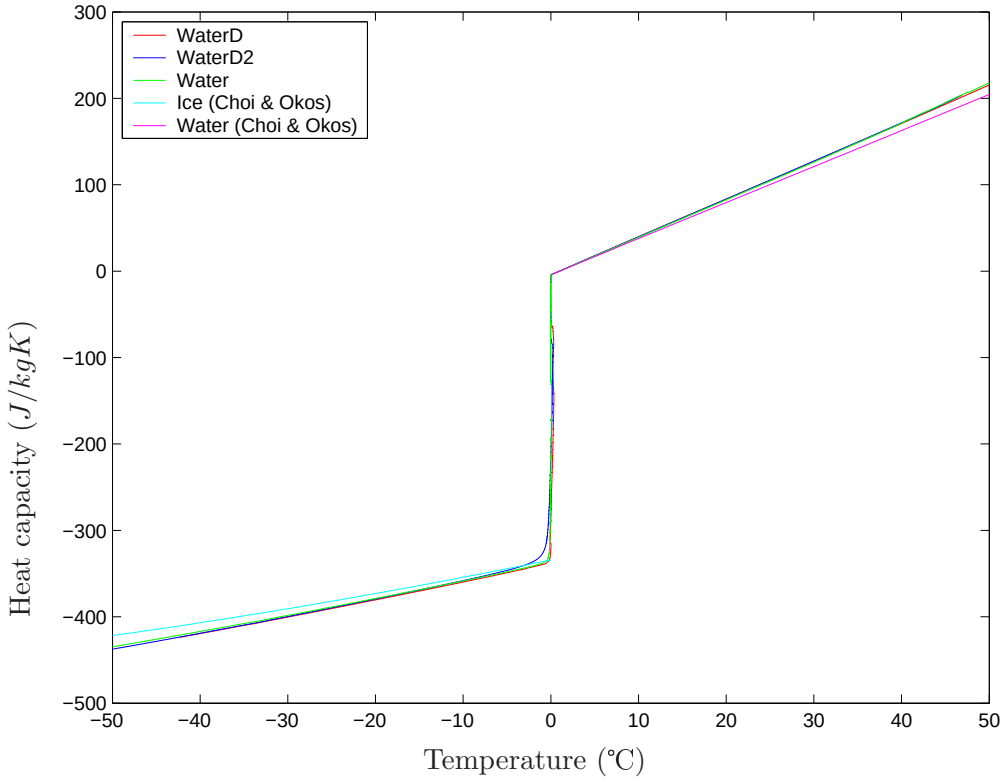

Figure 2.42: Enthalpy of water

The measurement is plotted together with data on enthalpy presented by Choi & Okos [60]

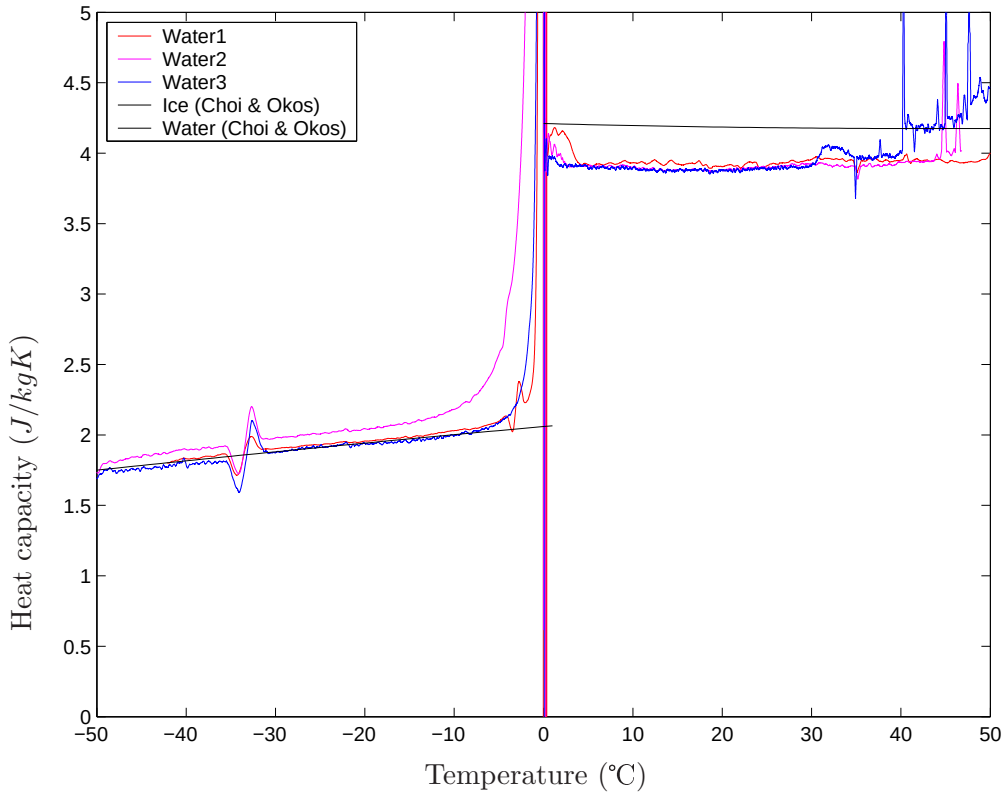

Figure 2.43: Heat capacity of water

The measurement is plotted together with data on heat capacity presented by Choi & Okos [60].

The measurement is 7% below the literature value for temperatures above the freezing point. The measured values below the freezing point are within 4%. It is unclear why there is noise at the end of one measurement, but it can be caused by a leakage of water from the sample container.

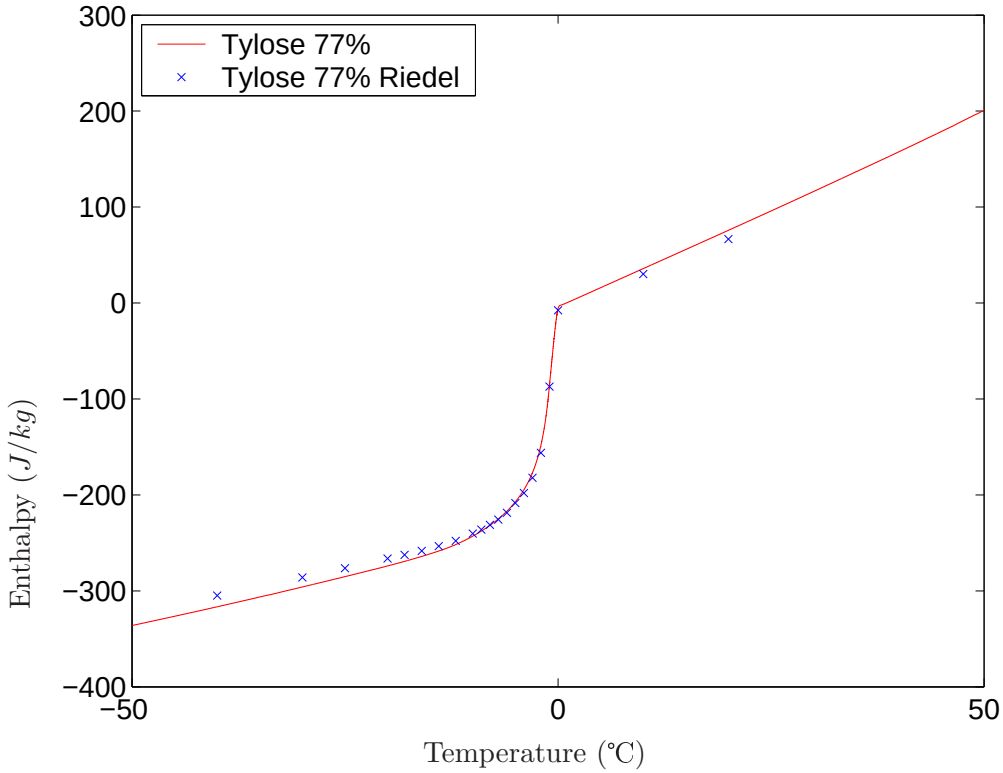

Figure 2.44: Heat capacity of tylose

The measurement is plotted together with data on enthalpy presented by Riedel [78]. The difference in measured enthalpy difference from -40 to +40 °C here and measured by Riedel is $21 J/kg$ or 5%.

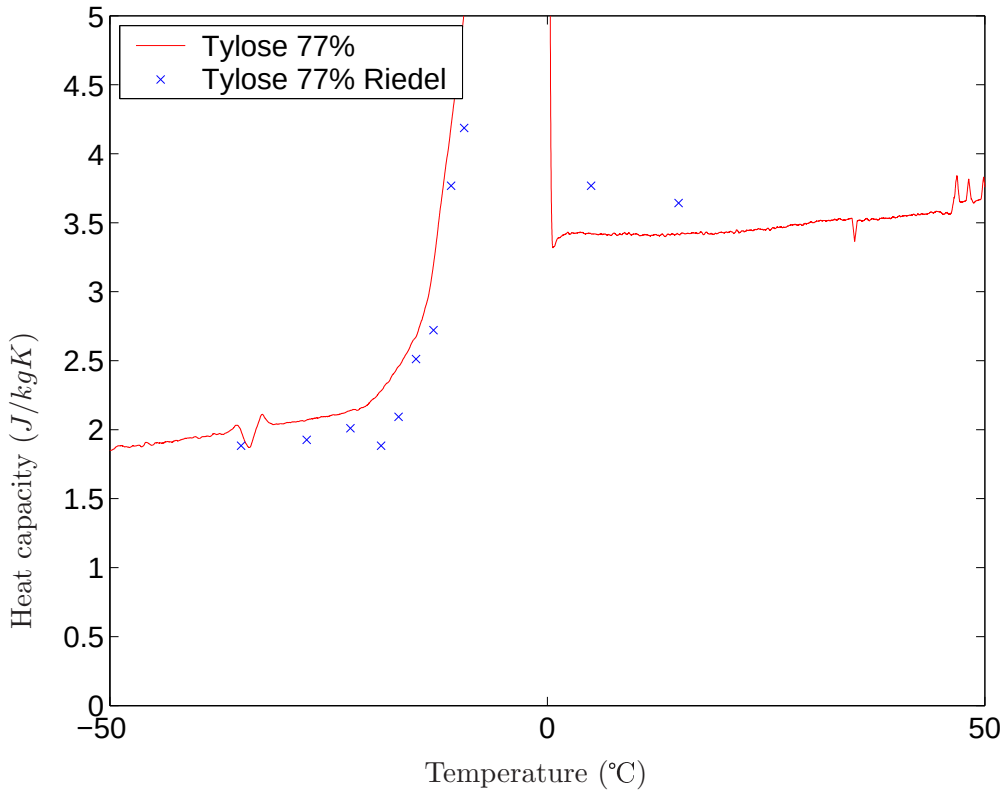

Figure 2.45: Heat capacity of tylose with 77% water

The measurement plotted together with data on heat capacity presented by Riedel [78]. Riedel gives enthalpy as function of temperature, which the heat capacity is calculated from.

Time-temperature progress, initial freezing point and density

Often it is interesting to measure the initial freezing point of food. In a measurement done by the thermal multimeter the initial freezing point is found by inspection of the temperature-time progress of BS_Pt100.

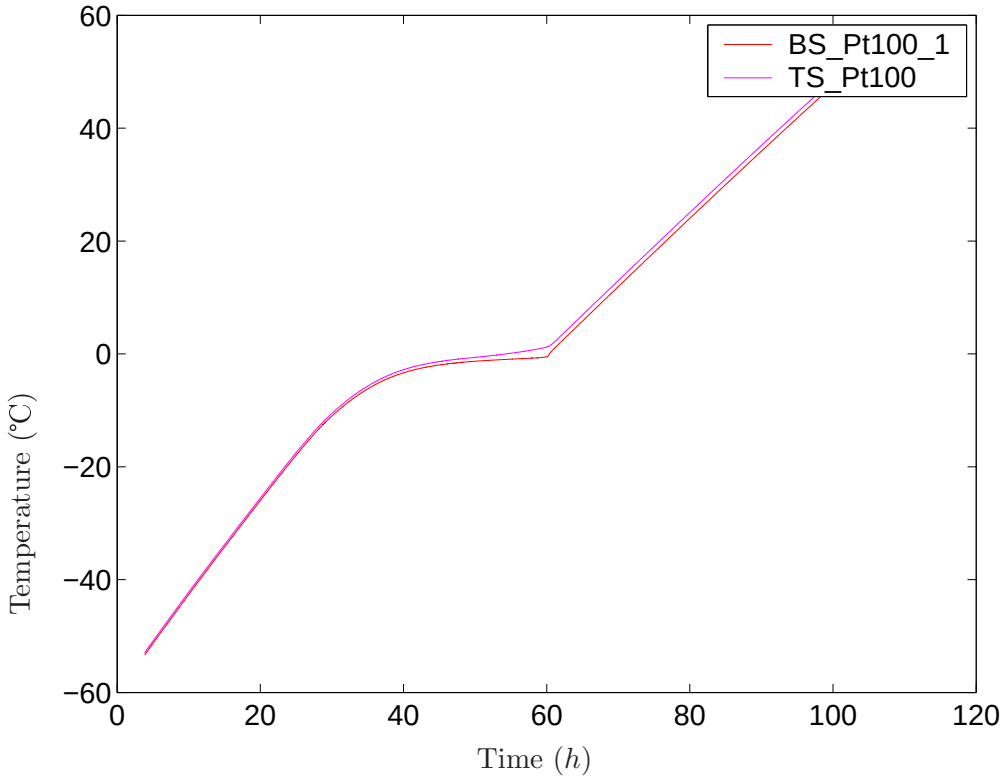

Figure 2.46: Time-temperature progress in the measurement on tylose 77%
Heat is added at constant rate. The temperature will then rise at a constant rate until the tylose starts to melt. Then the curve flattens off since supplied heat is used to melt the material. Since heat is added at TS tylose close to BS melts latest. When the last of the tylose melts there is a sharp knuckle point in the plot. The temperature at this knuckle point is the initial freezing temperature.

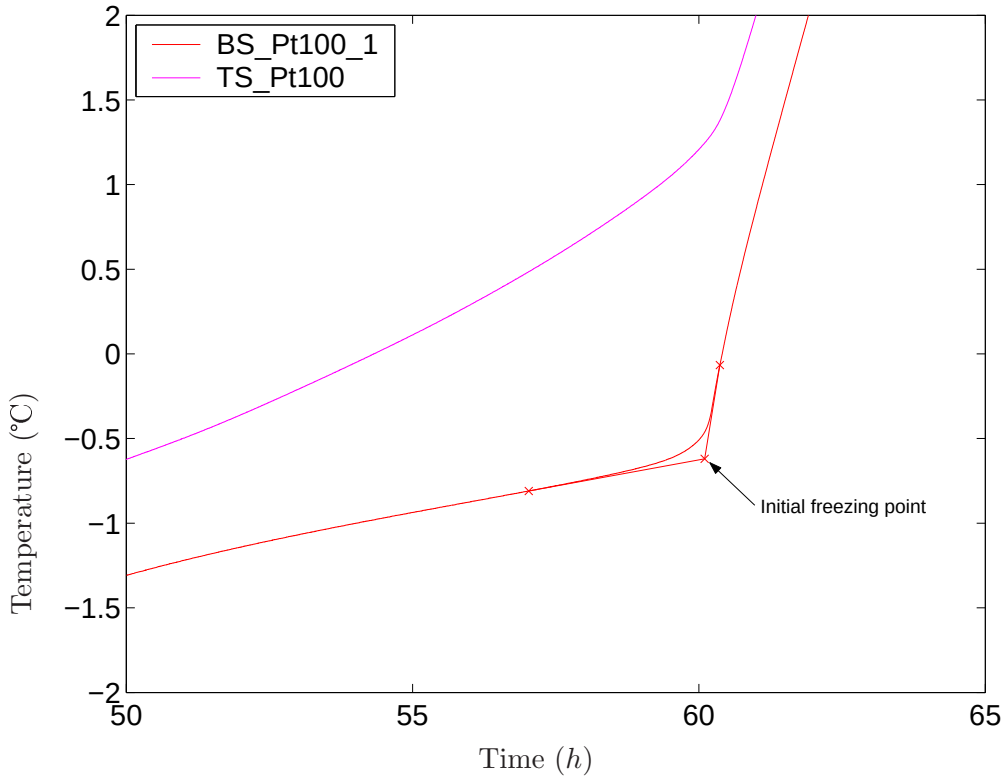

Figure 2.47: Time-temperature progress in the measurement of tylose 77% (Zoom)

The figure shows a close up of the Time-temperature progress in Figure 2.46. It is indicated how the initial friezing point can be found graphically.

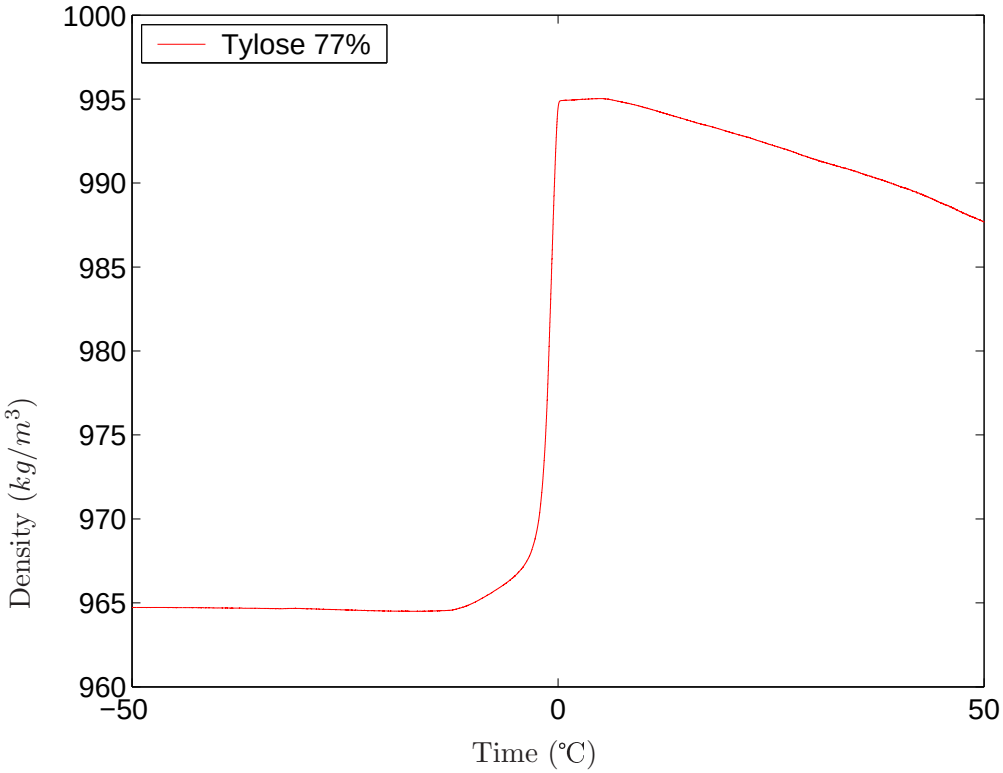

Figure 2.48: Measured density of tylose 77%

The figure shows the change in density as a function of temperature for Tylose with 77% water content.

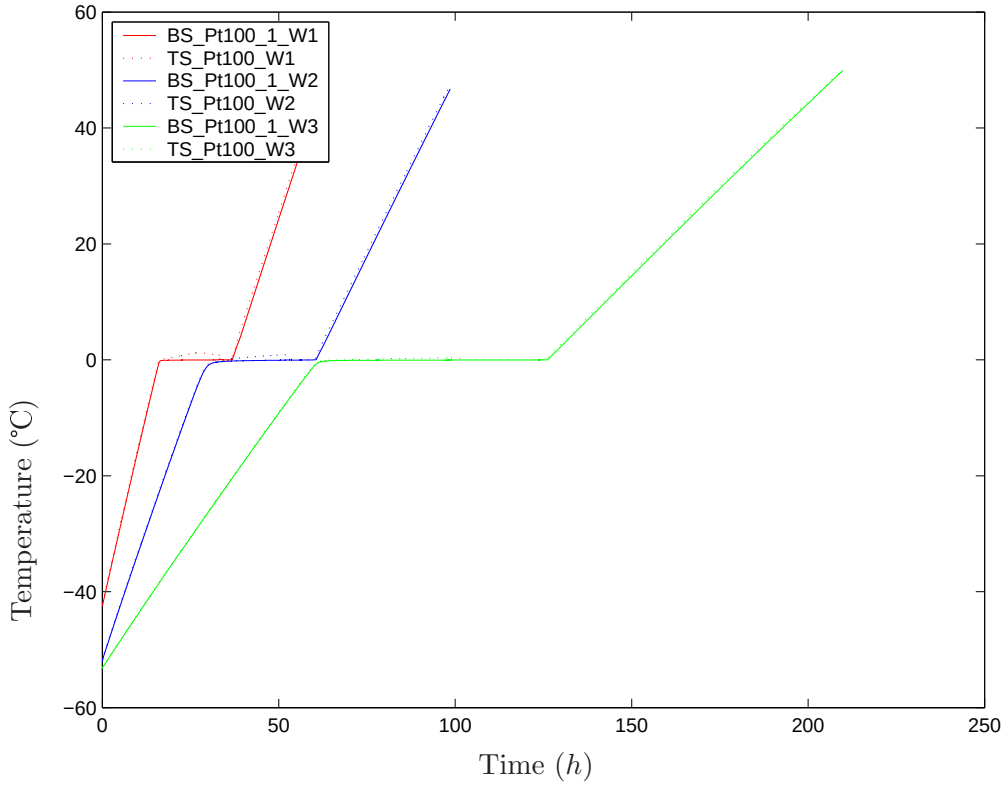

Figure 2.49: Time-temperature progress in the three measurements on water

The supplied heat was respectively 0.0461 W, 0.0932 W and 0.1400 W.This is the reason why the measurements have taken different times. Inspection of the relevant charts for thermal conductivity and heat capacity shows that the measured values also in real measurements are independent of the magnitude of supplied heat. TS_Pt100 shows that the temperature drops right before all the ice has melted. The ice at the bottom of the sample container has probably loosened and floated up

2.3.4 Raw data from measurements

The raw data file from a measurement is a tab separated array 29 columns wide and several thousand lines high. Each line gives data for one moment. Columns 1-6 are month, day, year, hour, minute and second. Columns 7-11 are temperatures measured with Pt100 elements, respectively ShC-Pt1000, SaC-Pt1000, BS-Pt100-1, TS-Pt100, and Air-Pt100. Column 12 is the temperature in the room (Room-Temp) where the thermal multimeter is placed measured with a thermoelement. For columns 7-12 the temperature is calculated by the Agielnt 34970A switch units. Columns 13-16 are the voltage over the ten point thermopile, respectively SaC-BHS-TP, BHS-BS-TP, THS-TS-TP and TS-BS-TP. These voltages are converted to temperatures by the post-processing program. Columns 17-22 are voltage to the heaters, respectively THS-H, TS-H, BS-H, BHS-H, SaC-H and ShC-H. Columns 23-28 are voltage over resistors with known resistance in parallel with the heaters, respectively THS-H (5), TS-H (20), BS-H (20), BHS-H (5), SaC-H (5) and ShC-H (5). The number in the brackets is the resistance. This gives enough data to calculate power to each heater. Column 29 is a voltage signal from the sensor for measuring length.

2.3.5 The post-processing program

The Matlab code for the post-processing program is available from this theses download page. (Se page 155.) The program consists of several procedures linked together by the master program called "Totalrun.m". First the procedure "Post-Processing.m" read the raw data file and store the data in several Matlab variables. Length of sample, power to the heaters and time in seconds is calculated. Then the procedures "CalibrationCharts.m" and "CalibrationCharts_comparason.m" prepares the data from calibration measurements. "Measurements_TM.m" starts by integrating the heat flux to find total heat capacity and enthalpy of the sample and sample container. Data from the calibration measurements are then interpolated to the measured data so they have the same number of points. Then the temperature difference over the thermopile TS_BS_TP is calculated. Thermal conductivity, heat capacity and density of the sample are then calculated from the equations presented in Section (2.2.3). The procedure "Charts.m" shows charts for calculated thermal conductivity, heat capacity, density performance of the shields etc. The procedure "Rapport.m" generates a report in PDF format where charts are included. Data are transferred between the procedures by Matlab mat-files, so when the whole program has run once any procedure can be run as an independent program. This saves time since if a change is done in the procedure "Charts.m"

only "Charts.m" and "Rapport.m" must be re-run. Most of the procedures call sub-procedures made for them, so the total program is comprehensive.

2.3.6 Sources of error and uncertainty

Many of the sources of uncertainties and errors are discussed earlier. Here the sources are collected, and their influence is estimated. It is also pointed out which sources of errors the user of the thermal multimeter must be aware of.

Accuracy of the temperature measurements

There are two types of temperature sensors in the thermal multimeter. They are Pt100 elements which measures absolute temperature and thermopiles which measures temperature difference.

TS_Pt100 and BS_Pt100_1 are used for measuring heat capacity. The absolute accuracy of elements are $\pm 0.06\ K$ but the repeatability is better than $\pm 0.01\ K$ as shown in Section 2.3.1. The repeatability is relevant for the measurement of heat capacity.

It is also shown in Section 2.3.1 that measured temperature difference done with the thermopile TS_BS_TP can be expected to have an uncertainty of $\pm 0.01\ K$ when the temperature difference is close to $0\ K$.

When a property is calculated from the measurement data, one way to evaluate how the uncertainty in one measured value influences the uncertainty in the property is to insert the measured value $\pm$ the measured values uncertainty into the equation used for calculating the property. If a variation of $\pm 0.01\ K$ in measured temperature is inserted into (2.31) for the measurement of frozen tylose at -24 ℃ measured heat capacity becomes

$$c_{Sa} = \frac{0.0947\ W \frac{2 \cdot 900\ s}{(-23.74 + -24.18 - -24.15 - -24.59) K \pm 0.01\ K)} - 29\ J/K}{0.0354\ kg} = 2270\ J/kgK \pm 3.2\%$$

There is still a $\pm 0.06\ K$ uncertainty in the absolute temperature this heat capacity is measured for.

As with the heat capacity, the uncertainty for thermal conductivity for tylose is calculated by (2.30). This because the uncertainty in measured temperature difference becomes

$$\lambda_{Sa} = \frac{58\ W/m^2 \cdot 0.0227\ m}{0.4856\ K \pm 0.01\ K} \cdot \frac{99\ J/K + 61\ J/K}{219\ J/K} = 1.98\ W/mK \pm 2.1\%$$

The magnitude of the uncertainty is dependent on the thermal properties of the sample.

Accuracy of measured supplied heat

There is an error of 0.5% in the measured supplied heat because the heat which is released from the wires which supplies the heaters with current is measured too. See Figure 2.12. This error is small compared with other errors and can therefore be ignored.

The uncertainty in measured supplied heat is very small.

Performance of the shields

As shown in Figure 2.29 the shields perform well. The performance must however be checked after each measurement because some examples of shield failure have been observed. Unstable regulation have been the most common cause of failure.

Heat leakage and varying contact heat resistance

Both numerical simulations and measurements show that there is a heat leakage between the sample and the shield caused by the temperature difference between TS and BS. This heat leakage is unavoidable, and influences both measured heat capacity and thermal conductivity.

The thermal contact between TS, the sample and BS is dependent of how carefully the copper surfaces are cleaned before they are put together. The thermal resistance is assumed to be the same from measurement to measurement.

Both heat leakage and thermal conductivity are corrected for, as described in (2.35), (2.42) and section 2.3.1. The error if the heat leakage is ignored is 5% according to Figure 2.33. The error if the thermal resistance between the copper plates is ignored is 10%. A doubling of the thermal resistance will cause an additional error of 10%. This can be seen form Figure 2.34. The magnitude of the error is dependent on the thermal properties of the sample. The errors are corrected for, but the magnitude of the correction gives an indication of how variation in internal heat leakage and thermal contact resistance influence the accuracy of the measurement.

Difference between sample containers

There are four copper plates, but only two of them are used in a measurement. The two others are spare. The difference in weight between the heaviest and the lightest are $1.3g$ or $0.5\ J/K$ For the duran sample this constitute 1% but it will constitute more for lighter samples. There is also some smaller variation in weight of the PEEK containers, but less than for the copper plates.

Measurement of sample weight and length

Weight can be measured accurately. It should however be measured both before and after the measurement, since liquids can disappear through leakage and evaporation, if the O-rings do not seal it completely. For solid samples the length of the sample can be measured before the sample is put into the instrument. The sample is 22 mm long, so an accuracy of 0.1 mm in the length measurements gives 0.5% inaccuracy. Liquid and plastic samples are prepared with a tool which is shown in Figure 2.37. This tool gives a sample length of 22 mm, but this length is influenced by freezing. It can also be difficult to ensure that no air is inside the sample container. Air can also be dissolved in water.

The instrument for measuring length of the sample during a measurement has an accuracy of 0.01 mm according to the manufacturer. Given the large changes in temperature, and that expansion of the sample is transferred to the length sensor through four thin steel tubes, measured length has larger uncertainty. It is still suited for measuring change in density during freezing. The length sensor should be calibrated by placing a sample with known length into the sample container regularly.

Leakage from liquid sample

To avoid leakage the O-rings must be greased every time a new sample is prepared. Measurements of liquids materials above 30 ℃ increases the chance of leakage.

Preparation of the sample

Here errors can be introduced by air inside the sample container. It is also important not to change the properties of the sample during preparation. If there is air in the sample and the sample is compressed thermal conductivity will increase in most cases. In general thermal conductivity can easily be changed when the sample is handled.

Natural variance between samples of same material

For most food materials it is important to be aware of natural variance. The thermal properties of salmon flesh are dependent on the amount of fat, muscle etc., which again can change from fish to fish.

2.4 Discussion and conclusions

When a measurement of thermal conductivity and heat capacity is done by constant heating of the sample from one side, the thermal conductivity is measured with accuracy better than 5% and the heat capacity with accuracy better than 7%. These numbers are based on measured values on materials where the thermal properties are known from the literature, and estimates of how uncertainties in measured temperatures influence the calculated thermal properties. The repeatability of the instrument is 2% for thermal conductivity. For heat capacity repeatability of up to 4% is observed.

The main sources of uncertainty are heat leakage around the sample and contact resistance between heater and sample. The leakage can be reduced by increasing the diameter of the sample. The area where there is a temperature difference will then become smaller compared with the cross-section area. This will reduce the percentage heat leak. A measurement will then of course demand more samples. It is also possible to increase the accuracy of the measured thermal conductivity by dividing TS into a heater and a guard, the same way as is done in hot plate apparatus. The heat capacity can then be found by adding heat supplied to the heater and the guard. This will not increase the accuracy of measured heat capacity.

A larger diameter combined with smaller distance between TS and BS will increase the accuracy in measured thermal conductivity for materials with thermal conductivity below $0.15 W/mK$. The reduced distance is necessary to decrease the temperature difference over the sample, and thereby the heat leakage on the edges. Reduced distance will make measurements on materials with medium thermal conductivity 0.5 to 4 W/mK less accurate since the accuracy of measured temperature difference becomes the limiting factor.

The problems with correcting for the thermal contact resistance can be eliminated if the sensors for measuring temperature difference are placed inside the sample instead of inside TS and BS, but it will be difficult to find a practical solution for doing this. The thermal contact resistance will also be less important when the thermal conductivity of the sample is low.

It is necessary to take more measurements of known materials to verify the readings and this may improve the accuracy of the instrument which at the moment is based on relatively few measurements. It is also necessary to find procedures for freezing samples so the thermal conductivity of frozen materials becomes reproducible. The accuracy of measured thermal properties is not outstanding, but the results can be used. The instrument also gives so many measurements at all temperatures that the curve for the thermal properties can be considered continuous. The sample size is large enough to measure inhomogeneous materials. The preparation of sample and measurement procedure is also simple. The instrument is robust, and over all well suited for measurements on difficult and messy materials like food.

Chapter 3

Measuring local heat transfer number (α) by shell freezing

3.1 Introduction

This Chapter shows how the local heat transfer number (α) can be found by shell freezing of transparent jelly. The ice shell thickness and the time the jelly is in the freezer are measured. α can be estimated by Plank's equation. This is posible because Plank's equation is not mathematicaly ill-posed with regard to α, contrary to the heat equation, (1.1). Transparent jelly is suited because the freezing front is destinct in this materiale when cut through.

3.1.1 Description of the heat transfer coefficient

The heat transfer coefficient (α) describes the heat flow between the surface of a solid object and a fluid flowing around the object. α is defined as

$$\alpha \equiv \dot{q} / (T_f - T_s) \tag{3.1}$$

T_f is the temperature in the main fluid stream and T_s is the temperature of the surface. $\dot{q}$ is the heat flux normal to the surface. Generally the fluid flow is so fast and the objects are so small that no temperature difference can be measured in

the free stream. α and the product surface temperature will however vary over one product. For simplicity α is therefore often defined as an average over the whole product. To define α for every point on the surface of the object demands that α can be measured at every point. When α is used to solve practical problems it is important to be aware that this is a simplification. α must be measured. To understand why, the factors which influence α must be identified. They are therefore outlined in the following paragraphs.

Since the fluid transports heat while moving (convection) the fluid flow field must be described in order to be able to describe the heat flow. When a fluid flows along a surface the surface will decelerate the fluid and create a speed profile in the fluid from zero speed at the surface to free stream velocity at a distance where the present of the surface no longer influence the fluid. This speed profile is known as the boundary layer. If the flow is turbulent, the boundary layer will consist of a laminar part close to the surface and a turbulent part farther out. The thickness of the laminar layer is dependent on the surface roughness, surface orientation, surface curvature, other objects close to the surface, free stream velocity and fluid properties. (See Figure 3.1)

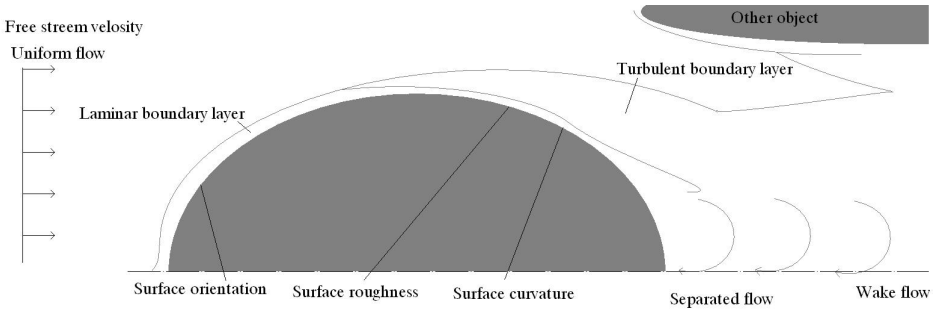

Figure 3.1: Fluid flow around an object

The number of factors, the problem in describing some of them accurately and the complexity of Navier-Stokes equations make it clear that calculating the fluid flow field in the boundary layer is a challenge.

Now, if there is a temperature difference between the surface and the free stream, there will be heat transport. Temperature is a continuous property, meaning that that there are no jumps as suggested by the definition of α. Since the temperature as function of position changes rapidly in the boundary layer a fine

grid is necessary to do simulations. Heat is transported by conduction, convection and radiation. The Navier-Stokes equations which describes the conservation of momentum must therefore be combined with equations for the conservation of energy when the heat transport is to be calculated. Carrying out such a calculation is beginning to become difficult.

In freezing, for unpacked food, latent heat is also transported by evaporation and sublimation. The α for this heat transport is normally given as a separate, latent α, since it can be calculated from the weight loss or gain to the object. Both surface properties and transport coefficients change with temperature, especially during freezing because of the change in the physical properties, and in some cases, the shape of the food. The temperature-dependent thermal properties of food must also be included in the calculations. It can be discussed if it is possible to include all these factors in a calculation of heat flow from the surface, but it is certainly too time consuming today for any practical purpose.

Therefore all these factors are hidden in α. Because of all these factors α must be measured. Regardless of measuring method, it is necessary to plan the experiment well to avoid changing any of the factors so much that a completely other α than the real one is measured.

Much work has been done to find correlations for α from the physical properties and the speed of fluid. Incropera and De Witt [22] list correlations for several objects with simple geometry in free stream. The correlations differ widely with geometry. For a sphere Whitaker [81] recommends an expression in the form (3.2)

$$\overline{Nu}_D = 2 + \left(0.4Re_D^{1/2} + 0.06Re_D^{2/3}\right) Pr^{0.4} \left(\frac{\mu}{\mu_s}\right)^{1/4} \tag{3.2}$$

$$\left[\begin{array}{l} 0.71 < \mathrm{Pr} < 380 \\ 3.5 < Re_D < 7.6 \cdot 10^4 \\ 1.0 < \left(\frac{\mu}{\mu_s}\right) < 3.2 \end{array}\right]$$

The Nusselt number is here an average for the whole sphere.

Because of the complex shape of frozen food products and the effects of shelves etc. such correlations for α are usually too inaccurate to be of any use in freezing technology research. A good method for measuring the α is therefore important.

3.1.2 Methods for measuring the heat transfer coefficient

The heat transfer coefficient α can be found in several ways. See Rahman [36] for a review of methods used in industrial food processing. Some of the common

methods are referred here.

α can be estimated by inverse heat conduction. The estimate is based on measuring the temperature history at two or more positions in the material. By combining measurements, knowledge of the thermal properties and position of the temperature sensors, heat flux and the temperature on the surface can be estimated. These are ill-posed problems, because the temperature history is to be calculated from the present internal heat profile. However, this is mathematically impossible. The reason is that the heat equation gets an infinite number of solutions if it is used backwards. A proof is presented by A. Iserles [73]. To solve this kind of problem you have to make a qualified guess about α, and then see if the simulations give the correct temperature in the measuring points. If the temperature is wrong, you correct your guess. This is very time consuming process. If α is time dependent, varies over the surface etc. it may not be possible to get a result at all. Some statistical methods are developed to solve ill-posed problems more efficiently. Se Beck et al. [82] for further details. To avoid ill-posed problems, constant heating can be supplied to the object of interest, to obtain a stationary problem. See Rahman [36] for a short review.

α can be measured with a suitable electric sensor. When using a sensor it is important to evaluate the disturbances the sensor introduce. The size of the sensor, and the heat flux from it should be considerably smaller than the size of the object and heat flux from the object. There are two types of electric sensors for measuring α, the heat flux sensor and the heat supplied sensor. Both sensors measure the average α over the area of the sensor. This means that the sensor must be as small as possible when measuring the local α. The accuracy of both sensors obviously depends on how accurately temperature and supplied heat can be measured. As the sensor size decreases, the accuracy is also increasingly limited by the heat leakage on the edge of the sensor. The leakage can be reduced by a guard. This means that the sensor is surrounded by a thin layer of insulating material, and outside the insulation the temperature is controlled to be the same as on the sensor. Since the guard needs a heat supply, the heat supplied sensor is usually chosen when small accurate sensors are required. This kind of sensor tends to become expensive.

The first type, which is also used as a heat flux sensor, consists of a thin plate of a material with known thermal conductivity and small heat capacity. The temperature difference over the plate is measured, usually with a thermopile. The surface temperature of the plate is also measured. The heat flow through the plate

can then be calculated by the formula

$$\dot{q} = \frac{\lambda}{L}\Delta T \tag{3.3}$$

where $\dot{q}$ is the heat flux, λ is the thermal conductivity, L is the thickness of the plate and ΔT is the temperature difference over the plate. To find α, the ambient fluid and surface temperature must be measured separately. Figure 3.2 shows how the sensor is placed on a material.

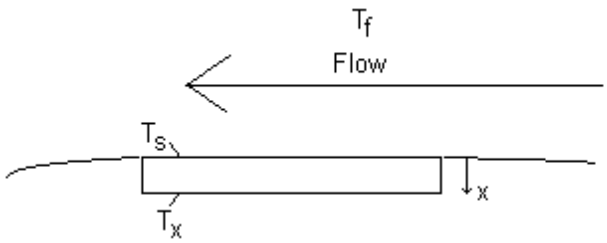

Figure 3.2: A heat flux sensor used for measuring the local α

Apart from accuracy in temperature measurements it is the uncontrolled heat flow on the edge which limits the accuracy of the sensor shown in Figure 3.2, especially for small sensors. This edge effect can be reduced by a guard, but introducing such a guard is technically difficult. Therefore, for this type of sensor usually no effort is made to reduce the edge effect. Still even small sensors of this type can be reasonably accurate because the sensor is thin which reduces the area heat can flow through in radial direction. The material the sensor is placed on will also act as a fairly good guard. The sensor can also be improved by placing an insulating material around the edge. It is suitable for measuring the transient α during freezing. If the object is not heated from the inside, the measurement will be dynamic. If the temperature on the surface is controlled, the sensor or the sample needs additional heating. Sensors of this type are robust.

The second type which is the heat supplied sensor shown in Figure 3.3, a known amount of heat is added to a plate of a material with relatively high thermal conductivity. The plate is insulated and guarded so (ideally) all the added heat leaves through the surface into the fluid. $\dot{q}$, T_s and T_f are measured directly. α is then calculated by (3.1).

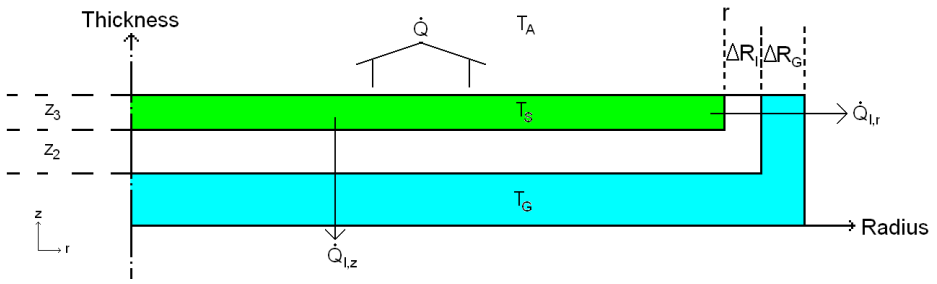

Figure 3.3: Guarded heat supplied sensor

The advantage of this sensor is that the temperature on the surface can be controlled separately from the object. As the size of the sensor decreases a higher accuracy is required when measuring temperatures and the heat flow. Therefore, such devices are usually relatively large and cannot be used to measure α on the surface of small objects. A large sensor will also make a larger disturbance in the heat flow by its presence, because it emits heat. Harris et al. [83] have made one only 40 mm in diameter, which is still large compared to many kinds of frozen products.

Another method for estimating α is to measure the heat flow indirectly. Kondjoyan & Daudin [13],[14],[15] have wetted objects of plaster and placed them in an air stream where temperature, air speed and air humidity are constant. After a while the plaster will obtain the wet bulb temperature. This temperature will be stable for a long time, until the surface of the objects dries, and water has to diffuse to the surface before it can evaporate. When the temperature is stable, the weight loss per time unit can be measured. All the energy needed to evaporate water is taken from the air, and an energy balance will give the heat flux and α.

Using Plank's equation to estimate α, is also an indirect method. Instead of the phase change of evaporation, Plank uses the phase change of freezing to calculate the heat flux. Since the freezing front is moving, it is a transient method. It is then also related to the method of estimating α by inverse heat conduction, but since Plank's equation is developed from the stationary heat equation, the problem is no longer ill-posed. This method is the subject for this chapter and is discussed more comprehensively later.

3.1.3 Methods for estimating or measuring the local α

With an exception of Kondjoyan's and Daudin's method, none of the methods mentioned in Section 3.1.2 are suitable to find the local α. A sensor with diameter of 40 mm can only measure local α for surfaces larger than 40 mm, and finding α by inverse heat conduction becomes very complex if the measured temperature inside the object is influenced by two or more surfaces with unknown α.

Kondjoyan's and Daudin's method is suitable since their whole object of plaster will have the same temperature. Since there is no tangential temperature gradient there is no heat flux along the surface. Since the measurement is done when the surface is fully wetted, there is no mass flux either, and the only problem is to measure the mass loss from different parts of the object. This can be done by constructing the object of units which are weighed separately.

The method presented here is to make a sample of jelly, and freeze it. After a measured time when the jelly is partially frozen the freezing is aborted, and the jelly is cut through with a sharp knife. The frozen layer (shell) thickness can then measured with a ruler, and local α can be calculated from the ice thickness. It can be performed this way since the freezing front is easy to see in the jelly as shown in Figure 3.6. There is some ice growth from the end of freezing to the jelly can be cut through and the shell thickness measured, but since latent heat is very large compared to sensible heat, and the frozen jelly in this time is heated by the surroundings, this growth can be neglected. Other methods for measuring the shell thickness are mentioned in the concluding remarks.

3.1.4 Range of application for the method

The method can be a valuable tool in the study of heat transfer in several settings. Jelly samples can be packed in different food packaging. Heat transfer through different parts of the packaging can be studied in detail. This is possible since the method finds the heat resistance independently of what is causing this resistance. Samples of jelly can be used as a sensor for finding changes in α in different settings of air freezing. In this way the effect of shelves and other obstructions from the air stream can be measured.

As seen from Figure 3.11 α is highly dependent on surface orientation and turbulent. In the industry the method is suitable for locating places in freezing tunnels, where freezing is not effective. This will be clearly visualised by differences in shell thickness for jelly samples at different places in the freezing tunnel.

3.2 Materials and methods

In freezing, when air temperature, geometry and the thermal properties is known, Plank's equation can be used to estimate α for a whole food sample. If the ice shell thickness of the food sample can be measured at two points in time, it should also be possible to use Plank's equation to estimate a local α by ignoring the tangential heat flux. α will be time average over a period. The reason that this is pointed out is that new methods for tracking the freezing front are now available and it is necessary to adapt Plank's equation to this method. The basis for the estimate of the local α is Plank's equation for rod, cylindrical shell and spherical shell.

The objective of this chapter is to show that the tangential heat flux in a frozen sample can be ignored if the frozen layer is thin. The chapter also shows how to quantify experimentally and by numerical simulations the accuracy of the the estimate of the local α. This will include estimates of the ratio between tangential and radial heat flux and some practical measuring problems. It will then be suggested how jelly can be used as a cheap and flexible sensor for estimating the local α, both for unpacked and packed products. Finally automatic methods for measuring the ice shell thickness are mentioned.

3.2.1 Plank's equation for a spherical shell

Plank's equation for freezing time is based on the simplification that food freezes at a fixed temperature, and that the latent heat is so much larger than the sensible heat that the sensible heat can be ignored.

Plank's equation is modified for several geometries, and a lot of work is done to incorporate pre- and after cooling in Plank's equation. See Cleland & Özilgen [84] for a review.

In this section Plank's equation is manipulated for objects of different shapes. This is done to show the relation between Plank's equation for different shapes, and to show for which ice thickens the choice of equation becomes important. Some of the deductions for Plank's equations for cylindrical and spherical shells are therefore presented here.

Ignoring sensible heat as Plank did when he deduced his equations, means that Fourier heat equation, (3.4), is reduced to Laplace's equation, (3.5), between the freezing front and the surface because c_p is zero and λ is constant.

$$\rho c_p \frac{\partial T}{\partial \tau} = \nabla \left(\lambda \nabla T \right) \tag{3.4}$$

$$\nabla^2 T = 0 \tag{3.5}$$

In spherical co-ordinates Laplace's equation becomes (3.6)

$$\frac{\partial^2 T}{\partial \hat{r}^2} + \frac{2}{\hat{r}} \frac{\partial T}{\partial \hat{r}} = 0 \quad r \leq \hat{r} \leq R \tag{3.6}$$

The boundary conditions for (3.6) is $T(R) = T_S$ on the sphere surface, and, $T(r) = T_{ff}$ on the freezing front. $\hat{r}$ because r is the position of the freezing front. The problem has a solution in (3.7)

$$T(\hat{r}) = \frac{(T_{ff} - T_S)\, rR \cdot \frac{1}{\hat{r}} + T_S R - T_{ff} r}{(R - r)} \tag{3.7}$$

The total heat flow through the sphere shell is described by (3.8).

$$\begin{aligned} \dot{Q} = -4\pi \hat{r}^2 \lambda \tfrac{\partial T}{\partial \hat{r}} \quad &= -4\pi \hat{r}^2 \lambda \tfrac{(T_{ff} - T_S) r R \cdot \frac{-1}{\hat{r}^2}}{(R-r)} \\ &= 4\pi R^2 \tfrac{r\lambda}{(R-r)R} (T_{ff} - T_S) \end{aligned} \tag{3.8}$$

By eliminating T_S from (3.8) with (3.1), (3.9) appears.

$$\dot{Q} = 4\pi R^2 \frac{r\lambda}{(R-r)\, R + \frac{\lambda r}{\alpha}} (T_{ff} - T_A) \tag{3.9}$$

If the heat flux at the freezing front is known, the differential equation (3.10) for the speed of the freezing front can be formulated.

$$\dot{Q} = -\frac{\frac{4}{3}\pi (r + dr)^3 \rho \Delta h_{ice} - \frac{4}{3}\pi r^3 \rho \Delta h_{ice}}{d\tau} \overset{\lim_{dr \to 0}}{=} -4\pi \rho \Delta h_{ice} r^2 \frac{dr}{d\tau} \tag{3.10}$$

This gives (3.11) which describes the rate of ice growth.

$$4\pi R^2 \frac{r\alpha\lambda}{(R-r)\, R\alpha + \lambda r} (T_1 - T_3) = -4\pi \rho \Delta h_{ice} r^2 \frac{dr}{d\tau} \tag{3.11}$$

(3.11) can be reformulated and integrated to (3.12).

$$\int_0^{\tau} \frac{(T_{ff} - T_A)}{\rho \Delta h_{ice}} d\tau = \int_R^{R_{ff}} -\frac{r \cdot ((R-r)\, R\alpha + \lambda r)}{R^2 \alpha \lambda} dr \tag{3.12}$$

$$\tau = \frac{\rho\Delta h_{ice}}{(T_{ff}-T_A)}\left(\frac{1}{3\alpha}R+\frac{1}{6\lambda}R^2-\frac{1}{2\lambda}R_{ff}^2 + \frac{1}{3R\lambda}R_{ff}^3-\frac{1}{3R^2\alpha}R_{ff}^3\right) \tag{3.13}$$

In (3.13) τ is then an expression for the freezing time of a sphere shell with outer radius R and inner radius ΔR_I. If $R_{ff} \to 0$, (3.13) becomes

$$\tau = \frac{\Delta h_{ice}\rho}{(T_{ff}-T_A)}\frac{1}{3}\left(\frac{1}{\alpha}R+\frac{1}{2\lambda}R^2\right) \tag{3.14}$$

(3.14) is Plank's equation for a sphere.

If $R_{ff} \to R$ and the shell thickness is defined as $L = R - R_{ff}$, $L \to 0$. (3.13) can then be reformulated to (3.15)

$$\tau = \frac{\rho\Delta h_{ice}}{(T_{ff}-T_A)}\left(+\frac{1}{\alpha}L+\frac{1}{2\lambda}L^2-\frac{1}{3R\lambda}L^3-\frac{1}{R\alpha}L^2+\frac{1}{3R^2\alpha}L^3\right) \tag{3.15}$$

When $L \to 0$ the terms in (3.15) with R in denominator is zero, and (3.15) becomes (3.16)

$$\tau = \frac{\rho\Delta h_{ice}}{(T_{ff}-T_A)}\left(\frac{1}{\alpha}L+\frac{1}{2\lambda}L^2\right) \tag{3.16}$$

(3.16) is Plank's equation for a rod which freezes from one side. The deduction to (3.16) proves that the equations give the same result if the frozen layer is thin. It also implicates that both (3.13) and (3.16) can be used to estimate a local α for a food sample of any shape if the frozen layer is thin.

Plank's equation for a cylinder shell can be developed by the same approach as for a sphere. The equation is:

$$\tau = \frac{\rho\Delta h_{ice}}{(T_{ff}-T_A)}\left(\frac{1}{2\alpha}R+\frac{1}{4\lambda}R^2+\frac{1}{2\lambda}R_{ff}^2\ln\left(\frac{R_{ff}}{R}\right) -\frac{1}{2R\alpha}R_{ff}^2-\frac{1}{4\lambda}R_{ff}^2\right) \tag{3.17}$$

(3.17) is also the result of an integration from R_{ff} to R of Equation 3 in Plank's [85] original article. Plank operates with an inner α between the frozen and unfrozen material. This inner α is set to infinite in the integration which leads to (3.17). If $R_{ff} \to 0$ (3.17) becomes Plank's equation for a cylinder. If $R_{ff} \to R$ the (3.17) becomes Plank's equation a for rod.

This proves that if the frozen layer is thin, Plank's equation for a spherical shell (3.13), Plank's equation for a cylindrical (3.17) shell and Plank's equation

for a rod (3.16) give the same result for estimated α (α). As long as the frozen layer is thin it is therefore indifferent which ((3.13), (3.17) or (3.16)) is used. The equation for a rod can therefore be used independently of the shape of the object.

When using the equation for a rod, (3.16), instead of the correct equation for spherical or cylindrical geometry, which ever is appropriate, α predicted wil be too high. The chart in Figure 3.4 shows how large the over prediction is compared to the relative shell thickness.

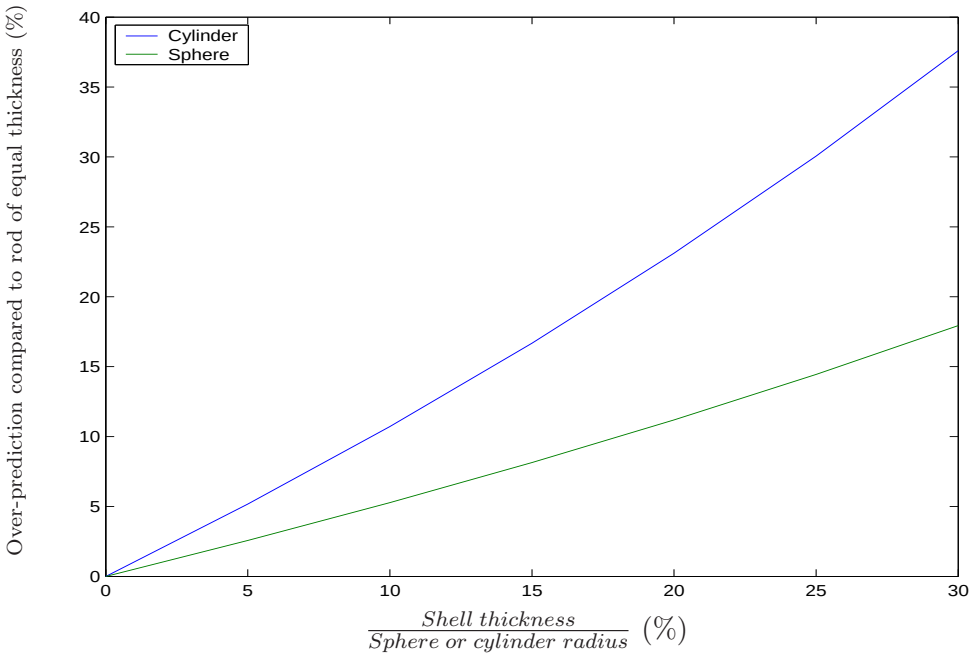

Figure 3.4: Over prediction of α by using Plank's equation for a rod

An example: A sphere with radius of 10 cm is put into a freezer where α is the same everywhere on the sphere surface. It is taken out when the outer 1 cm (10% of total radius on the x-axis) of the sphere has frozen into a spherical shell. If the equation for a slab (3.16)) is used to estimate α ($L = 1\ cm$) the estimated α is approximately 10% (find 10% on the x-axis and read the value for the blue line on the y-axis) to0 high compared to the correct α found by using the equation for a spherical shell (3.13) with $R = 10\ cm$ and $R_{ff} = 9\ cm$.

The choice of equation, ((3.13), (3.17) or (3.16)), becomes increasingly important with shell thickness. Figure 3.4 shows how important. Choice of equation depends on which geometry describes the surface where α shall be estimated. An example is shown in Figure 3.5

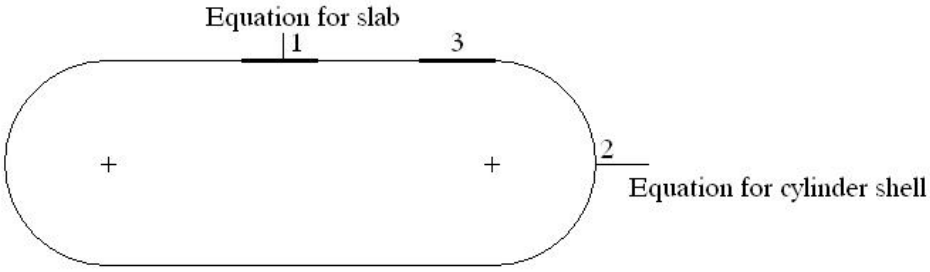

Figure 3.5: Choice of equation for estimating α

The picture shows a cross-section of an infinite long object. At position 2 in the figure, Plank's equation for a cylindrical (3.17) shell will give the best estimate of α, while at position 1 Plank's equation for a rod (3.16) gives the best result. At position 3 the best result is something in between.

3.2.2 Use of Plank's equation to estimate the local α on a sphere of jelly

This section describs how local α can be found by shell freezing of a half sphere of jelly.

Description of jelly

Jelly is chosen since it is simple to shape. When made in a mould, it is possible to make more or less identical samples. Once frozen, jelly changes consistency, and becomes opaque. It is therefore possible to see which part of the jelly has been frozen, even after the jelly has melted. When the jelly freezes, it looks like there are a lot of small needles which grow into the unfrozen jelly.

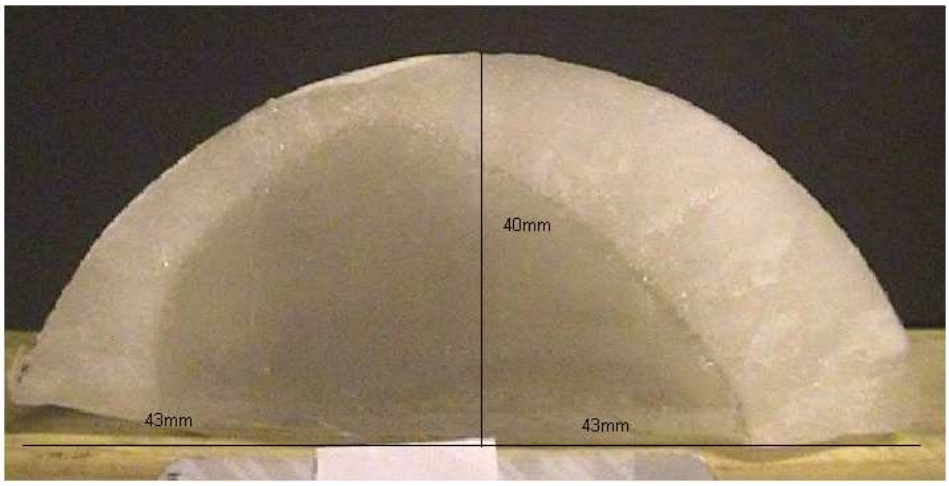

Figure 3.6: Picture of partially frozen jelly hemisphere

Mark the short side of a credit card visible in the bottom of the picture

Figure 3.6 shows a cut through a hemisphere of jelly which has been in experimental freezing tunnel for 60 minutes. The half sphere was cut with a sharp knife while still frozen. The radius of the jelly samples varied from 40 mm to 43 mm. The scaling card in bottom of Figure 3.4 is 54 mm long.

The jelly was made of water and Gelita Gelatine plates produced by DGF Stoess AG. (D69402 Eberbach/Baden, Germany) 20 plates in one litre of water gave a jelly which retained its shape when removed from the mould and placed on a shelf without support. By using the informative label on Gelita Gelatine the composition of the jelly was calculated by weight to be 97.28% water, 2.66% animal protein, and 0.06% mineral salt. Initial freezing point was measured to -0.235 ℃, by measuring centre temperature during a freezing experiment. The temperature will then stabilized on the initial freezing point for a while, before the temperature suddenly drops when all the jelly is frozen. From this, the thermal properties of the jelly were estimated based on theories presented in Schwartsberg's [86] article.

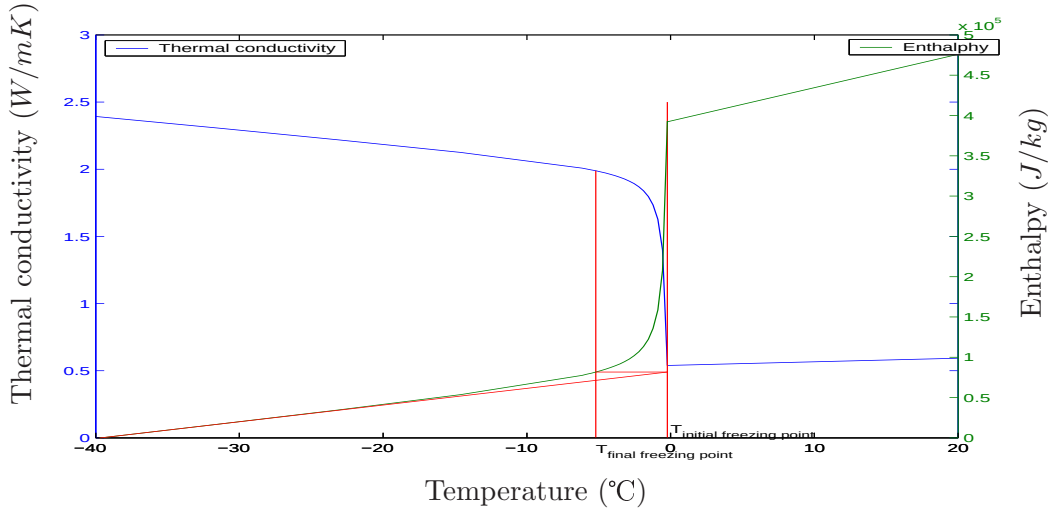

Figure 3.7: Thermal properties of jelly - h and λ

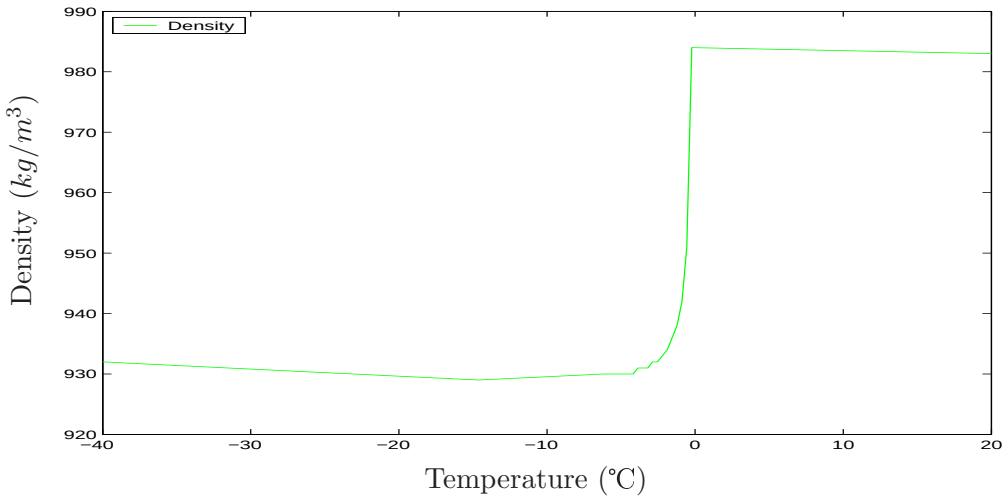

Figure 3.8: Thermal properties of jelly - ρ

To use the data in Plank's equation of frozen shell values for thermal conductivity, latent heat of melting and density must be assigned to the jelly. This is done graphically, the way Pham [59] suggests in Figure 3.7. The resulting values is presented in Table 3.1 together with other pre-set or pre-estimated values for the freezing experiment.

Table 3.1: Estimate of thermal properties of jelly used in Plank's equation

Thermal conductivity	1.99 $W/(m \cdot K)$
Density	930 kg/m^3
Latent heat of melting	311 kJ/kg
Time	3600 s
Temperature difference	29.165 K
Radius of half sphere of jelly	0.042 m
Air temperature	-29.4 °C
Initial freezing point	-0.235 °C
Final freezing point	-5.2 °C

Description of freezing tunnel

Figure 3.9 is a sketch of the principle in our mobile refrigeration tunnel and its air supply.

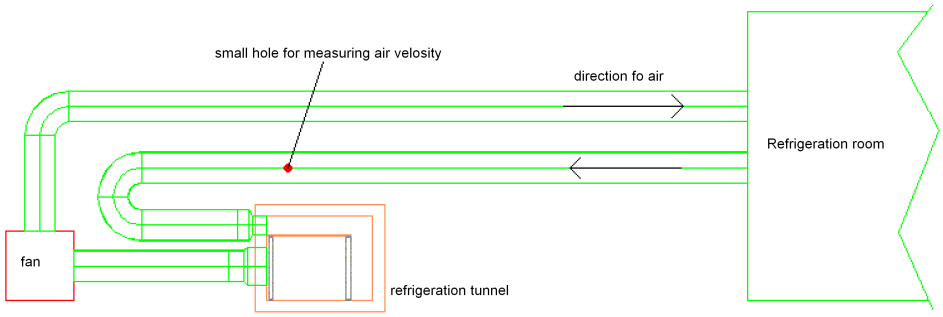

Figure 3.9: The complete freezing tunnel with its supply of cold air

Air is drawn from a refrigeration room, through a duct. The air passes through the tunnel before it reaches the fan. From the fan the air is blown back into the refrigeration room. The air velocity can be measured at a defined mark in the pipe (see Figure 3.9). Here the air has gone through a straight pipe that is long enough for a fully developed air velocity profile to be established. From the measured air speed at the centre of the duct, the air volume flow can be calculated. The pipe diameter at the measuring point is 315 mm. All parts of the system are well insulated from the surroundings. Temperature in the refrigeration room used in the experiment, is controlled within ± 1 K by a on/off regulation system. Minimum temperature the room can reach is about -35 ℃. The fan engine is controlled by a frequency regulator. At max the average air speed in the tunnel is about 4 m/s. Temperature difference in the air, air humidity, pressure loss over the fan and between inlet and outlet of the freezing compartment, are measured. Air speed was measured with a Schiltknecht MiniAir 2.

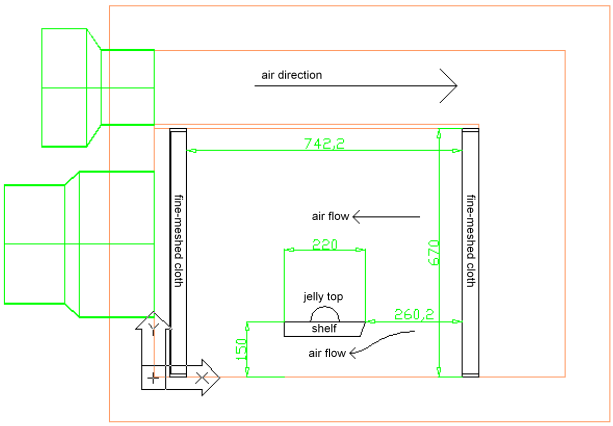

Figure 3.10: The chamber (freezing tunnel) where the product was frozen.

Figure 3.10 shows the freezing tunnel. The measurements are in mm. The chamber is 610 mm wide in the z-direction. Five jelly samples were usually frozen

at the same time. The one in the centre was placed on a plate in a hole with radius 73 mm in the shelf. The plate was connected to a scale in order to log weight loss during the freezing experiments. A fine-meshed cloth 26 cm upstream to the sample was used to get a even air distribution in front of the hemispheres in the freezing chamber.

Description of the experiment

Jelly was mixed, and was allowed to stiffen in ladle which had the shape of hemispheres inside. When set, the jelly was turned on a sheeting by holding the moulder in boiling water. The jelly was then packed in the foil, and stored on ice so that the initial temperature was close to 0 ℃ when the experiment was started. Cold air was blown through the freezing tunnel so it should be stable when the experiment was going to be started. Then the jelly was unpacked. All the foil except the circle under the half sphere was cut away. The foil under the jelly was kept to prevent the jelly from getting stuck in the foamed rubber and the thermocouple placed under the half sphere. The jelly was then kept in the freezing chamber for 60 minutes with air temperature -29.4 ℃ and air speed 1.2 m/s from the left side of the photo in Figure 3.6.

3.3 Results

In a smoke test it was possible to se the lines of smoke, but the lines moved around in the chamber. The smoke test and air speed measurements also showed that the air speed was largest at the bottom of the chamber, but the air speed was relatively constant in the area where the jelly was placed. In the freezer, the jelly sample was placed on foamed rubber so that the boundary condition at the bottom was assumed to be close to perfect insulation. According to boundary layer theory for laminar fluid-flow over a plate, presented by Kays & Craford [87], the displacement thickness is described by (3.17).

$$\delta_1 = 1.73\sqrt{\nu x/u_\infty} \tag{3.18}$$

Using tabulated properties for air at -30 ℃, the air speed in the chamber and length of shelves from this experiment the displacement thickness is 2 mm when the air has moved from the beginning of the shelves to the centre of the jelly sample, and 3 mm when it reach the end of the shelf. Since the jelly sample is 40 mm high, the effect of the shelf on the air stream can be ignored around the

jelly sample. This means that the jelly sample can be modelled as a sphere in free stream. For symmetrical reasons it can be expected that α and the shell thickness are the same if the angle between the vector from centre to the surface of the jelly sphere and the x-axis on Figure 3.6 is constant. This means that any cut through the centre parallel to the x-axis will have the same profile. It also means that the problem is reduced from 3 to 2 dimensions in spherical co-ordinates. This is valid if the air steam is parallel to the x-axis. The air stream is not so well defined, but cuts through several jelly samples show that it is close enough for this introductory experiment.

3.3.1 Estimate of the local α

Since the object shape is almost spherical it is natural to use the sphere form of Plank's equation. The choice of equation (rod, cylinder, sphere or something between) depends on geometry. The choice is only important when the frozen layer becomes thick. As shown above in Figure 3.7 all equations give same result if the frozen layer is thin compared with the total thickness of the sample. From (3.13) α can be placed on left-hand side, and becomes.

$$\alpha = 2\lambda \frac{R^3 - R_{ff}^3}{6\tau\lambda R^2 \frac{(T_{ff}-T_A)}{\rho\Delta h_{ice}} - R^4 + 3R_{ff}^2 R^2 - 2R_{ff}^3 R} \tag{3.19}$$

Everything on the right-hand side, can then be measured. In Figure 3.11 which is the same picture as Figure 3.6, the freezing front is marked by visual inspection, and L is measured. $\Delta R_I = (R - L)$ is then calculated.

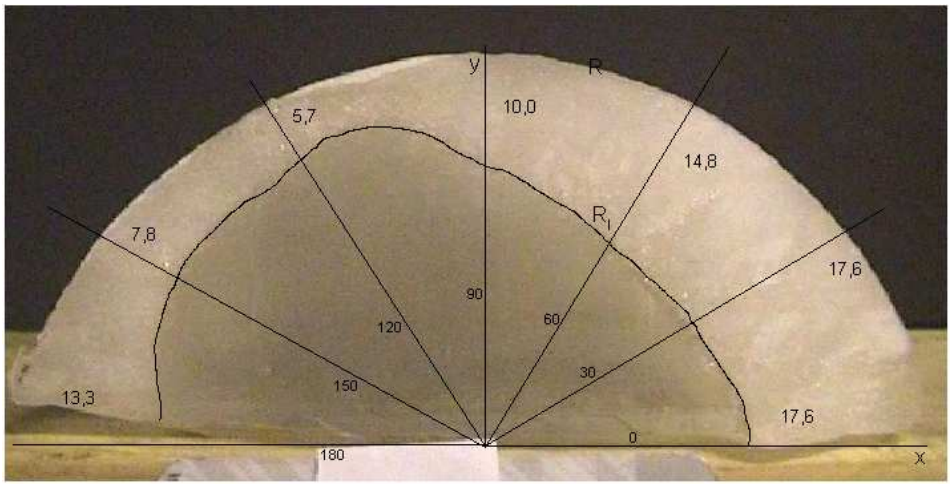

Figure 3.11: Partially frozen jelly hemisphere

Contour of inner radius (R_{ff}) is emphasised. Values for R_{ff} and angles are written on the figure.

The heat flux and the surface temperature can be estimated from (3.20) and (3.21).

$$\dot{q} = \frac{\Delta R_I \lambda}{(R - R_{ff})\, R + \frac{\lambda R_{ff}}{\alpha}} \left(T_{ff} - T_A\right) \tag{3.20}$$

$$T_S = \frac{\dot{q}}{\alpha} + T_A \tag{3.21}$$

(3.20) is (3.9) divided on the area of a sphere, ($4\pi R^2$), and (3.21) is the definition of α. Table 3.2 shows α, heat flux and surface temperature at different angles based on (3.19), (3.20) and (3.21).

Table 3.2: α, heat flux and temperature estimated from Plank's equation for sphere

Angle	L	R_{ff}	α_{sphere}	$\dot{q}$	T_S		α_{rod}		$\Delta r_{ig}(\%)$
0	0.0176	0.0244	36.6	686	-10.7		61.7		8.7
30	0.0176	0.0244	36.6	686	-10.7		61.7		8.7
60	0.0148	0.0272	31.8	678	-8.0		48.0		5.2
90	0.01	0.032	22.8	578	-4.1		29.6		1.9
120	0.0057	0.0363	13.9	389	-1.5		16.1		0.5
150	0.0078	0.0342	18.4	493	-2.6		22.4		1.0
180	0.0133	0.0287	29.0	660	-6.7		41.7		3.9

The second last column in Table 3.2 is α estimated by (3.16) which is Plank's equation for a rod. The relative large difference shows that the frozen layer is so thick that choice of equation has become important. The last is the maximum possible ice growth after the jelly is removed from the freezer because of cooling of the ice below the freezing point.

3.3.2 Error sources

Accuracy of shell thickness measurement

Jelly freezes over a temperature interval. Because of this there is an uncertainty connected to the definition of the position of the freezing front, in addition to the uncertainty in the measurement of length. Even if the jelly had a fixed freezing point like water, the front would not be smooth because of the nature of the crystals growing during freezing. In the results presented here, it was also necessary to cut through the jelly sample before the ice thickness could be measured with a ruler, which may disturb the freezing front. The uncertainty to the position measurement of the freezing front was estimated to $\pm 0.5\ mm$. Because the accuracy of the estimated heat transfer number is dependent on the relative accuracy of the ice shell thickness, a very thin shell will give a large uncertainty.

The ice thickness will increase a little when the jelly is removed from the freezer. This is because the ice is cooled below -0.235 ℃. Δr_{ig} in Table 3.2 is the maximum possible ice growth because of this effect if all the heat is taken from the freezing front. For thin ice shell the cooling below freezing is small and there is little ice heat can be removed from. The effect is therefore neglible. For a thicker

ice shell the ice growth is small compared to the total thickness of the shell.

Tangential internal heat flow

As for a temperature based sensor the heat leaving through the edge of an area on the jelly sample is a source of uncertainty, when estimating α. The heat flowing tangentially increases with the ice shell thickness. The ice layer must reach some thickness before it can be measured since the freezing front is not exactly defined.

Inaccuracy connected to the use of Plank's equation

As shown in Figure 3.11 it is not obvious which values the thermal properties are to be given when used in Plank's equation. According to the literature Plank's underpredicts the freezing time by 20-40% ([26]). This 20-40% is mostly caused by pre-cooling before freezing and cooling after freezing. See Pham [27, 28] and Cleland et al. [84]. Jelly freezes over a short temperature interval compared to fish, meat etc. Since this is closer to assumptions for which Plank's equation is developed, the prediction may be more precise. Pre-cooling is reduced by storing the jelly samples on ice. The average temperature in the jelly when removed from the freezer is according to simulations -4 ℃. This reduces the after-cooling. It is therefore likely that the uncertainty in α estimated based on Plank's equation is considerably more precise than 20%. More research is necessary to figure out how accurate α estimate is.

Inaccuracy in the initial conditions

It takes 2-3 minutes to prepare an experiment. This causes rise in the initial temperature in the jelly samples before the experiment starts. It also takes about 1 minute before the conditions in the freezing tunnel become steady after start. These errors are assumed to be small since the time is so short.

Uncertainty in boundary conditions

In the simulation there was perfect insulation under the jelly. In reality the jelly was placed on rubber foam. Rubber foam is a good insulator, but imperfect. Some heat therefore leaves the jelly through the insulation. Another problem was that a small air gap between the jelly and the foam was generated during freezing because of expansion. Cold air can then flow under the jelly and remove some heat. Both error sources influence the estimated α at 0 and 180 degrees in Figure

3.11. The influence for other angles is neglible because the temperature difference in the unfrozen jelly is small.

3.3.3 Estimate of magnitude of uncertainty

The $\%\alpha$ in Table 3.3 gives the error in % caused by $\pm 0.5\ mm$ uncertainty in the measurement of the shell thickness.

Table 3.3: Uncertainty in estimates caused by a measuring error in shell thickness

Angle	L	R_{ff}	α	$\alpha+$	$\alpha-$	$\%\alpha$	$\dot{q}$	T_S
0	0.0176	0.0249	35.8	34.9	36.6	2.4	687	-10.2
30	0.0176	0.0249	35.8	34.9	36.6	2.4	687	-10.2
60	0.0148	0.0277	30.9	30.0	31.8	2.9	673	-7.6
90	0.01	0.0325	21.8	20.8	22.8	4.5	561	-3.7
120	0.0057	0.0368	12.8	11.7	13.9	8.7	361	-1.3
150	0.0078	0.0347	17.4	16.3	18.4	6.0	470	-2.3
180	0.0133	0.0292	28.1	27.2	29.0	3.3	651	-6.3

To be able to estimate other sources of errors the following estimates is presented. 1% uncertainty in $\rho \cdot \Delta h_{ice}$ gives 1.2% uncertainty in α. 1% uncertainty in the thermal conductivity gives 0.2% uncertainty in α. These uncertainties are dependent on how the properties are estimated from Figure 3.11. 1 K uncertainty in the air temperature in this experiment gives 4% uncertainty in α. In sum there is about 5% uncertainty from other sources than the ice shell thickness measurement.

3.3.4 Comparison with numerical simulations

To be able to give a better prediction of the accuracy of the method of estimating the heat transfer method by measuring the shell thickness during freezing of jelly, αs found in Table 3.2 were used as input in a numerical simulation. The code was based on Forward Euler in 2-d spherical coordinates. The time steps were 0.5 milliseconds, and the grid was $(\pi/128)$radians x 0.25 mm wide. The thermal properties were updated at every time step. In the simulation the jelly sample was assumed to be a perfect sphere. α was interpolated between the angles where it was estimated in Table 3.2. The thermal properties were given in Figures 3.7 and

3.8. The density was held constant at $930 kg/m^3$ and shape change during freezing was ignored.

In agreement with assumptions for Plank's equation a rapid change in the heat flux from almost 0 to a high value marks the freezing front. Figure 3.12 is therefore an illustration of the absolute value of the heat flux in the jelly after 60 minutes in the freezing tunnel.

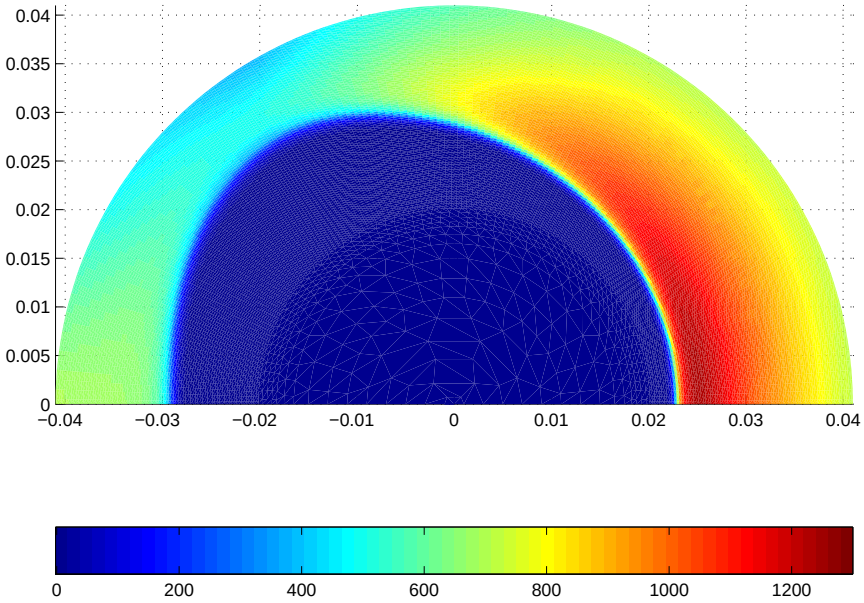

The unit for x and y axis is meter. The colours gives heat flux in W/m^2.

Figure 3.12: Simulated heat flux based on estimated α in Figure 3.3

As seen from Figure 3.12 the variation in heat flux is from 0 to 600 W/m^2 or more within $1.5mm$. Figure 3.12 shows the heat flux as a function of radius. In the non-frozen jelly the heat flux is close to zero. Then it increases fast in the freezing front before it decreases again through the frozen layer. The reason why the heat

flux decreases is the sphere geometry. In a rod the heat flux would be slightly increasing towards the surface.

Since a defined position of the freezing front is demanded in Plank's equation, the freezing front is defined as the intersection of the largest derivative of the heat flux, and the smallest derivative further out. See the lines between the circles in Figure 3.13. The smallest derivative had to be calculated with 5 points due to noise, which probably was caused by the differences in α around the sphere.

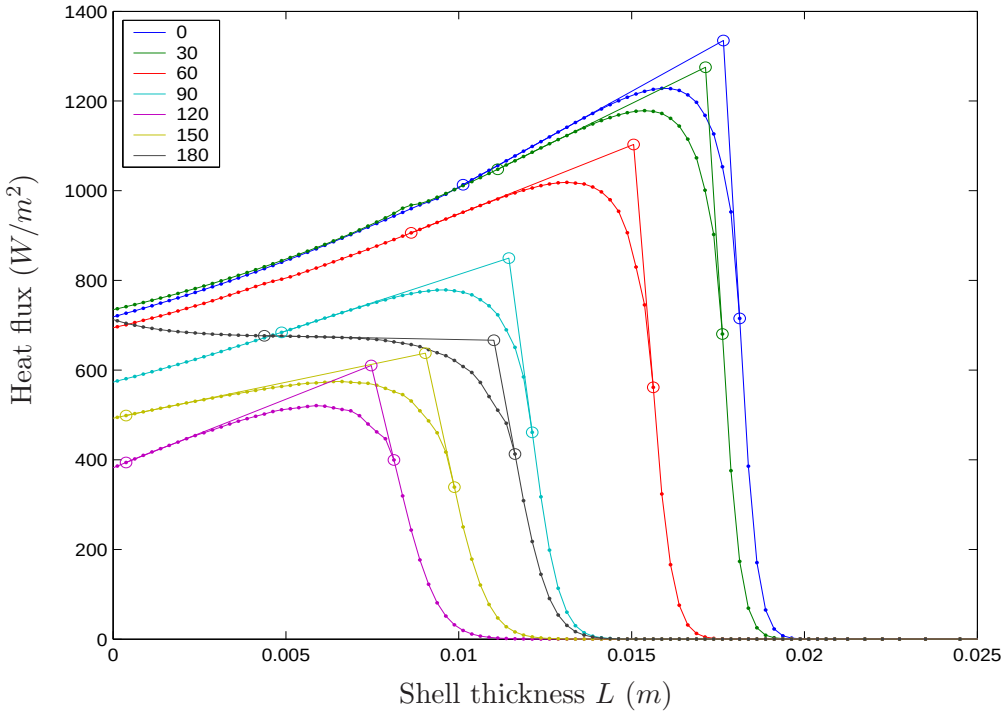

Figure 3.13: Heat flux as a function of shell thickness at different angles after 60 minutes

The figure shows cross-sections at different angles through Figure 3.12. The knuckle point shows the estimated position of the freezing front.

If Plank's assumptions were exact, the heat flux would have the shape of the

unit step function at the freezing front. This way to estimate the freezing front position is chosen because it gives a result which is close to a unit step function. The simulated result is compared with the one measured in Table 3.4.

Table 3.4: Comparison between the measured and simulated freezing front at different angles

	Least square, 2 and 5 points		
Angle	L Simulated	L Measured	% Error
0	0.0187	0.0176	6.3
30	0.0181	0.0176	2.8
60	0.0161	0.0148	8.8
90	0.0124	0.01	4.0
120	0.0085	0.0057	49.1
150	0.01	0.0078	28.2
180	0.012	0.0133	-9.8

The error in the simulation is up to 50%, but this is not bad for estimating a local α. It is worth noting that the simulation based on the estimated αs over predicts the shell thickness, which may indicate that the estimated αs is too high. The most likely systematic error is the method of estimating the freezing front in the numerical simulation. To measure the temperature when the jelly changes from transparent to white, and uses this temperature as the position of the freezing front, would probably been better, but the necessary experiment has not been performed. The error is largest where the shell thickness is small. This is because the relatively shell thickness measurement is at its largest here. It is also because heat flows away from this point in both directions. Then there is no levelling because heat is leaving at one side and entering at the other. The method does not compensate for this tangential heat flow. In Figure 3.14 the temperature, the radial heat flux, and the tangential heat flux are plotted from the simulation every 10 minutes.

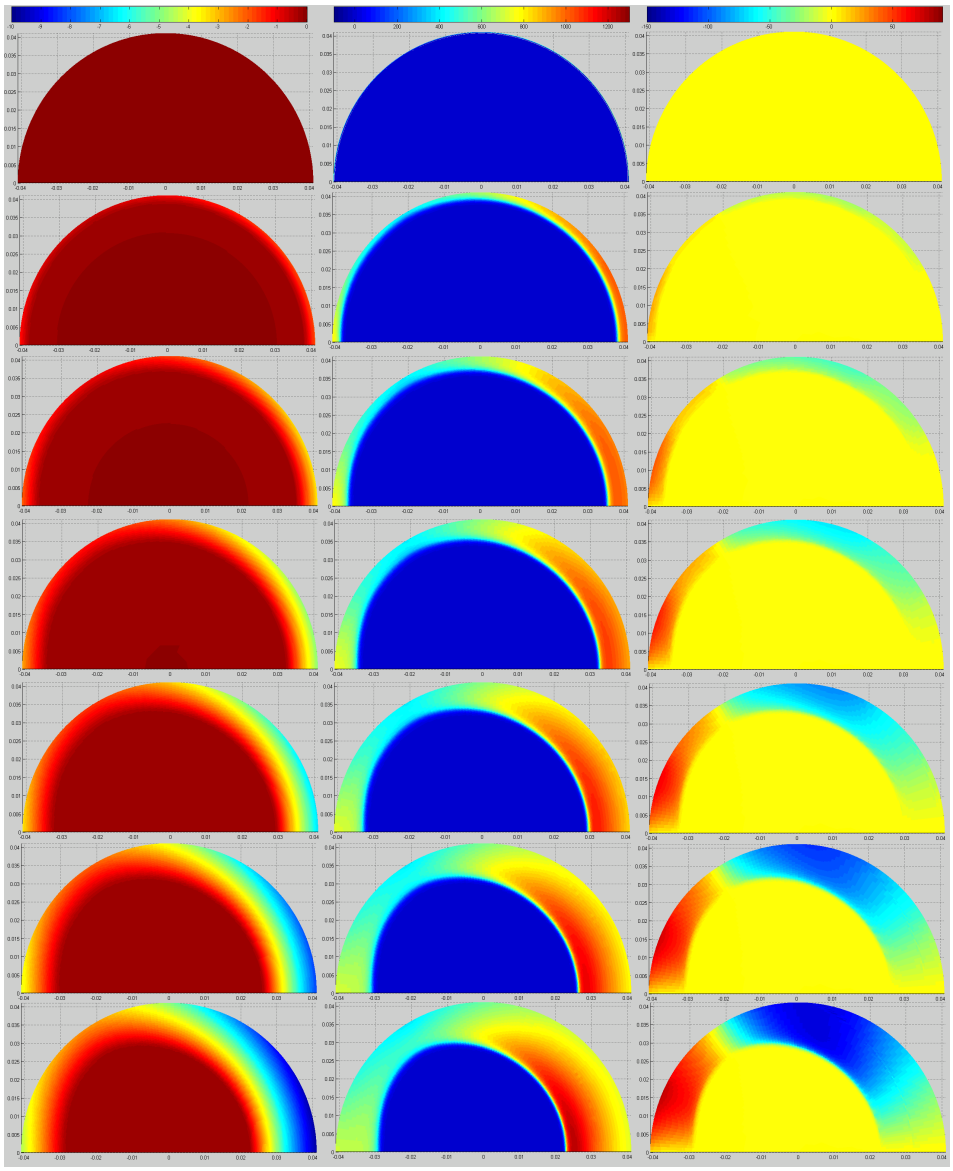

Temperature (-10 to 0 ℃) – Radial heat flux (-0 to 1300W/m^2) – Tangential heat flux (-150 to 100 W/m^2)

Figure 3.14: Temperature and heat flux evolution in 10 minute time steps

The first row of Figure 3.14 is at 0 minutes and the last is at 60 minutes. The tangential heat flux has a positive direction counter-clockwise around the origin. From 3.14 it is clear that heat will flow from the freezing front at an angle of 120 $^\circ$ and leave the half sphere at other angles, causing a too high estimated α at 120 $^\circ$ and nearby angles and too low in other places. The ratio between the tangential and radial heat flux indicates that the error is around 10-15%, but it can be lower because the tangential heat flux is smaller at the beginning of the experiment.

3.4 Discussion and conclusion

The thickness of the frozen shell in jelly combined with Plank's equation can give a usable estimate of the local α. More work on different geometries needs to be done to find out what accuracy can be expected by the method, and find the application area of the method. Very high or very low Biot's numbers can cause problems. So can large changes in the local α during freezing.

It is also necessary to find ways to correct for the tangential heat flux, and see if accuracy can be improved by using one of the many modifications of Plank's equation. Another method for measuring the shell thickness than visual inspection may improve the accuracy, and will allow estimation of α as a function of time. It was tried unsuccessfully to measure the shell thickness during freezing with sonar designed for finding cracks in steel. This failed because the echo from the freezing front was blurred.

Other possible methods are for instance, to measure thickness optically, since the jelly is transparent before it freezes, or to measure it with magnetic resonance (MR). Since MR can be used to find the freezing front in any food with high water content, an MR study will be particularly interesting.

Chapter 4

Concluding remarks

Chapter 2 describes an instrument called thermal multimeter developed for finding the thermal properties of materials where the thermal properties are highly dependent on temperature. Chapter 3 describes a method for finding α during freezing. The subjects are related in the way that successful measurement of the thermal properties makes it possible to find α in new ways and with higher accuracy. It is also necessary to have good control of the boundary conditions for a sample to measure its thermal properties with high accuracy.

Some measurements were made with the thermal multimeter. These measurements indicate an accuracy of 5% for measured thermal conductivity and 7% for heat capacity everywhere except close to the initial freezing point. Measured enthalpy is correct everywhere. The accuracy of the density measurement is estimated. More measurements are necessary to optimise the instrument and verify and possibly improve the accuracy. The method has proven to be reliable, and well suited for measuring change in thermal properties as a function of temperature. The instrument has performed well in measuring difficult materials between -50 and +40 ℃. The measuring time is long, up to four days. However, it is considerably shorter than the time needed to get enough measuring points with plate apparatus and adiabatic calorimeter to show how the thermal properties for a food material changes with temperature. A method for freezing food with high water content should be developed so that the thermal conductivity of the samples is reproducible . Other possibilities for the instrument should also be explored. Heat can be added so the whole sample and the whole shield have the same temperature. The instrument will then perform like an adiabatic calorimeter. Heat can

be supplied and drained from the sample so the temperature and the temperature difference over the sample is constant. The instrument will then operate similar to a plate apparatus. It will not perform as well as a plate apparatus, since there is no guard but the measurement will be more accurate than a transient measurement. Finaly heat can be removed from the sample. This is in principle the same as constant heating which is tested, but it makes it possible to investigate phenomena such as sub cooling, hysteresis between cooling and heating and controlled freezing of the sample inside the instrument.

The methods for using jelly to estimate local α must be regarded as interesting. Its simplicity and ability to make differences in α visible make it practicable, well suited for education and use in situations where it is important to prove without doubt for non scientists that a local low α gives slow freezing. The method is particular suited for showing:
- how α varies with the shape on object.
- how heat conduction through the support for the object influences freezing.
- how packaging influences α and which parts of the packaging causes most resistance to heat flow.
- a visualization of α.

Research should be done to improve the accuracy of α which is measured by this method. A weakness is that there is no easy way to make the collection of measurement data automatic.

References

[1] D.Q. Wang and E. Kolbe. Thermal conductivity of surimi - measurements and modelling. *Journal of Food Science*, 55:1217–1221, 1990.

[2] K. Hayakawa. *Estimation of heat transfer during freezing or defrosting of food Science et Technique du Froid. Freezing, frozen storage and freeze drying.* Institut International du Froid, Commission C1 et C2 :239, 1977.

[3] R. Simpson and C. Cortés. An inverse metod to estimate thermophysical propperties of foods at freezing temperatures: apparent volumetric specific heat. *Journal of Food Engineering*, 64:89–96, 2004.

[4] A.C. Cleland. *Food refrigeration processes: analysis, design and simulation.* Elsevier Applied Science, :28, London, 1990.

[5] W.M. Magee, R. Deal, J, and J.C Blanco. High-temperature adiabatic calorimeter for constant-volume heat capasity measurements of compressed gases and liguides. *Journal of Research of the National Institute of Standards and Technology*, 103(63):63–75, 1998.

[6] P. Nesvadba. Methods for the measurement of thermal conductivity and diffusivity of foodstuffs. *Journal of Food Engineering*, 1:93–113, 1982.

[7] Q.T. Pham. Detemination of the enthalpy of foods by an adiabatic calorimeter. *Journal of Food Engineering*, 21:137–156, 1994.

[8] R. Pongsawatmanit, O. Miywaki, and T Yano. Measurement of thermal conductivity of unfrozen and frozen food materiales by a steady state method with coaxial dual-cylinder apparatus. *Bioscience, Biotechnology and Biochemistry*, 57(7):1072–1076, 1992.

[9] R. Jowitt, F. Escher, Hallström, H.F.Th. Meffert, W.E.L. Spiess, and G. Vos. *Physical properties of foods (COST90).* Applied science publishers, London, 1983.

[10] Q.T. Pham. Modelling thermal processes: cooling and freezing. *Food Process Modelling (Book by Tijskens)*, :312–339, 1994.

[11] U Danielsson. Convective heat transfer measured directly with a heat flux sensor. *Journal of Applied Physiology*, 68(3):1275–1282, 1990.

[12] S Whitaker. Forced convection heat transfer correlations for flow in pipes, past flat pipes, single cylinders, single spheres, and for flow in packed beds and tube bundles. *AIChE Journal*, 18(2):361–371, 1972.

[13] A. Kondjoyan and J.D. Daudin. Determination of transfer coefficients by psychrometry. *International Journal Heat and Mass Transfer*, 36(21):1807–1808, 1992.

[14] A. Kondjoyan and J.D. Daudin. Heat and mass transfer coefficients at the surface of a pork hindquarter. *Journal of Food Engineering*, 32:225–240, 1997.

[15] A. Kondjoyan and J.D. Daudin. Effects of free stream turbulence intensity on heat and mass transfers at the surface of a circular cyllinder and an elliptical cylinder, axis ratio 4. *International Journal Heat and Mass Transfer*, 38(25):1735–1749, 1995.

[16] C.H. Edwards Jr. and D.E. Penney. *Elementary differential equations with boundary value problems.* Prentice-Hall, London, 3^{rd} edition, 1993.

[17] E. Kreyszig. *Advanced engineering mathematics.* Wiley, New York, 1993.

[18] M.N. Özisik. *Heat conduction.* Wiley, New York, 2^{nd} edition, 1993.

[19] H.K. Versteeg and W. Malalasekera. *Computational fluid dynamics.* Longman Scientific and Technical, Harlow, 1995.

[20] R.W. Lewis, K. Morgan, and O.C. Zienkiewicz. *Numerical methods in heat transfer.* John Wiley & Sons, Chichester, 1981.

[21] H. Anton and C Borres. *Elementary linear algebra.* Wiley, NY, 6^{th} edition, 1991.

[22] F.P. Incropera and D.P. DeWitt. *Fundamentals of heat and mass transfer.* Wiley, 4^{th} edition, 1996.

[23] G.F. Hewitt, G.L. Shires, and T.R. Bott. *Process heat transfer*. CRC Press, 4^{th} edition, 1994.

[24] R. Plank. Uber die gefrierzeit von eis ind. wasserhallegen lebensraitteln. *Beihefte Z ges Kelte-Ind Reihe*, 39(14), 1932.

[25] R. Plank. Beitrage nur berechnung und bewertung der gefriergesch - windigkeit von lebensmitteln. *Beihefte Z ges Kelte-Ind Reihe*, 3(25):1–16, 1941.

[26] R.L Cleland, A.C.;Earle. A comparason of methods for predicting the freezing times of cylindrical and spherical foodstuffs. *Journal of Food Science*, 44:958–963, 1979.

[27] Q.T. Pham. Extension of Plank's equation for predicting freezing times of foodstuffs of simple shapes. *Revue Internationale do Froid*, 7(19):377–383, 1984.

[28] Q.T. Pham. Analytical method for predicting freezing times of rectangular blocks of fooodstuffs. *Revue Internationale do Froid*, 8(1):43–47, 1985.

[29] Q.T. Pham. Simplified equation for predicting the freezing time of foodstuffs. *Journal of Food Technology*, 21:209–219, 1986.

[30] D.J. Cleland, A.C. Cleland, and R.L. Earle. Prediction of freezing and thawing times for multi-dimensional shapes by simple formulae part1: regular shapes. *International journal of refrigeration*, 10:156–164, May 1986.

[31] A.C. Cleland, D.J. Cleland, and L.M Davey. Accuracy of simplified approach for finding geometric factor of regular geometric shapes during freezing and thawing time prediction. *19^{th} International Congress of Refrigeration*, 2:57–64, 1995.

[32] A.C. Cleland and R.L Earle. Assessment of freezing time prediction methods. *Journal of Food Science*, 49:1034–1042, 1984.

[33] M.M Hossain. A simple method of freezing time calculation for foodstuffs of varius shapes. *Food Australia*, 47(3):March, 1995.

[34] Md.M Hossain, D.J. Cleland, and A.C Cleland. Prediction of freezing and thawing times for foods of tree-dimensional irregular shape by using semi-analytical geometric factor. *Revue International Froid*, 15(4):241–246, June 1992.

[35] Ilcal Coskan, Metin Cetin, and S. Cetin. Methods for the freezing time of ellipses. *Journal of Food Engineering*, 28:361–372, September 1996.

[36] S. Rahman. *Food properties handbook*. CRC Press, 1995.

[37] Q.T Pham. Prediction of caloremetric properties and freezing time of foods from composition data. *Journal of Food Engineering*, 30:95–107, April 1996.

[38] Q.T. Pham. Prediction of thermal conductivity of meats and other animal products from composition data. *Proceedings from the 5th International Congress on Engineering and Foods (ICEF 5) (Cologne)*, 5:408–423, 1989.

[39] I. Lind. The measurement an prediction of thermal properties of food during freezing and thawing - a review with particular reference to meat and dough. *Journal of Food Engineering*, 13:285–319, 1991.

[40] J.D. Mellor. Thermophysical properties of foodstuffs 3^{rd} - measurements. *International Institute of Refrigeration (IIR)*, 59:551–564, 1979.

[41] M. Kent, K. Christiansen, I.A Haneghem, E. Holz, M.J. Moerly, P. Nesvadba, and K.P Poulsen. Cost 90 collaborative measurements of thermal properties of food. *Journal of Food Engineering*, 3:117–150, 1984.

[42] V. Harðarson. *Matvarers termofysiske egenskaper og deres betydning ved dimensjonering av frysetunneler*. NTH-Trykk, Trondheim, 1995.

[43] *Encyclopaedia Britannica*. Chicago, 15th edition, 2002.

[44] William Ramsay. *The life and letters of Joseph Balck*. Constable and Co Ltd, London, 1918.

[45] L. Riedel. Enthalpy and specific heat of fats and oils. *Ketechnik*, 8(3):8–10, 1956.

[46] L. Riedel. Calorimetric investigations of the meat freezing process. *Ketechnik*, 9:38–40, 1957.

[47] L. Riedel. Calorimetric investigations of the freezing of egg white and yolk. *Ketechnik*, 9:342–345, 1957.

[48] L. Riedel. Eine prüfsubstanz fûr gefrierversuche. *Ketechnik*, 12:222–225, 1960.

[49] Fleming. Calorimetric properties of lamb and other meats. *Journal of Food Technology*, 4:199–215, 1969.

[50] D.T. Lindsay and S.J. Lovat. Further enthalpy values of foods measured by an adiabatic calorimeter. *Journal of Food Engineering*, 23:609–620, 1994.

[51] K. Kobashi, T. Kyomen, and M. Oguni. Construction of an adiabatic calorimeter in the temperature range between 13 and 505 k, and thermodynamic study of 1-chloroadamantane. *Journal of Physics and Chemistry of Solids*, 59(5):667–677, 1998.

[52] A.M. Tocci, S.E. Ethel, and R.H Mascheroni. Enthalpy, heat capacity and thermal conductivity of boneless mutton between -40 and +40 c. *Lebensm,. Wiss u.-Technol*, 30:184–191, May 1996.

[53] G. Höhne, W. Hemminger, and H. Flammersheim. *Differential Scanning Calorimetry*. Springer-Verlag Berlin, Heidelberg, 2^{nd} edition, 2003.

[54] N. Garti, J. Schlichter, and S. Sarig. DSC studies concerning polymorphism of saturated monoacid triglycerides in the presence of food emulsifiers. *Fett wissenschaft technologie*, 90:295–299, 1988.

[55] W. Brill and E. Gmelin. Disc - a differential isoperibol scanning calorimeter. *Journal of Thermal Analysis*, 33:365–370, 1988.

[56] P. Meuter, H. Rahier, and B Mele. Disc - a differential isoperibol scanning calorimeter. *International Journal of Pharmaceutics*, 192:77–84, 1999.

[57] S. Ozilgen and D.S. Reid. The use of DSC to study the effects of solutes on heterogeneous ice nucleation kinetics in model food emulsions. *Food Science and Technology-Lebensmittel-Wissenschaft & Technologie*, 26(2):116–120, 1993.

[58] W. Hemminger and G. Höhne. *Calorimetry - fundamentals and practice*. Verlag Chemie, 1984.

[59] Q.T. Pham. Calculation of bound water in frozen food. *Journal of Food Science*, 52(1):210–212, 1987.

[60] Y. Choi and M.R. Okos. Effect of food temperatures and composition on the thermal properties of foods. *Journal of Food Process Engineering*, 1:93–101, 1982.

[61] A.M. Howatson, P.G. Lund, and J.D. Todd. *Engineering tables and data*. Chapman & Hall, London, 2^{nd} edition, 1991.

[62] Q.T. Pham and J. Willix. Thermal conductivity of fresh lamb meat, offals and fat in the range -40 to +30℃: Measurements and correlations. *Journal of Food Science*, 54(3):508–515, 1989.

[63] Q.T. Pham and C.G. Smith. Thermal imbalance errors and effective area in guarded hot plates. *Review of Scientific Instruments*, 57(1):408–423, 1986.

[64] J. Willix, S.J. Lovat, and N.D. Amos. Additional thermal conductivity values of foods measured by a guarded hot plates. *Journal of Food Engineering*, 37:159–174, 1998.

[65] Silas E. Gustavsson. Transient plane source tecniques for thermal conductivity and thermal diffusivity measurements of solid materials. *Rev. Sci. Instruments*, 62(3):797–804, 1991.

[66] Silas E. Gustavsson, Ernest Karawacki, and M.Nazim Khan. Transient hot-strip method for simultaneously measuring thermal conductivity and thermal diffusivity of solids and fluids. *Appl. Phys.*, 12:1411–1421, 1979.

[67] Silas E. Gustavsson, Ernest Karawacki, and M.Nazim Khan. Thermal transport studies of electrically conducting materiales using the transient hot-strip technique. *Appl. Phys.*, 19:727–735, 1986.

[68] A.B. Buhri and R.P. Singh. Measurement of food thermal conductivity using differential scanning calorimetry. *Journal of Food Science*, 58(5):1145–1147, 1993.

[69] P. Nesvadba. A new transient method for the measurement of temperature dependent thermal diffusivity. *Appl. Phys.*, 15:725–738, 1982.

[70] A.L. Fitch. A new thermal conductivity apparatus. *Am. Phys. Teach.*, pages 135–136, 1935.

[71] G.E. Myers. *Analytical methods in conduction heat transfer.* McGraw-Hill, New York, 1971.

[72] H.G. Schwartzberg. Effective heat capacities for the freezing and thawing of foods. *Journal of Food Science*, 41:152–156, 1976.

[73] A. Iserles. *Numerical analysis of differential equations.* Cambridge University Press, Cambridge, 1996.

[74] R. Siegel and J.R. Howell. *Thermal radiation heat transfer.* Hemisphere, Washington, 1992.

[75] E.D. Palik, editor. *Handbook of optical constants of solids.* Academic Press handbook series, 1998.

[76] CRM 039 Certified Reference Material, editor. *Pyrex Glass*. Community Bureau of Reference BRC, Brussels, 1990.

[77] Y.S. Touloukian, editor. *Thermophysical properties og high temperature solid materiales*. Macmillan, New York, 1967.

[78] L. Riedel. Eine prfsubstanz fr gefrierversuche. *Kaltetechnik*, 12:222–225, 1960.

[79] Q.T. Pham and J. Willix. Effect of biot number and freezing rate accuracy of some food freezing time prediction methods. *Journal of Food Science*, 55(5):1429–1434, 1985.

[80] E. Brendeng and P.E Frivik. On the design of a guarded hot plate apparatus. *Annexe 1969-7 Bulletin, International Institute of Refrigeration*, pages 281–288, 1969.

[81] S. Whitaker. *Elementary heat transfer analysis*. Pergamon Press inc., New York, 1976.

[82] J.V. Beck, B. Blackwell, and C.R. St.Clair Jr. *Inverse heat conduction*. Wiley, New York, 1985.

[83] M.B. Harris, S.J. Lovatt, and J. Willix. Development of a sensor for measuring local HTCs on carcass-shaped objects. *20 th International Congress of Refrigeration, IIR/IIF, Sydney*, IV(352), 1990.

[84] A.C. Cleland and S. Özilgen. Thermal design calculations for food freezing equipment -past present and future. *International journal of refrigeration*, 21(18):359–371, 1998.

[85] R. Plank. Die gefrierdauer von eisblöcken. *Zeitschrift für die gesamte Kälte-Industrie*, 6:109–114, June 1913.

[86] H.G. Schwartsberg. Effective heat capacities for the freezing and thawing of food. *Journal of Food Science*, 41:152–156, 1976.

[87] W.M. Kays and M.E. Crawford. *Convective heat and mass transfer*. McGraw-Hill, New York, 2^{nd} edition, 1980.

Appendices

A Technical drawings

Figure A1, A2, A3 and A4 shows some of the parts in Figure 2.4. They are Technical drawings with measurements in mm (red text). The numbers reference to details on each part.

1 Holes for steel tubes which holds the instrument together. (Figure A2 and A3)
1 Holes for heat bridge between ShC and SaC (Figure A1).
2 Screw holes for fastening the heater to each part.
3 Holes for thin steel pipes. These are the pipes which holds the sample in place.
4 Holes for Pt100 and thermopile sensors.
5 (Holes for) heat bridges between SaC and BS.
6 Slot for steel shield (2 in Figure A1).
7 The part of TS and BS which enclose the sample.
8 (Holes for) heat bridges between ShC and BHS.

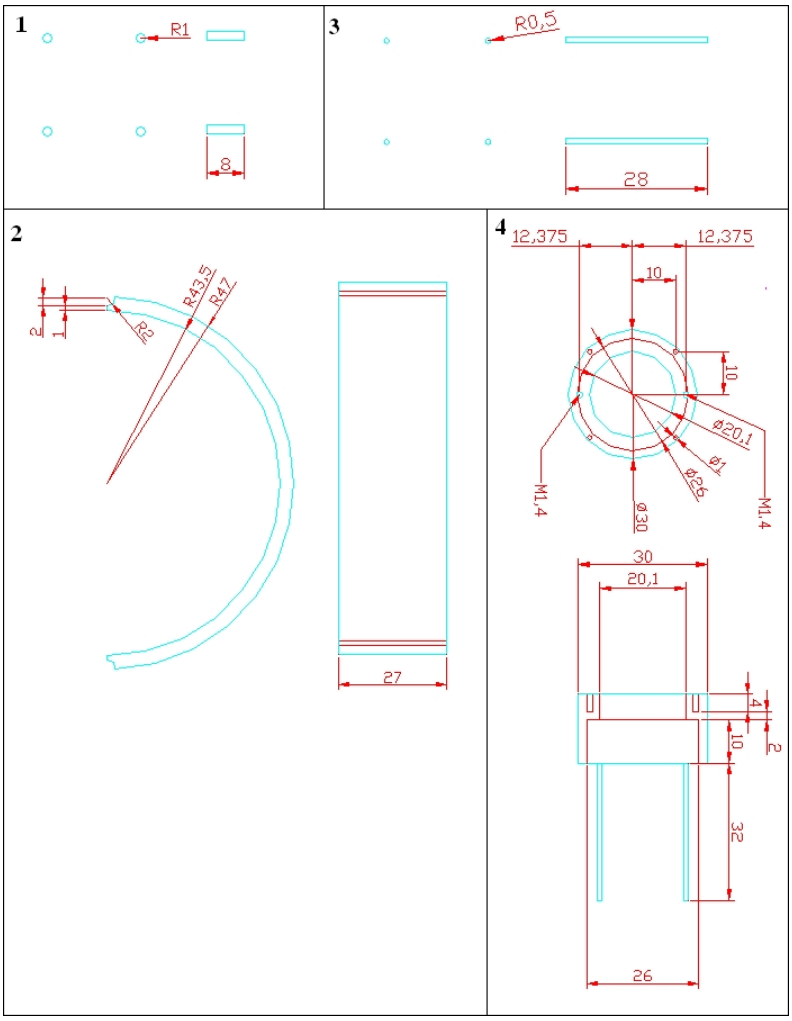

Figure A1: Technical drawings of some important parts of steel

1 Steel rods between SaC and ShC.
2 One of two steel shield between THS and BHS.
3 Steel tubes which holds the sample in place.
4 Device for handling sample expansion.

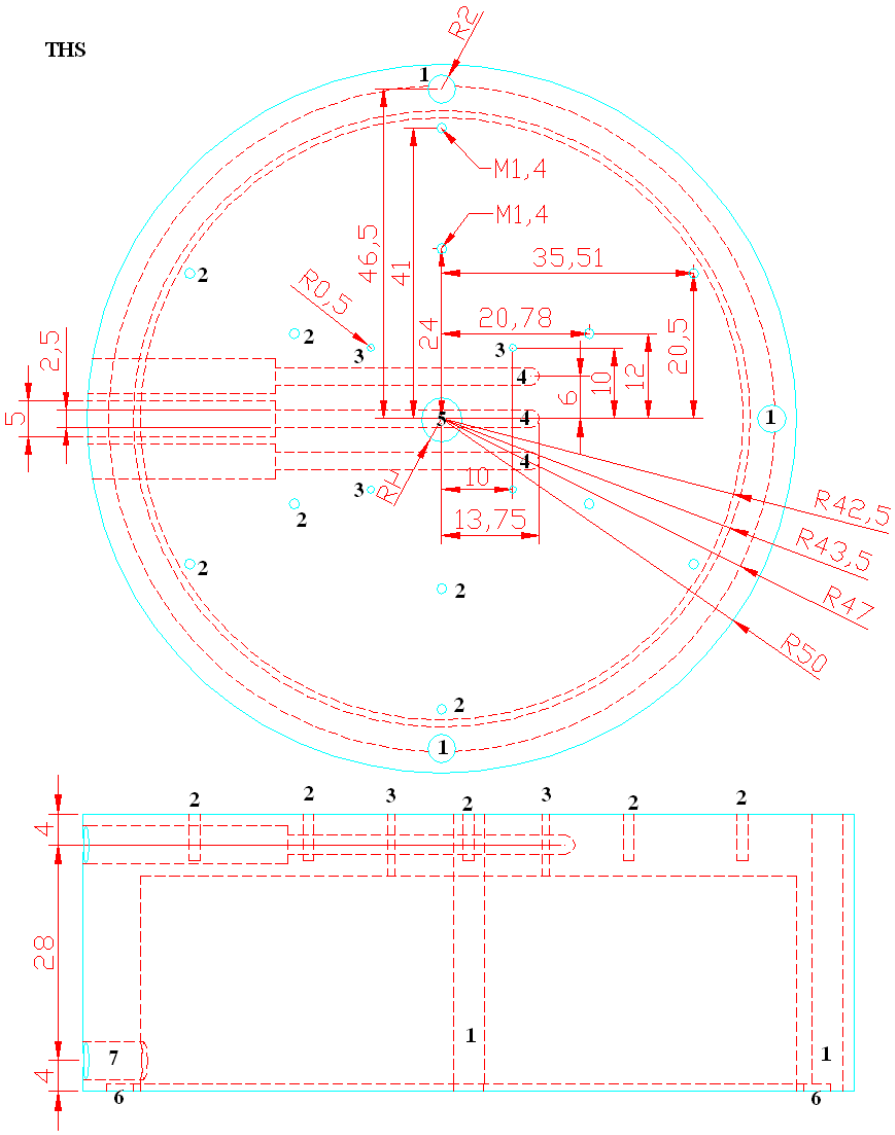

Figure A2: Technical drawings of THS

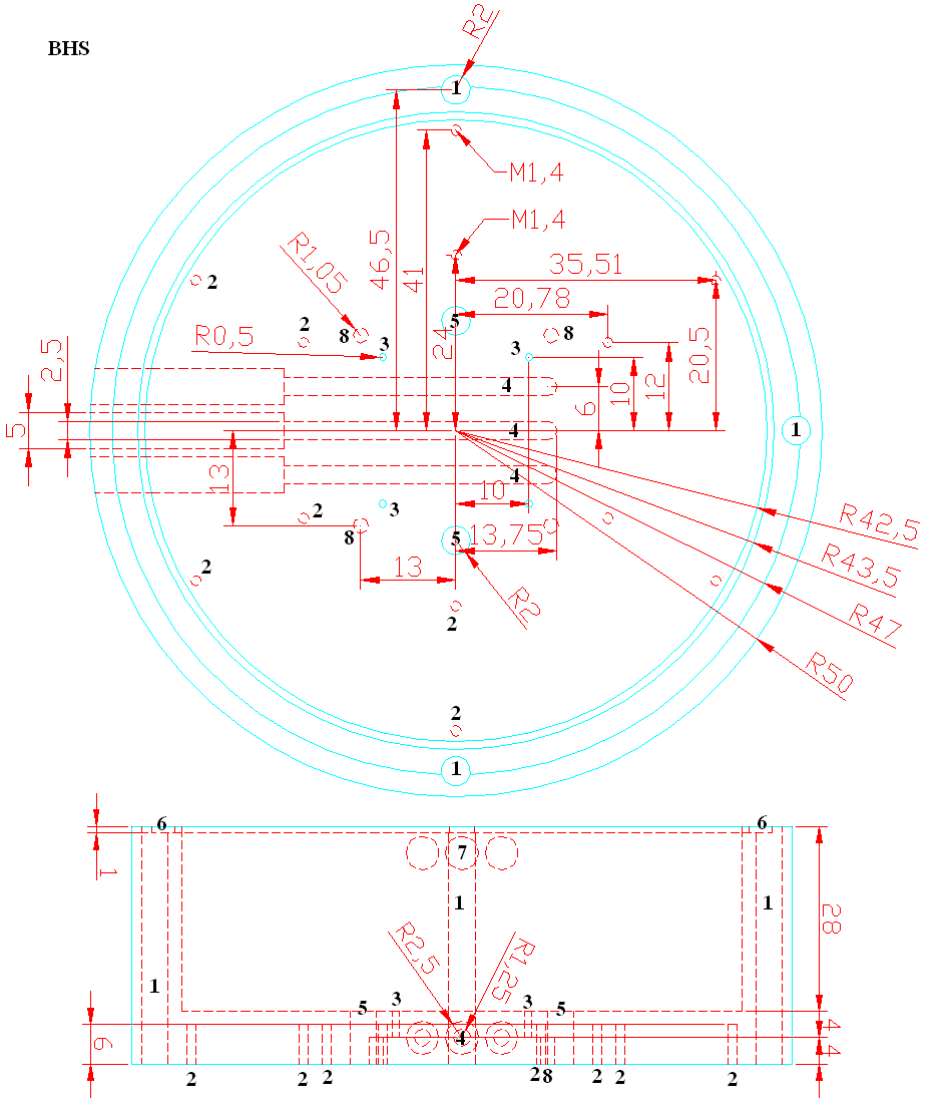

Figure A3: Technical drawings of BHS

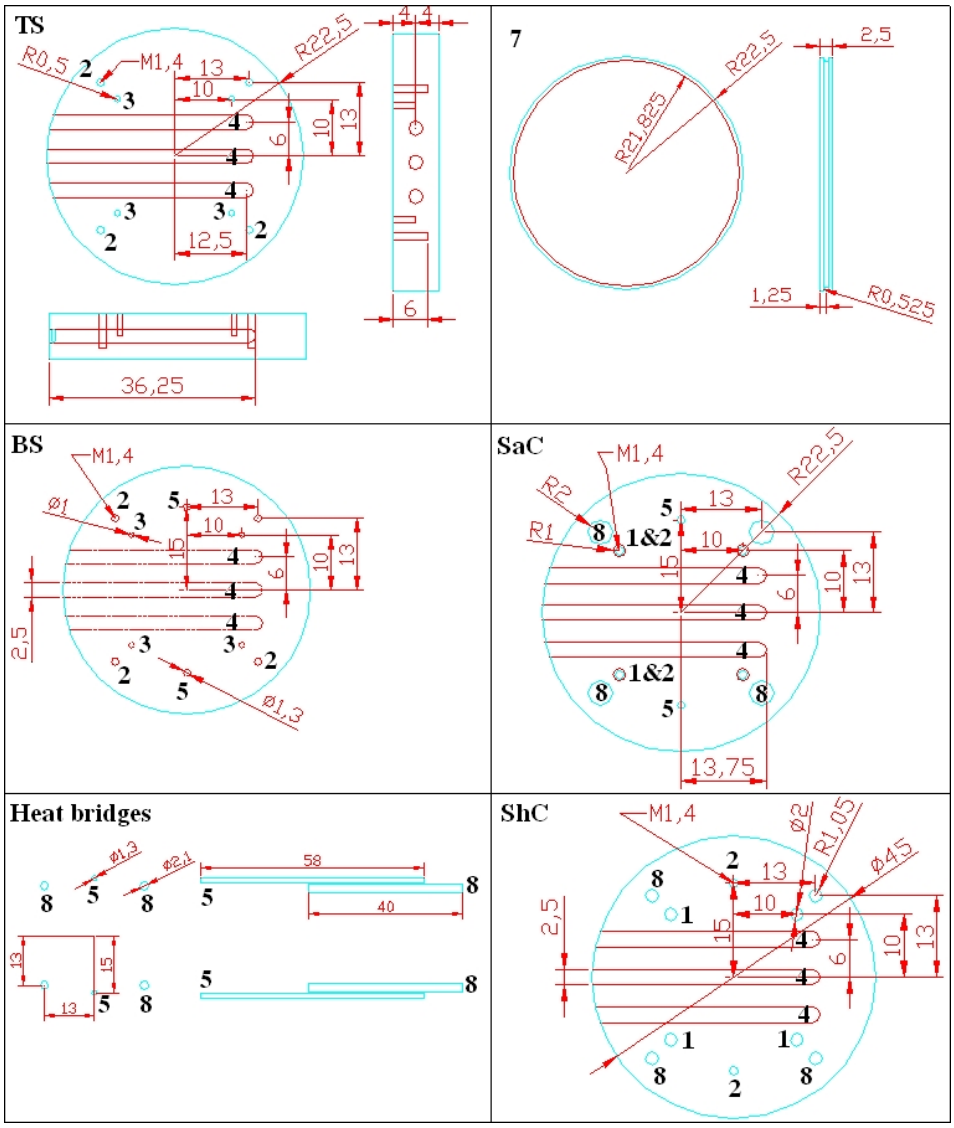

Figure A4: Technical drawings of some important parts of copper

B Attached files

This thesis can be downloaded in PDF format from
http://urn.ub.uu.se/resolve?urn=urn:nbn:no:ntnu:diva-979
together with some of the files used for numerical simulation,
data acquisition, construction etc.
Se http://www.ub.ntnu.no/dravh/Brennvall_attachment.zip

Explanation to attached files

Avhandling.pdf	This thesis
FourierCoolingSlab.m	Analytical solution for cooling of slab. (Section 1.3.1)
Simulation of jelly tops	
GeletopShow-Chart.m	Presents charts from simulation of jelly tops (geltop12r4.f90)
GeletopVideo.m	Make videos from charts shown in GeletopChowChart.m
geltop12r4.f90 *	Source code simulation program for jelly tops
Matmatrix3.f95	Prepare result from geltop12r4.f90 to presentation in Matlab
GeltopT.avi	Video, Temperature progress
GeltopQ.avi	Video, Total heat flux progress
GeltopQR.avi	Video, Radial heat flux progress
GeltopQA.avi	Video, Tangential heat flux progress
{res}	Folder, data from simulations of jelly tops
Simulation of thermal multimeter	
MultimeterVis.m	Program for visualising in Matlab
fs.m	Function to GeletopChowChart.m and MultimeterVis.m
Multimeter.f90 *	Program for thermal simulation of the thermal multimeter
Matmatrix3.f95	Prepare result from Multimeter.f90 to presentation in Matlab
{MPV}	Folder, data from simulations
{Multimeter}	Folder, data from simulations
{Multimeter_Para-meter_Variation}	Folder, data from simulations
AutoCAD model	
k40.dwg	AutoCAD model of the thermal multimeter

Simulation of freezing of 10 mm deep water (Section 1.3.2)
These files are placed in the folder {Freezing_of_ice}

\Freezing.m	Simulation program
\Chart.m	Show result from simulation (Figure 1.3).
\ThermalProp	Function to Freezing.m

Calculation of thermal properties from measured heat flux and temperatures in the thermal multimeter
These files are placed in the folder {TM_data_acquisition_program}

\Totalrun.m	Program for calculating thermal properties from measured data

Main functions in Totalrun.m. Can be run as separate programs

\PostProsessing.m	Preparation of data from measurement for Matlab
\CalibrationCharts.m	Treating data from calibration runs
\CalibrationCharts_-comparason.m	Show results from calibration measurements
\Measurements_TM.m	Calculating thermal properties
\Charts.m	Generates charts from measurement
\Report.m	Generates report from measurement

Sub functions are not included
\TargetDirectory.DAT

All the f90 simulation programs marked with a * ran on gridur.ntnu.no .
Se http://www.notur.org .

Jon Eirik Brennvall

ISBN 978-82-471-0119-3 (printed ver.)
ISBN 978-82-471-0122-3 (electronic ver.)
ISSN 1503-8181

Doctoral Theses at NTNU, 2007:6

NTNU
Innovation and Creativity

NTNU